Rheological evaluation and printability guidelines of high-performance amorphous thermoplastics and carbon fiber-reinforced composites for additive manufacturing

A Dissertation Presented for the
Doctor of Philosophy
Degree
The University of Tennessee, Knoxville

Christine Ajinjeru
August 2020

Copyright © 2020 by Christine Ajinjeru.
All rights reserved.

I dedicate this dissertation to my mother, Margaret Baba Diri, who has sacrificed so much for me to be where I am today.

ACKNOWLEDGEMENTS

This dissertation research was sponsored by the U.S. Department of Energy, Office of Energy Efficiency and Renewable Energy, Advanced Manufacturing Office, under contract DE-AC05-00OR22725 with UT-Battelle, LLC. I also received partial support from the Center for Materials Processing, a Tennessee Higher Education Commission (THEC) supported Accomplished Center of Excellence, for the use of various processing equipment to conduct parts of this research. Part of the dissertation research was funded by the National Science Foundation, grant number A19-0175. I would like to thank the facilities at which the research was conducted especially the Manufacturing Demonstration Facility (MDF) at Oak Ridge National Laboratory, for providing me access to the equipment and resources that I needed for this work to be a success. I would also like to thank Cincinnati Inc for providing the Big Area Additive Manufacturing (BAAM) system at the MDF on which most of the experiments were performed. Materials used throughout this dissertation were supplied by Techmer PM, SABIC, and BASF and I would like them for ensuring that there was plenty of material for research purposes.

I would like to thank my advisor, Dr. Chad Duty, for introducing me to the world of additive manufacturing and training me to be the scholar that I am today. I would also like to thank the Bredesen Center and in particular, the current and former program directors, Dr. Suresh Babu and Dr. Lee Riedinger, respectively for ensuring that I thrived in the program and had all the support I needed to excel.

I would like to thank my PhD committee members; Drs. Vlastimil Kunc, Brett Compton, and Mark Dadmum for the mentorship and support I received from them throughout my training.

I am grateful to my family for their support and encouragement throughout the PhD journey. It was difficult being thousands of miles away from them but they constantly checked up on me and on days when I could not keep going, they were my motivation. Thank you Robert Lemeriga, Gerald Guma, Richard Sanya, Grace Anika Diri, Walter Awule, Evelyn Kobusingye, Christine Amulen, Dorothy Guma, Remmy Amandru, Sam Duku, and Susan Apai. To my nieces and nephews who look up to me, Queen, Denaya, Benita, Dominic, Ethan, Elaine, Eugenia, Molen, Adrian, Cherry, Meghan, Napiso, and Happy, may I continue to serve as a role model in your lives.

I would also like to thank my Bredesen Center colleagues; Tracey-Ann Wellington, Akinola Oyedele, Maria Fernanda Campa, Mallory Ladd, Jayde Aufrecht, Ishita Ray, Eva Mutunga, Anna Wanhala, Adeola Adediran, Kristine Cabugao, Jeff Beagle, Tony Bova, Michelle Halsted, and Alex Pawlowski.

I would like to thank my support system; Rhnea Raegan and Ruthann Moyers in the MABE department for making sure that the lab supplies I needed for my research were ordered and delivered in time. I would also to thank the Bredesen Center staff; Wanda Davis for being a mother figure and confidant, Allie Burns and Rebecca Christ for always worrying about logistics which freed up space in my brain for research.

I am grateful for the support of my lab mates: James Brackett, Dylan Hoskins, Tyler Smith, and Jake Dvorak. I have so many memories to cherish from our time together. A special shout out to Vidya Kishore who has been a pillar of support and knowledge through our time working together with Dr. Chad Duty. Thanks to the undergraduate interns in the lab over the years; Jordan Failla, Dakota Cauthen, Carter Sutton, and Daniel Johnson for conducting numerous experiments that made this dissertation possible. I would also like to thank members of the MDF and Oak Ridge National Laboratory especially Ahmed Arabi Hassen, John Lindahl, Christopher Hershey, Seokpum Kim, and Halil Tekilnap for their support and collaboration on various projects. I would like to thank the collaborative efforts of Dr. Brett Compton's research group, in particular, Nadim Hmeidat and Madeline Wimmer for the experiments they conducted in support of this research.

Thanks to my friends; Kaydi-Ann Newsome, Marissa Robinson, Chainky Reindorf, Tolu Alabi, and Kaya Matson for cheering me on every single day. Thanks to Maria Namwanje, Colette Aba, Sheila Namirembe, Ashley Mayanja, and Maureen Njuguna for being great sounding boards and a strong familial support. I would like to extend my gratitude to Coach Jeff Pedersen, Glendon and Charmaine Newsome, Terry Wellington, Father Alex, Dr. Stephen Opiyo, Gladys Opiyo, Adonis Ajayi, Father Ruffino Ezama, Lisa George-Sharpe, Tyler, George and Lucy Njuguna, Natalie Richardson Gentil, Heidi Ostby, Zoe Whitlock, Loriade Akin-Olugbade, Oladoyin Phillips, Samantha Pilicer, Bridget Kayitesi, Adewale Odukoimaya, and Kertesha Riley for the unwavering support over the course of my PhD.

ABSTRACT

Although additive manufacturing (AM) has revolutionized the manufacturing industry through rapid and complex geometry fabrication capabilities at a fraction of the cost, only a small fraction of the materials used for traditional manufacturing are compatible with AM. Emerging applications in polymer AM motivate the need for production and development of new materials with a broader range of thermal and mechanical properties. Advancements in AM have also led to new system development such as Big Area Additive Manufacturing (BAAM) systems at Oak Ridge National Laboratory, capable of processing high-performance thermoplastics and composites. As the application space for three-dimensional printed components continues to grow, it is necessary to identify appropriate processing conditions and expand the current selection of high-performance thermoplastics and fiber reinforced composites for AM systems. However, there is no formal process for designing, screening, and evaluating the printability of these high-performance thermoplastics and composite systems. Traditional polymer characterization techniques utilizing thermal and rheological material properties have been effectively employed in other polymer processing methods such as injection molding to identify suitable processing conditions. Therefore, to expand the current high-performance material selection for BAAM using industrial grade pellets, these techniques are employed to establish the relationships between fundamental material properties such as thermal and rheological properties and AM processing parameters. Overall, this work is an attempt to expand the current selection of high-performance feedstock on large format AM systems such as BAAM using thermal and rheological characterization techniques. This is achieved by predicting their extrudability through the nozzle, quantifying the impact of pressure transients on extrusion, and identifying appropriate processing conditions for these materials to provide a basis for optimizing the use of current high-performance materials as AM feedstock.

TABLE OF CONTENTS

Chapter One Introduction 1
Motivation 1
Extrusion-Based Additive Manufacturing Systems 2
High-Performance Amorphous Thermoplastics in AM 3
Acrylonitrile Butadiene Styrene (ABS) 4
Polyetherimide (PEI) 4
Polyphenylsulfone (PPSU) 6
Use of Rheological Characterization in AM 6
Existing Challenges and Research Objectives 7
Specific Research Objectives 8
Chapter Two Predicting the extrudability of additive manufacturing feedstock using a pressure-driven flow model 9
Introduction 9
Overall Objective 11
Primary Research Questions 11
Approach for Predicting Material Extrudability on AM Systems 12
Modeling Pressure-Driven Extrusion in DW 12
Modeling Pressure-Driven Extrusion in FFF and BAAM 15
Pass/fail criteria for pressure-driven flow during extrusion 16
Experimental Methods 16
Materials 16
Rheological Characterization 18
Epoxy/Nano-Clay Ink Formulations 18
PLA and ABS Samples 19
CF-Reinforced PPS Grades 19
Material Extrusion 20
DW 20
FFF 20
BAAM 21
Results and Discussion 21
Rheological Characterization 21
Frequency Sweep 23
Extrudability Trials 23
Effect of Viscosity Modifiers 27
Effect of Temperature 29
Effect of Carbon Fiber Loadings 36
Summary and Conclusions 39
Chapter Three Investigating the effects of transient start-up pressure during the start/stop process of large area additive manufacturing systems 40
Introduction 40
Overall Objective 42

Primary Research Questions 42
Numerical Modeling 42
Experimental Methods 43
Materials and Material Properties 43
Capillary Rheometry Characteristic Decay Time Measurements 43
BAAM Extrusion 45
Results and Discussion 48
BAAM Extrusion: ABS 20 wt.% CF 48
BAAM Extrusion: PPSU 25 wt.% CF 48
Relationship Between Transient Start-up and Steady-State Pressures 69
Stress Relaxation 69
Characteristic Decay Time 72
Capillary Rheometer 72
BAAM 74
Influence of Characteristic Decay Time on BAAM Processing Conditions 78
Summary and Conclusions 79
Chapter Four Determination of melt processing conditions for high-performance amorphous thermoplastics for big area additive manufacturing 80
Introduction 80
Approach 81
Overall Objective 83
Primary Research Questions 83
Experimental Methods 83
Materials 83
Thermal Analysis 85
Dynamic Rheological Characterization 85
Results and Discussion 87
Thermal Analysis 87
Dynamic Rheological Characterization 87
Strain Sweep 87
Storage modulus, loss modulus, and tan $\boldsymbol{\delta}$ 92
Complex Viscosity 101
Summary and Conclusions 108
Chapter Five Conclusions and future outlook 109
Summary of Research Work 109
Predicting Material Extrudability 109
Research Questions 109
Overall Conclusions 109
BAAM System Pressure Monitoring in the Nozzle 110
Research Questions 110
Overall Conclusions 110
Determining Melt Processing Conditions 111
Research Questions 111
Overall Conclusions 111

Practical Printing Application 111
List of Publications 112
List of References 114
Appendix 125
BAAM as a Rheometer 126
Determining Power Law Variables from BAAM Data 126
Power Law Variables from BAAM Data for ABS 20 wt.% CF 128
Power Law Variables from BAAM Data for PPSU 25 wt.% CF 129
Calculated Viscosities as a Function of Shear Rate for ABS 20 wt.% CF and PPSU 25 wt.% CF 132
Mesh Sensitivity Study 132
Influence of Exit Geometry and Entry Angle on Simulated Pressure Predictions 132
Vita 141

LIST OF TABLES

Table 2.1. Typical printing parameters for DW, FFF, and BAAM. 14
Table 2.2. Composition of DW epoxy/nano-clay ink formulations 17
Table 2.3. Experimentally calculated power-law n and C values for ABS 24
Table 2.4. Experimentally calculated power-law n and C values for PLA 25
Table 2.5. Experimentally calculated power-law n and C values for CF-reinforced PPS 26
Table 2.6. Pressure drop predictions as well as experimental pressure values for epoxy/nano-clay ink formulations on DW system 28
Table 2.7. Elastic modulus, tensile strength, and calculated pressures of ABS and PLA used to assess the pressure-driven model 30
Table 2.8. Model predicted extrusion pressure values at various temperatures and print speeds along with Pass/Fail print criteria for ABS on the FFF system, P_{max} = 2.65 MPa 31
Table 2.9. Model predicted extrusion pressure values at various temperatures and print speeds along with Pass/Fail print criteria for PLA on the FFF system, P_{max} = 3.02 MPa 33
Table 2.10. Q values and Hagen-Poiseuille pressure drop predictions for CF-PPS at various screw speeds and an extrusion temperature of 370 °C 38
Table 3.1. Thermal and rheological parameters of ABS 20 wt.% CF and PPSU 25 wt.% CF used in the COMSOL simulation 44
Table 3.2. Average mass flow rate of deposited ABS 20 wt.% CF and PPSU 25 wt.% CF beads 44
Table 3.3. Parallel-plate rheological parameters of ABS 20 wt.% CF and PPSU 25 wt.% CF used in the COMSOL simulation 62
Table 4.1. Effect of temperature, carbon fiber loading, and frequency on the complex viscosity of ABS, PEI, and PPSU 106
Table A.1. BAAM process parameters for ABS 20 wt.% CF 128
Table A.2. BAAM nozzle dimensions for ABS 20 wt.% CF 128
Table A.3. BAAM shear rates for ABS 20 wt.% CF 128
Table A.4. Numerically solved Power-Law exponent, n for ABS 20 wt.% CF 129
Table A.5 Guess n values for ABS 20 wt.% CF 129
Table A.6. BAAM process parameters for PPSU 25 wt.% CF 129
Table A.7. BAAM nozzle dimensions for PPSU 25 wt.% CF 130
Table A.8. BAAM shear rates for PPSU 25 wt.% CF 130
Table A.9. Numerically solved Power-Law exponent, n for PPSU 25 wt.% CF 130
Table A.10 Guess n values for PPSU 25 wt.% CF 131

LIST OF FIGURES

Figure 1.1. Chemical structure of the ABS terpolymer 5
Figure 1.2. Chemical structure of PEI 5
Figure 1.3. Chemical structure of PPSU 6
Figure 2.1. Schematic illustration of typical extrusion orifices used in (a) DW and (b) FFF and BAAM showing deposition parameters for these systems 13
Figure 2.2. Log-log plots of G' and G" as a function of oscillatory shear stress for epoxy/nano-clay ink formulations along with experimentally determined τy values 22
Figure 2.3. Complex viscosity plots of ABS as a function of angular frequency at various extrusion temperatures in air 24
Figure 2.4. Complex viscosity plots of PLA as a function of angular frequency at various extrusion temperatures in air 25
Figure 2.5.Complex viscosity plots of CF-reinforced PPS at 370 °C in nitrogen as a function of angular frequency 26
Figure 2.6. Volume flow rate (Q) values of ABS as a function of print speed and extrusion temperature on the Lulzbot TAZ6 FFF printer 34
Figure 2.7. Volume flow rate (Q) values of PLA as a function of print speed and extrusion temperature on the Lulzbot TAZ6 FFF printer 35
Figure 3.1. Custom designed BAAM nozzle with port for pressure transducer ... 46
Figure 3.2. BAAM extruder end cap fitted with a custom designed 0.762 cm nozzle and pressure transducers 47
Figure 3.3. Measured volumetric flow rate vs screw speed for ABS 20 wt.% CF 49
Figure 3.4. BAAM transient and steady-state pressure in the nozzle during ABS 20 wt.% CF extrusion at different screw speeds using the 1.016 cm nozzle 50
Figure 3.5. Measured volumetric flow rate vs screw speed for PPSU 25 wt.% CF 53
Figure 3.6. BAAM build sheet showing three kinds of flow instabilities (a) irregular bead width, (b) lack of material, and (c) surface roughness on PPSU 25 wt.% CF deposited beads using a 1.016 cm diameter nozzle at all screw speeds 54
Figure 3.7. BAAM transient and steady-state pressure in the nozzle during PPSU 25 wt.% CF extrusion at different screw speeds using the 1.016 cm nozzle 56
Figure 3.8. BAAM steady-state pressures vs volume flow rate (Q) for ABS 20 wt.% CF and PPSU 25 wt.% CF for different nozzle sizes 59
Figure 3.9. Complex viscosity vs angular frequency for neat and ABS 20 wt.% CF at 250 ºC in air 60
Figure 3.10. Complex viscosity vs angular frequency for neat and PPSU 25 wt.% CF at 376 ºC in nitrogen 61
Figure 3.11. ABS 20 wt.% CF BAAM steady-state pressures, Hagen-Poiseuille predicted pressure drop, and COMSOL simulated nozzle pressures as a function of volume flow rate (Q) 62

Figure 3.12. PPSU 25 wt.% CF BAAM steady-state pressures, Hagen-Poiseuille predicted pressure drop, and COMSOL simulated nozzle pressures as a function of volume flow rate (Q) 63
Figure 3.13. Theoretical and experimental ΔP for ABS 25 wt.% CF as a function of measured volumetric flow rate (Q) 65
Figure 3.14. Theoretical and experimental ΔP for PPSU 25 wt.% CF as a function of measured volumetric flow rate (Q) 66
Figure 3.15. Transient and steady-state pressures during BAAM extrusion of ABS 20 wt.% CF beads at all screw speeds and different nozzle sizes (Deposition temperature: 250 °C) 67
Figure 3.16. Transient and steady-state pressures during BAAM extrusion of PPSU 25 wt.% CF beads at all screw speeds and different nozzle sizes (Deposition temperature: 355 °C) 68
Figure 3.17. Relaxation modulus of ABS 20 wt.% CF at 230 ºC, strain = 0.06% and PPSU 25 wt.% CF at 340 ºC, strain = 1% 71
Figure 3.18. Transient and steady-state pressure of ABS 20 wt.% CF extrusion at different shear rates and L/D ratios in the capillary rheometer 73
Figure 3.19. Characteristic decay time for ABS 20 wt.% CF on the capillary rheometer as a function of shear rate for varying L/D ratios and die diameter = 0.749 mm (Test temperature = 250 ºC) 75
Figure 3.20. Transient and steady-state pressure profile of ABS 20 wt.% CF at 150 RPM deposited at 250 ºC 76
Figure 3.21. BAAM characteristic decay times for ABS 20 wt.% CF and PPSU 25 wt.% CF as a function of screw speed for nozzle diameters (ABS 20 wt.% CF was deposited at 250 ºC, PPSU 25 wt.% CF was deposited at 355 ºC) 77
Figure 4.1. Determination of the BAAM processing temperature window using DSC and TGA thermograms. DOT is the decomposition onset temperature. 82
Figure 4.2. Neat and CF-reinforced ABS, PEI, and PPSU used for thermal and rheological characterization 84
Figure 4.3. TA Instruments' DHR-2 fitted with 25-mm disposable parallel-plate fixture used for SAOS measurements 86
Figure 4.4. DSC Thermograms for ABS, PEI, and PPSU as well as their CF reinforced composites 88
Figure 4.5. TGA Thermograms for ABS, PEI, and PPSU as well as their CF reinforced composites 90
Figure 4.6. Strain sweeps for ABS, PEI, and P as well as their CF reinforced composites 94
Figure 4.7. G', G", and tan δ vs angular frequency at various temperatures for neat and CF reinforced ABS in air 96
Figure 4.8. G', G", and tan δ vs angular frequency at various temperatures for neat and CF reinforced PEI in air 97
Figure 4.9. G', G", and tan δ vs angular frequency at various temperatures for neat and CF reinforced PPSU in nitrogen 99

Figure 4.10. Complex viscosity vs angular frequency at various temperatures for neat and CF reinforced ABS in air 102
Figure 4.11. Complex viscosity vs angular frequency at various temperatures for neat and CF reinforced PEI in air 103
Figure 4.12. Complex viscosity vs angular frequency at various temperatures for neat and CF reinforced PPSU in nitrogen 104
Figure 4.13. Complex viscosity and shear viscosity curves of neat (unfilled symbols) and carbon fiber reinforced (filled symbols) ABS at 230 C° 105
Figure A.1. Viscosity vs shear rate calculated from BAAM steady-state pressure values for ABS 20 wt.% CF and PPSU 25 wt.% CF 133
Figure A.2. Mesh independence study for the 0.508 cm and 1.016 cm nozzle 134
Figure A.3. Exterior image of mesh on the 1.016 cm nozzle 135
Figure A.4. COMSOL nozzle geometries: 0.508 cm nozzle diameter 136
Figure A.5. COMSOL nozzle geometries: 0.762 cm nozzle diameter 137
Figure A.6. COMSOL pressure drop predictions for ABS 20 wt.% CF using BAAM nozzles with varying exit lengths and entry angles 139
Figure A.7. COMSOL pressure drop predictions for PPSU 25 wt.% CF using BAAM nozzles with varying exit lengths and entry angles 140

CHAPTER ONE
INTRODUCTION

Motivation

Additive manufacturing (AM) has revolutionized the manufacturing industry through rapid and complex geometry fabrication capabilities at a fraction of the cost. For instance, the cost and lead-time of composite tooling are a major hindrance to the application of composite materials. By switching from traditional tooling methods to AM, the cost of tooling is estimated to reduce by 10 - 100 times and reduce the amount of time from concept to tool by an order of magnitude [1]. These savings extend well beyond the manufacturing sector and are trickled down into other sectors of the economy.

Despite the recent progress in material development for extrusion-based AM, only a small fraction of the materials used for traditional manufacturing are compatible with AM [2,3]. Emerging applications in polymer AM motivate the need for production and development of new materials with a broader range of thermal and mechanical properties. Advancements in AM have also led to new system development such as Big Area Additive Manufacturing (BAAM) systems, capable of processing high-performance thermoplastics and composites. BAAM was developed by Cincinnati Inc in conjunction with the Manufacturing Demonstration Facility at Oak Ridge National.

As the application space for three-dimensional (3D) printed components continues to grow, it is necessary to identify appropriate processing conditions and expand the current selection of high-performance thermoplastics and fiber reinforced composites for AM systems. However, there is no formal process for designing, screening, and evaluating the printability of these high-performance thermoplastics and composite systems. Traditional polymer characterization techniques utilizing thermal and rheological material properties have been effectively employed in other polymer processing methods such as injection molding to identify suitable processing conditions. Therefore, to expand the current high-performance material selection for BAAM using industrial grade pellets, these techniques are employed to establish the relationships between fundamental material properties such as thermal and rheological properties and AM processing parameters.

This work is an attempt to expand the current selection of high-performance feedstock on large format AM systems such as BAAM using thermal and rheological characterization techniques. This is achieved by predicting their

extrudability through the nozzle and identifying appropriate processing conditions for these materials to provide a basis for optimizing the use of current high-performance materials as AM feedstock.

Extrusion-Based Additive Manufacturing Systems

AM commonly referred to as 3D printing, offers the ability to directly fabricate parts with complex geometry from a 3D Computer-Aided Design (CAD) system. To use extrusion-based AM systems, first a 3D solid model is created on any of the several commercially available CAD packages such as Solidworks. The model is then exported to a slicing software using the stereolithography (STL) format, which breaks down the part into triangles. The STL file is then sliced into many horizontally thin sections which represent two-dimensional contours that the AM process then generates and when stacked on top of one another, result in a part that resembles the three-dimensional part [4,5]. AM techniques have evolved over time and can process materials such as polymers, metals, and ceramics [4,6–9].

Fused filament fabrication (FFF) is the most common extrusion-based AM technique used to make cheap prototypes mostly out of Acrylonitrile Butadiene Styrene (ABS) plastics and other amorphous thermoplastics [10]. The physical process of FFF involves a thermoplastic filament such as ABS being fed into a heating element where it then becomes semi-molten. The melt is pushed through the print nozzle by the filament entering the heating element onto the print surface. The newly deposited material is able to fuse with the material deposited before because the extrusion is in a semi-molten state and it has been shown that bonding between the layers by the roads is thermally driven [4,11–13]. The print head moves in the X-Y plane depositing material based on the geometry of the part while the platform that holds the part moves vertically in the Z plane to start depositing a new layer on top of the previous layer. The quality and strength of FFF parts depends greatly on the various process parameters selected for part fabrication. These process parameters include bead width, air gap, build temperature, and raster orientation [5]. FFF uses a variety of unreinforced thermoplastics [4,12,13]. Those commonly used on the FFF system are available in filament form from several vendors and these include ABS, polycarbonate (PC), poly(lactic)acid (PLA), polyetherimide (PEI) and blends such as PC/ABS and PEI/PC.

There are extrusion-based systems that do not rely on a filament to generate the extrusion pressure such as direct write (DW) and large format AM systems such as BAAM [14–18]. In DW, viscoelastic ink formulations are deposited via extrusion through micro to sub-millimeter nozzles at room temperature without the need to melt the material prior to, or cure immediately following deposition [17,19,20]. DW ink formulations must possess sufficient yield stress and shear

thinning behavior so that they can be extruded through fine nozzles under ambient conditions. In addition, after exiting the nozzle, these viscoelastic inks must possess a high elastic modulus to maintain their shape after deposition [17,19,21,22].

BAAM on the other hand, is a large scale polymer extrusion AM technique that uses a single screw extruder to melt pelletized feedstock developed in conjuction with Cincinnati Inc at the Manufacturing Demonstration Facility at Oak Ridge National Laboratory. The single screw extruder increases the deposition rate up to 50 kg per hour, which is 200 times faster than conventional AM systems [14]. Using a pellet-based feedstock allows BAAM to leverage lower cost and standard materials that are used in high volume production (e.g. injection molding, extrusion, etc.). In addition, BAAM is capable of depositing materials that contain significant amounts of fillers such as glass and carbon fiber reinforcements to make high-performance composite structures such as demonstration vehicles, molds, dies, and autoclave tools used to fabricate Tier 1 composite structural components with very low void content (i.e. <5%) [1,23]. Compared to the neat resin, fiber reinforced polymers increase the strength of the part by a factor of 4 to 7 times and reduces the coefficient of thermal expansion (CTE) by an order of magnitude [24–26]. In addition, the build volume of the BAAM system can accommodate parts that are 6 m long, 2.4 m wide and 1.8 m high over a wide range of temperatures up to 510 °C [27]. Reducing the CTE with the use of fiber reinforced polymers minimizes the shrinkage as the part cools from the deposition temperatures to ambient temperatures and results in significantly reduced part distortion [24]. However, the presence of fibers in the polymer matrix presents a processing challenge due to fiber orientation during flow and modified rheology of the polymer system.

High-Performance Amorphous Thermoplastics in AM

The polymer AM market is growing and for the transition from prototyping to production of end use parts on AM systems to be realized, the ability to manufacture parts with desired thermomechanical properties needs to be fulfilled. As a result, high-performance thermoplastics as well as their fiber reinforced composites are of interest as feedstock for the BAAM extruder at the Manufacturing Demonstration Facility, Oak Ridge National Laboratory due to their superior thermal and mechanical properties [1,28–31].

High-performance thermoplastics are characterized by distinguishing features such as high strength and stiffness, resistance to many chemicals, and outstanding electrical properties [32]. They are also considered to have a short-term heat resistance of 250 °C and can withstand long-term heat resistance of 160 °C. Some of these high-performance polymers include polyethersulfone (PES), polyphenylene sulfide (PPS), polyphenylsulfone (PPSU),

polyetherketoneketone (PEKK), and polyetherimide (PEI). Compared to commodity plastics, the base resins for these high-performance thermoplastics tend to be more expensive.

High-performance plastics can also be classified as either semi-crystalline or amorphous polymers. Semi-crystalline polymers have highly ordered molecular structures attributed to formation of solid crystals having a definite geometric form. Semi-crystalline thermoplastics are noted for very good electrical properties, ability to withstand both high heat and severe chemical environments. PPS and PEKK are examples of high-performance semi-crystalline polymers. Amorphous polymers on the other hand, are devoid of crystallinity and are made up of random entanglements of polymer chains. They are known for very good mechanical properties (strength and stiffness) and dimensional performance. ABS, PPSU, PEI, and PES are examples of amorphous polymers. The polymer systems investigated in this work are neat and carbon fiber reinforced ABS, PEI, and PPSU.

Acrylonitrile Butadiene Styrene (ABS)

ABS is the most commonly used thermoplastic in extrusion-based polymer AM systems such as FFF and BAAM because of its excellent processability and dimensional stability [25,26,33]. However, it has a relatively low glass transition temperature (T_g) of 105 °C which restricts its use in advanced applications that demand continuous use of printed components at elevated temperatures. ABS is a terpolymer synthesized from three monomers: acrylonitrile, butadiene and styrene (Figure 1.1). Each of the three monomers of ABS is important because acrylonitrile contributes chemical resistance, heat resistance and high strength; butadiene is responsible for the toughness, impact strength and low-temperature property retention; while styrene contributes rigidity, surface appearance and processability. The ratios of the monomers may vary and the manner in which they are arranged to form the final polymer also tends to vary making the range of ABS-type polymers quite large [34].

Polyetherimide (PEI)

PEI, commonly known as ULTEM™, holds great potential for high-temperature AM applications [35]. It is mainly used to manufacture end-use products such as high performance electronic parts and under-the-hood automotive parts due to its enhanced rigidity at high temperatures [36]. PEI's chemical structure consists of repeating aromatic imide units connected by relatively flexible aromatic ether units (Figure 1.2). This allows PEI to have a high glass transition temperature of 217 ºC [37], good melt flow characteristics, and sufficient high-temperature stiffness [38]. Several researchers have used PEI in FFF applications to manufacture components at deposition temperatures ranging between 330 ºC – 380 ºC [16, 25–31].

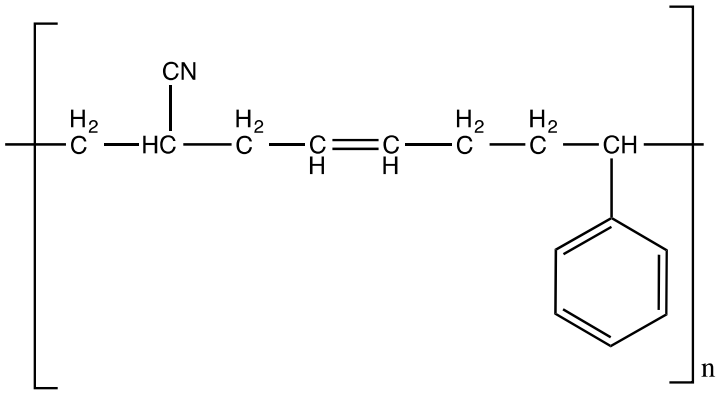


Figure 1.1. Chemical structure of the ABS terpolymer

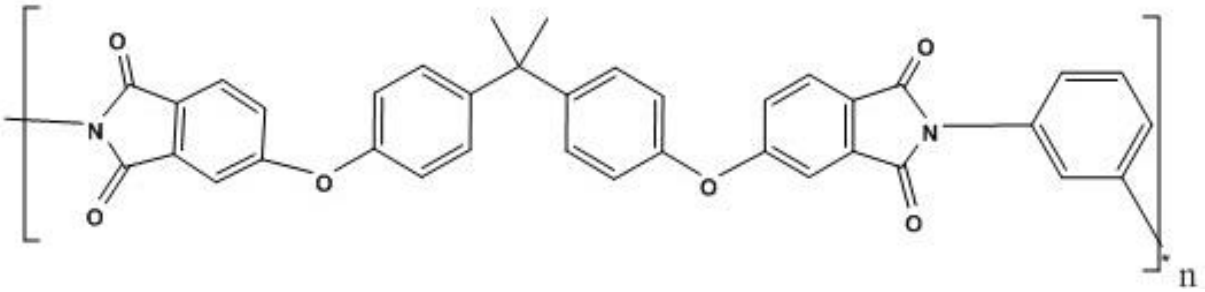


Figure 1.2. Chemical structure of PEI

Polyphenylsulfone (PPSU)

PPSU is the highest performance amorphous thermoplastic, made by nucleophilic aromatic substitution between difluorodiphenyl sulfone and the sodium salt of 4,4-dyhydroxybyphenyl with elimination of sodium fluoride (Figure 1.3) [32]. The biphenylene ether unit of PPSU markedly increases the impact strength and contributes to ease of melt fabrication. PPSU is known for high stiffness, good chemical resistance, flame resistance, and high T_g of 220 °C. The high continuous use temperature of 205 °C allows applications in high heat environments [32].

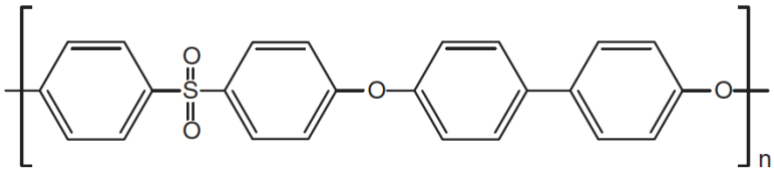


Figure 1.3. Chemical structure of PPSU

Use of Rheological Characterization in AM

When evaluating potential AM feedstock, understanding the melt dynamics is crucial for identifying inherent material properties that are necessary for potential AM feedstock [39]. Rheological characterization of polymers can provide screening methodologies that prevent a costly trial-and-error approach to evaluating potential feedstock materials [40].

Rheological studies help to understand the dynamics associated with the AM process for polymeric materials in areas such as pressure driven flow through the nozzle during extrusion, formation of a free-standing bead of adequate height on the deposition bed, and ability of the bead to support subsequent layers deposited during printing, and obtaining a quality bead with minimal void fraction [28,31,41–43]. Since most of the thermoplastic AM process occurs in the melt state, entanglement dynamics and microstructure can have significant influence on the printability of the feedstock material. Stress relaxation tests are commonly employed to observe the timescales at which polymer chains relax through short-range and long-range thermal motions [44]. When entanglements hinder chain relaxation, a stress plateau or rubbery regime is observed, for which the plateau modulus is defined. The magnitude of this plateau modulus is related to the

molecular weight of polymer segments between entanglements; a property unique to the structure of the polymer chain [45]. Beyond the plateau regime, with sufficient time, terminal relaxation results in a total stress reduction. For neat resins, an increase in molecular weight prolongs the stress relaxation to longer time scales. Since time and temperature are proportional, the terminal region may be entered with higher processing temperatures [46]. The added complexity of filler reinforcement can lead to networks which must first be destroyed to sufficiently reduce the stress. However, the buildup of a filler network after flow cessation is much quicker than the buildup of entanglement networks [47]. By controlling temperature, molecular weight, and filler concentration, a polymer can exhibit significant shear thinning behavior from filler network breakdown to allow extrusion through the nozzle, high zero-shear viscosity within extruder torque limits, and fast filler network buildup to maintain the shape of the deposited bead.

Existing Challenges and Research Objectives

As the application space for 3D printed parts continues to grow, there is a need to expand the current AM material selection. However, only a fraction of the materials used for traditional manufacturing are compatible with AM despite recent advancements in AM [3]. The current limited material selection is a motivation for production and development of new AM materials with broader thermal and mechanical properties for various applications. The challenge with this is that there is no formal process for designing, screening and evaluating the printability of polymers as feedstock for extrusion-based AM.
Advancements in AM system development have also led to production and utilization of extrusion-based systems such as BAAM that do not require a filament and are capable of processing high-performance thermoplastics and fiber reinforced composites. The BAAM system is capable of processing thermoplastics up to 510 °C and the challenge lies in identifying the range of temperatures at which high-performance polymer systems can be extruded at high temperatures without degrading and compromising structural integrity.

This dissertation proposes extrudability guidelines and processing conditions of high-performance amorphous thermoplastics and composites in attempt to expand the current selection and applications of high-performance feedstock for large scale extrusion-based AM systems. The major challenges in expanding feedstock selection on AM systems and opportunities for valuable fundamental input lie in;

1. Predicting successful extrudability of viscoelastic ink formulations and polymer melts using a pressure-driven flow model.

2. Characterizing and quantifying the occurrence of pressure transients during extrusion using custom-design extrusion BAAM nozzles fitted with a pressure sensor.
3. Determining the appropriate processing conditions of high-performance amorphous thermoplastics and carbon fiber composites on BAAM using thermal and rheological measurements.

Specific Research Objectives

With the main objective being to expand the current material selection for AM feedstock by predicting material extrudability, measuring in-situ nozzle pressures, and developing processing conditions, this work focuses on the following research questions for the challenges discussed:

i. Predicting extrudability: Can a simple pressure-driven flow model be used to predict extrudability on various extrusion-based AM platforms? Can you relate experimental laboratory based measurements to real life AM processes? This work is discussed in Chapter Two.
ii. BAAM system pressure monitoring in the nozzle: How do the transient start-up pressures in the nozzle relate to steady-state pressures and influence extrudability? How do pressure predictions from analytical models and numerical simulations compare to experimentally measured nozzle pressures? This work is discussed in Chapter Three.
iii. Melt processing conditions: Can thermal and rheological properties be used to identify suitable processing windows for amorphous thermoplastics on BAAM? How are key BAAM processing parameters such as screw speed and deposition temperature influenced by a material's melt flow behavior? This work is discussed in Chapter Four.

CHAPTER TWO

PREDICTING THE EXTRUDABILITY OF ADDITIVE MANUFACTURING FEEDSTOCK USING A PRESSURE-DRIVEN FLOW MODEL

Introduction

Historically, AM has proven useful for making models and prototypes but the number applications is increasing. In addition, the processes are developing and improving to use specialized and high-performance thermoplastics. Developing new materials and expanding the current selection of materials for AM systems requires screening across all areas of the printing process, from material selection to final part properties. A few research efforts have focused on creating a formal process for designing, screening, and evaluating the printability of polymers as feedstock materials across various extrusion-based AM platforms, including DW, FFF, and BAAM.

However, the majority of efforts to establish material extrusion criteria and rapid screening processes have focused largely on FFF [48–50]. In the FFF process, the thermoplastic filament acts as both the piston driving the extrusion process and as the material being deposited [4]. The filament is fed through motorized wheels into a heated extrusion head where it is melted [49]. The pressure drop in the liquefier influences the force required to push the filament [49,50]. The primary failure modes tend to be filament buckling, inconsistent filament diameter and annular backflow [8,48,50]. In the FFF process, a filament fails due to buckling, when the pressure applied by the rollers exceeds the material's critical buckling load. Venkataraman et al. found that feedstock materials whose ratio of the elastic modulus to apparent viscosity was greater than a critical value of (3 x 20^5 to 5 x 10^5 s^{-1}) tend not to buckle while those whose ratio is less than this range will buckle during extrusion [3]. Gilmer et al. built upon this by applying the filament buckling analysis and incorporating flow and geometry considerations to predict a material's propensity to backflow using a dimensionless Flow Identification Number [48]. A sensitivity analysis of their model indicated that propensity to fail during extrusion is mostly due to fluctuations in filament diameter and the degree of shear-thinning. Other approaches aimed at expanding the applicability of FFF have focused on designing material extrusion based feedstocks with targeted physical properties [51–54].

Ramanathan et el. were the first to develop a general model for analyzing and simulating the flow behavior of materials in FFF [55]. They modeled the melt flow behavior of poly-ε-caprolactone (PCL) in the FFF flow channel using mathematical modeling and finite element analysis (FEA). They studied the melt flow behavior with the use of an accurate channel geometry and by varying filament velocity at the entry, nozzle diameter and entry angle at the exit. They observed that the flow behavior of PCL melt in the channel was influenced by pressure gradient, velocity profile, temperature, and physical properties such as the melt temperature and rheology. The results of their mathematical modeling and FEA suggested that the pressure drop is higher when nozzle diameter is smaller, and less pressure drop is observed when the nozzle diameter is larger [55]. Several other researchers have since explored the deformation and melt flow behavior of thermoplastic melts in FFF nozzles [56,57].

There has been some progress made towards modeling and quantifying the pressure in the nozzle of an FFF printer during extrusion [58–62]. For instance, Phan and Mackay determined pressure by monitoring the power needed to drive the counter-rotating gears which grip the fiber and force it through the nozzle [60]. The measured pressure drop data during printing was then used to determine the extrudate temperature to ascertain heat transfer coefficients. Coogan and Kazmer directly measured the melt pressure by incorporating an in-line rheometer into the FFF printer [59]. They validated the accuracy of the pressure measurements acquired by the on-line rheometer using offline rheological measurement techniques such as rotational and capillary rheometers.

Advancements in AM systems development have led to utility of extrusion-based AM systems such as DW and BAAM that do not need filaments. In DW, viscoelastic ink formulations are extruded using a syringe at room temperature, without the need to melt the material prior to, or cure following deposition [17,21,63]. To design successful DW ink formulations, they must possess sufficient yield stress and shear thinning behavior that they can be extruded through fine nozzles under ambient conditions. In addition, after exiting the nozzle, these viscoelastic inks must possess a high elastic modulus to maintain their shape after deposition [17,21,63]. BAAM on the other hand, is a large scale polymer extrusion AM technique that uses a single screw extruder and is capable of depositing high performance thermoplastics and highly filled composites at temperatures as high as 510 °C [18]. The BAAM extruder at the Manufacturing Demonstration Facility was developed by Oak Ridge National Laboratory, in conjunction with Cincinnati Inc.

To advance rapid material screening across various extrusion-based AM platforms, Duty *et. al* recently published a practical model for evaluating the printability of polymer feedstock for three AM platforms namely DW, FFF, and BAAM [41,64]. The proposed model uses viscoelastic properties of materials in

a four- part framework to assess 3D printability. For a successful print, the first criterion requires pressure-driven flow of the polymer through the nozzle. Second, the deposited material must form a stable bead with the right geometry. Third, the deposited bead must be able to support the weight of other subsequent layers and bridge a free spanning gap. Finally, the AM printed structure needs to be dimensionally stable during the transition to the final part through cooling to ambient temperature.

In this chapter, the extrudability of high-strength epoxy nano-composites and shear-thinning polymer melts is evaluated on AM systems using a pressure-driven flow model. The AM systems investigated include DW, FFF, and BAAM. The extrusion criterion is modeled by calculating the pressure drop (ΔP) across the nozzle that is required to extrude the material and comparing it against the system maximum pressure. In DW, the extrusion of epoxy nanocomposites is calculated using the Benbow-Bridgewater equation for the flow of pastes since these materials behave as Bingham fluids [65]. In FFF and BAAM, the Hagen-Poiseuille (HP) equation is used to calculate the required ΔP for extrusion because the feedstock behave as power-law fluids at the shear rates of interest [50]. The proposed approach for predicting successful extrusion is demonstrated with candidate materials such as epoxy/nano-clay ink formulations, acrylonitrile butadiene styrene (ABS), poly(lactic)acid (PLA), and carbon fiber (CF) reinforced polyphenylene sulfide (PPS). The key variables investigated include (1) the role of viscosity modifiers on ink formulations used in DW, (2) the effect of varying extrusion temperature on FFF systems, and (3) the effect of high CF loadings on material extrusion in BAAM. Extrusion trials of the candidate materials on the AM platforms validate model predictions.

Overall Objective

Develop a simple material screening methodology to evaluate the extrudability of potential AM feedstocks to allow for a more rapid introduction of new materials to AM.

Primary Research Questions

i. Can a simple pressure-driven flow model be used to predict extrudability on various extrusion-based AM platforms?
ii. Can you relate experimental laboratory based measurements to real life AM processes?

Approach for Predicting Material Extrudability on AM Systems

The two models used to predict material extrudability; Benbow-Bridgewater equation for DW systems and HP equation for FFF and BAAM are described in detail in the following sections. Figure 2.1 illustrates the common extrusion orifice geometries encountered in DW, FFF, and BAAM. The basic printing parameters for each system are outlined in Table 2.1.

Modeling Pressure-Driven Extrusion in DW

High-strength epoxy nano-composites used in DW behave like Bingham fluids in that they do not flow until a certain level of stress is achieved within the nozzle that exceeds the shear yield stress. Above this yield stress, motion occurs and the material flows [65,66]. The pressure drop for DW extrusion of a viscoelastic ink can be calculated using the Benbow-Bridgewater equation for paste extrusion [67]. Benbow and Bridgewater's paste flow model has two parts: flow from the barrel into the die land (ΔP_1) and flow in the die land (ΔP_2). The die land is the region marked L in Fig. 2.1(a) of the DW system corresponding to the exit length.

The motion of the epoxy nano-composite from the syringe barrel into the die entry region in Fig. 2.1(a) is given by;

$$\Delta P_1 = 2\sigma_y ln\left(\frac{D_o}{D}\right) \tag{2.1}$$

where σ_y is the uniaxial yield stress, D_o is the barrel diameter, and D is the die land diameter. It is assumed that the barrel and the die land both have circular cross-sections. This expression is applied to dies with abrupt contractions and to dies with conical or tapered entries when wall friction is not thought to be significant. In the die land, the paste is assumed to flow as a rigid plug that is surrounded by a thin layer of lubricating liquid separating it from the wall, and thus is described by;

$$\Delta P_2 = 4\tau_y(L/D) \tag{2.2}$$

where τ_y is the shear yield stress and is expected to be about half the uniaxial yield stress, σ_y using Tresca's yield criterion which predicts that τ_y is equal to $\sigma_y/2$ [67]. The Tresca yield criterion states that yield will occur when the maximum shear stress on any plane reaches a critical value. The von Mises criterion on the other hand, states that yield will occur when the elastic shear strain energy density reaches a critical value and is equal to $\sigma_y/\sqrt{3}$ [68]. The Tresca yield criterion is used because it is more conservative than the von Mises criterion and it predicts a narrower elastic region, which can be safer from the

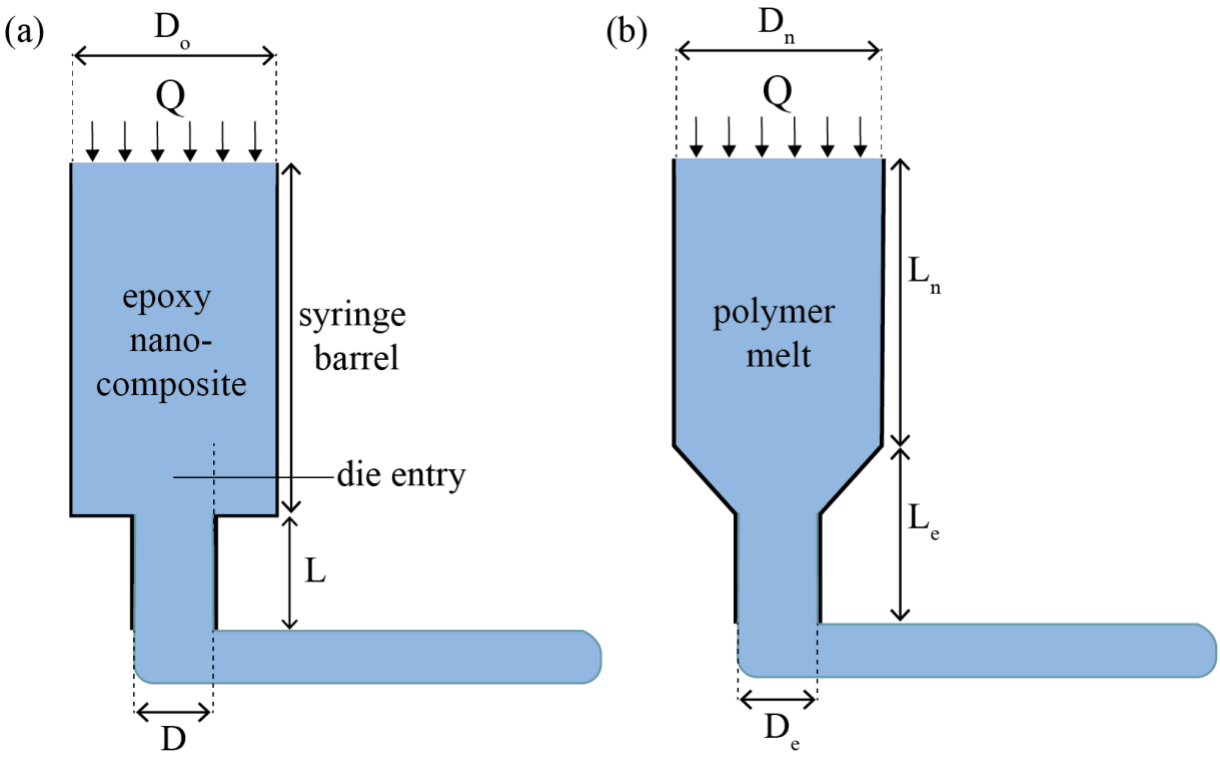


Figure 2.1. Schematic illustration of typical extrusion orifices used in (a) DW and (b) FFF and BAAM showing deposition parameters for these systems

Table 2.1. Typical printing parameters for DW, FFF, and BAAM.

Print Parameters	**DW**	**FFF**	**BAAM**	**units**
Nozzle diameter (D_n)/D_o	0.977	0.32	1.02	cm
Nozzle length (L_n)	-	1.05	6.40	cm
Exit diameter (D_e)/D	4.2 x 10^{-3}	0.05	0.76	cm
Exit length (L_e)/L	3.00	0.15	0.86	cm
Bead height	0.02	0.03	0.38	cm
Bead width	0.04	0.62	0.84	cm
Mass flow rate	2.78 x 10^{-3}	0.002	5.40*	g/s
Maximum pressure (P_{max})	4.34	3.02+	6.89	MPa
Volume flow rate (Q)	2.26 x 10^{-3}	0.0063*	7.34*	cc/s

*Material and temperature dependent

+Material dependent, values used are for PLA

design point of view [68]. The overall pressure drop in the DW system, is thus given by;

$$\Delta P_{DW} = \Delta P_1 + \Delta P_2 = 2\sigma_y \ln\left(\frac{D_o}{D}\right) + 4\tau_y(L/D) \tag{2.3}$$

Modeling Pressure-Driven Extrusion in FFF and BAAM

The HP equation (Eq. 2.4) is used to calculate the pressure drop required to drive a polymer melt in FFF and BAAM systems, and is given by [41];

$$\Delta P = \frac{8\,\eta\,Q\,L}{\pi R^4} \tag{2.4}$$

where Q is the volumetric flow rate, η is the viscosity of the polymer melt at extrusion temperature, L is the length of the nozzle, and R is the radius of the nozzle. Equation 2.4 may be modified to calculate the required pressure to achieve the desired volume flow rate to drive a non-Newtonian polymer melt through the nozzle during extrusion. The standard HP equation assumes that a liquid is incompressible and Newtonian while flow is steady, fully developed, isothermal, and laminar. Other assumptions include: no slip occurs between the wall and the melt, shear rate is zero at the center and maximum at the wall, and the velocity is maximum at the center of the tube and zero at the wall.

To adapt the HP equation to predict extrudability of non-Newtonian, shear thinning polymer melts typically used in FFF and BAAM, the viscosity of the polymer melt as a function of shear rate is modeled as a power-law fluid using Eq. 5 [39]. The power-law model is used in this study for simplicity and it sufficiently describes the AM feedstocks across the range of shear-rates of interest [39]. The power-law states:

$$\eta = C\dot{\gamma}^{n-1} \tag{2.5}$$

where n is the power-law index, C is the consistency index, η is the viscosity and $\dot{\gamma}$ is the shear rate. The power-law index, n, is a measure of the shear-thinning behavior and typically varies between zero and one for thermoplastics. During extrusion, the apparent shear rate $(\dot{\gamma}_a)$ at the wall (assuming no slip) can be determined from the flow rate by:

$$\dot{\gamma}_a = \frac{4\,Q}{\pi R^3} \tag{2.6}$$

However, $\dot{\gamma}_a$ corresponds to Newtonian behavior with fluids that exhibit constant viscosity. For shear-thinning fluids like polymer melts, the Rabinowitsch

correction is applied to account for a non-parabolic velocity profile, and the true shear rate ($\dot{\gamma}$) for the power-law model now becomes;

$$\dot{\gamma} = \frac{4Q}{\pi R^3}\left(\frac{3n+1}{4n}\right) \tag{2.7}$$

Pass/fail criteria for pressure-driven flow during extrusion

Equations 2.1 and 2.4 are used to calculate the pressure drop required to achieve the desired volume flow rate of a non-Newtonian AM feedstock through the extrusion nozzle during deposition. According to the pressure predictions, a given AM feedstock will successfully extrude if the calculated ΔP is less than the maximum AM system pressure (P_{max}) and will "pass" this condition if:

$$\Delta P < P_{max} \tag{2.8}$$

However, if the calculated $\Delta P > P_{max}$, the model predicts that the feedstock will "fail." In such instances, it does not necessarily mean that the system will clog, but that the material will not be extruded at the desired volumetric flow rate [41]. The proposed pressure-driven model in this section, does not account for the role that reinforcing fillers play during extrusion other than their effect on viscosity. A secondary condition introduced in the printability model accounts for the potential of fibers to entangle as they approach the flow restriction of the extrusion nozzle and clog [41].

Experimental Methods

Materials

The epoxy resin used for DW is EPON826 epoxy resin (Momentive Specialty Chemicals, Inc., Columbus, OH) with a density of 1.16 g/cc. 1-Ethyl-3-methylimidazolium dicyanamide (VS03) with a density of 1.20 g/cc was the curing agent used to initiate the chemical reaction required for crosslinking (Basionics VS03, Sigma-Aldrich, Inc., St. Louis, MO). Garamite 7305 nanoclay platelets (BYK-Chemie GmbH, Inc., Wesle, Germany) with a density of 1.60 g/cc were used as the nano-scale filler material. The nano-clay readily disperses in the epoxy and imparts the rheological properties (shear thinning and shear yield stress requirements) needed for DW, enabling the fabrication of stable and fully dense structures with good mechanical properties [17]. The ink formulations were prepared following the matrix in Table 2.2 using a procedure detailed by Hmeidat et. al [64].

Table 2.2. Composition of DW epoxy/nano-clay ink formulations

EPON826 (g)	VSO3 (g)	Nano-clay (wt.%)	Nano-clay (g)	Nano-clay (vol.%)
20	1	10	2.33	7.47
20	1	12.5	3.00	9.40
20	1	15	3.71	11.36
20	1	17	4.45	13.35

For FFF, two commonly used and commercially available thermoplastics (ABS and PLA) are used to demonstrate the effectiveness of the model on the FFF system. Both materials were obtained in filament form from Makerbot Industries. The product and lot numbers for the PLA filament were MP05612 and 72175, respectively while the production-grade ABS filament reel from MakerBot Industries did not have the product or lot number. The filament diameter (d_f) for both materials was 1.75 mm. ABS is an amorphous thermoplastic with a T_g of 105 °C. PLA is a semi-crystalline thermoplastic with a T_g of 60 – 65 C, melting temperature (T_m) of 150 °C. The T_g and T_m values were verified experimentally using differential scanning calorimetry. The densities for ABS and PLA were experimentally determined using an ultrapycnometer to be 1.0196 g/cc and 1.2157 g/cc, respectively. The melt densities for ABS and PLA utilized in this study were 0.97 g/cc and 1.13 g/cc, respectively and were obtained from literature [69,70]. The recommended extrusion temperatures of ABS and PLA on FFF systems from the filament manufacturer is 230 °C and 215 °C, respectively.

To take advantage of BAAM's ability to extrude high loadings of fiber-reinforced thermoplastics, CF-reinforced PPS grades are used to evaluate the effectiveness of the model. Three 3D printing grades of PPS, ELECTRAFIL PPS/F CF HS 3DP, containing 40%, 50%, and 60% by weight of CF were compounded and supplied by Techmer Engineered Solutions in pellet form. The lot numbers for the 40%, 50%, and 60% CF reinforced PPS grades used in this study were TL1511018064, TL1507020701, and TL1511018066, respectively. Thermal analysis of 40 wt.% and 50 wt.% CF PPS grades determined the T_m to be in the range of 280 – 285 °C [42].

Rheological Characterization

The rheological properties of the materials used to assess the pressure-driven extrusion model were determined from measurements on a 25-mm parallel-plate rheometer, Discovery Hybrid Rheometer-2 (DHR-2) from TA instruments (TA Instruments, New Castle, DE). All measurements were conducted in air unless otherwise specified.

Epoxy/Nano-Clay Ink Formulations

Oscillatory stress sweep tests were performed on all four DW epoxy/nano-clay ink formulations at oscillatory stresses ranging from 50 to 5000 Pa with a gap of 0.5 mm and angular frequency of 10 rad/s. Oscillatory stress sweep tests are a form of amplitude sweeps that are useful for describing the viscoelastic behavior of pastes, gels, or polymer melts. During an oscillatory sweep test, the angular frequency is held constant and the amplitude of the deformation signal (oscillatory stress) is varied. The results of the oscillatory stress sweep test are

presented as a log-log plot of the viscoelastic moduli (storage (G') and loss (G") moduli) vs oscillatory stress. From this plot, the limit of the linear viscoelastic (LVE) regime, a region in which the test can be carried out without destroying the structure of the sample is first determined. Oscillatory stress sweeps are also used to determine the yield stress, the value of the shear stress at the limit of the LVE region, at which material flows. The ink formulations were pre-conditioned at a constant shear rate of 0.01 s^{-1} for 120 s followed by an equilibration step for 120 s. The equilibration step is an approximate time in order for any structure to build and/or sample geometry to come to thermal equilibration before data collections begins. Tests were performed at ambient room temperature (~ 23 °C).

PLA and ABS Samples

Small amplitude oscillatory shear (SAOS) measurements of ABS and PLA were conducted using commercial filament material. The filaments were chopped into pellets, dried in a vacuum oven and directly melted onto the 25-mm aluminum disposable plate fixture for testing. PLA was dried at 55 °C and ABS was dried at 85 °C for 4 hours each prior to testing. First, an oscillatory strain sweep test was used to determine the LVE region of these resins. Similar to the oscillatory stress sweep test described above, an oscillatory strain sweep is an amplitude sweep test in which angular frequency is kept constant while the strain amplitude is varied. The results of the oscillatory strain sweep test are presented as a log-log plot of the viscoelastic moduli (G' and G") vs strain amplitude. From this plot, the limit of the LVE regime, a region in which the test can be carried out without destroying the structure of the sample is determined. For ABS and PLA, the strain amplitude was varied from 0.01% to 100%, and angular frequency kept constant at 10 rad/s. Then, frequency sweep measurements to determine the complex viscosities of these thermoplastics at various angular frequencies (628 – 0.1 rad/s) and extrusion temperatures were made. In a frequency sweep test, angular frequency is varied, whereas the strain amplitude is kept constant. The selected strain amplitude used is from the previously performed amplitude sweep tests. The strain amplitude used for the frequency sweeps was 0.5% at 10 rad/s for both ABS and PLA and the gap between the plates was kept at 1.5 mm. Measurements for ABS were made between 190 and 250 °C in increments of 10 °C, while those for PLA were made between temperatures of 155 °C and 220 °C, in increments of 10 °C. A fresh batch of pellets was used for frequency sweep measurements for each temperature.

CF-Reinforced PPS Grades

The process used here for the SAOS measurements is identical to that described for ABS and PLA above. First, an oscillatory strain sweep test was conducted to determine the LVE region followed by a frequency sweep. The applied strain

used for frequency sweep measurements was 0.04%. Increase of CF loading to the neat polymer matrix decreases the LVE region due to a phenomenon known as the Payne effect, and so the chosen strain corresponds to the lower limit obtained from PPS 60 wt.% CF [71]. The pellets were dried in a vacuum oven at 104.4 °C for 8 hours, using the same drying conditions for extrusion on the BAAM extruder located at the Manufacturing Demonstration Facility, Oak Ridge National Laboratory. The rheological measurements for PPS were conducted in nitrogen at 370 °C to mimic the BAAM print conditions and temperature of the melt during deposition. An inert environment through the use of a cover gas minimizes viscosity build-up during extrusion on BAAM [1,28].

Material Extrusion

DW

The epoxy/nano-clay ink formulations were loaded into 3-cc syringe barrels (Nordson EFD, Westlake, OH) using a spatula. The protocol described by Hmeidat et al. is followed to eliminate bubbles and amplify the pressure in the syringe [17]. A 0.0422 cm-diameter straight Luer-lock syringe tip (Mcmaster-Carr, Elmhurst, IL) was used to extrude all ink formulations. Each ink formulation was used to print a bead that is 2 cm long, 0.0422 cm wide and 0.0211 cm high. The pressure required to print a stable bead with comparable width and height was manually controlled by varying the air pressure gauge. Increasing nano-caly content was extruded with a target flow rate of 0.00226 cc/s, and the air pressure was recorded. The stand-off distance between the substrate and nozzle tip and the printing speed were held constant at 0.025 cm and 2.5 cm/s, respectively. The cross-sectional area of the printed beads was measured using a VHX-5000 digital microscope (Keyence Corporation of America, Itasca, IL).

FFF

Extrusion of ABS and PLA was performed on a Lulzbot Taz 6 3D printer (Aleph Objects, Inc., USA) at varying deposition temperatures and print speeds. A 0.05 cm diameter nozzle was used to extrude a free standing bead with a width of 0.062 cm and thickness of 0.03 cm. The dimensions of the extruded bead were measured using a VHX-5000 digital microscope (Keyence Corporation of America, Itasca, IL). Starting at 250 °C for ABS and 220 °C for PLA, the extrusion temperature was lowered by 10 C until it was not possible to extrude molten material through the nozzle at each print speed (0.05 cm/s, 0.08 cm/s, and 0.13 cm/s). To verify the actual volumetric flow rate, Q, mass flow rate tests were conducted as a function of print speed and extrusion temperature. To obtain mass flow rate, material was extruded until steady flow was observed at each given print speed and temperature, the extrudate was cut, and immediately

a timer was started. The extrudate was collected for 150s. The mass of the extrudate was measured and divided by the collection time. The mass flow rate was then divided by the material melt density to obtain Q.

BAAM

Three grades of PPS containing 40%, 50%, and 60% by weight of CF were extruded and deposited on the BAAM extruder at the Manufacturing Demonstration Facility, Oak Ridge National Laboratory using a non-mixing single screw at a nominal temperature of 338 °C. All three PPS grades were dried at 104.4 °C for 8 hours prior to extrusion. The BAAM single screw extruder contains five heating zones and the temperature profile for these zones were set at; 315.5 °C, 326.7 °C, 332.2 °C, 332.2 °C, and 338 °C for the CF-reinforced PPS grades [72]. All BAAM extrusion trials were performed at the Manufacturing Demonstration Facility, Oak Ridge National Laboratory. The temperature of the melt stream was determined to be between 365 °C and 383 °C. A single elliptical bead measuring 152.4 cm long, 0.84 cm wide, and 0.38 cm high was extruded using a 0.762 cm diameter nozzle, and a screw speed of 300 revolutions per minute (RPM). During BAAM extrusion, the screw speed controls the volumetric flow rate of the material out of the extruder. The volumetric flow rate was measured at screw speeds of 100, 200, 300, and 400 RPM by weighing the amount of material extruded in 120s and dividing by the material melt density. For these CF-reinforced PPS grades, the experimentally determined melt density values at 370 C averaged 1.42 (+/- 0.03) g/cc. The melt density is calculated by dividing mass of the extrudate from the capillary rheometer by the product of extrudate collection time and volumetric flow rate. On a capillary rheometer, Q, is a product of plunger speed and barrel cross sectional-area.

Results and Discussion

Rheological Characterization

Figure 2.2 plots G' and G" as a function of oscillatory shear stress for the four epoxy/nano-clay ink formulations; 10 wt.%, 12.5 wt.%, 15 wt.%, and 17.5 wt.%. Overall, G' and G" increase with increase in nano-clay content and G' is higher than G" especially at lower oscillatory shear stresses. This observed phenomenon suggests that the inks display solid-like behavior at the low shear stress region [17]. However, as the applied oscillatory stress increases above a certain value, G' decreases and becomes less than G". The crossover point for this transition defines the material's shear yield stress (τ_y). Above τ_y, the inks behave more liquid-like [22–24]. These values are recorded in Fig. 2.2 and demonstrate that increasing the nano-clay content increases the shear yield stress values. Similar behavior was observed by Hmeidat et. al using inks with varying nano-clay content [17].

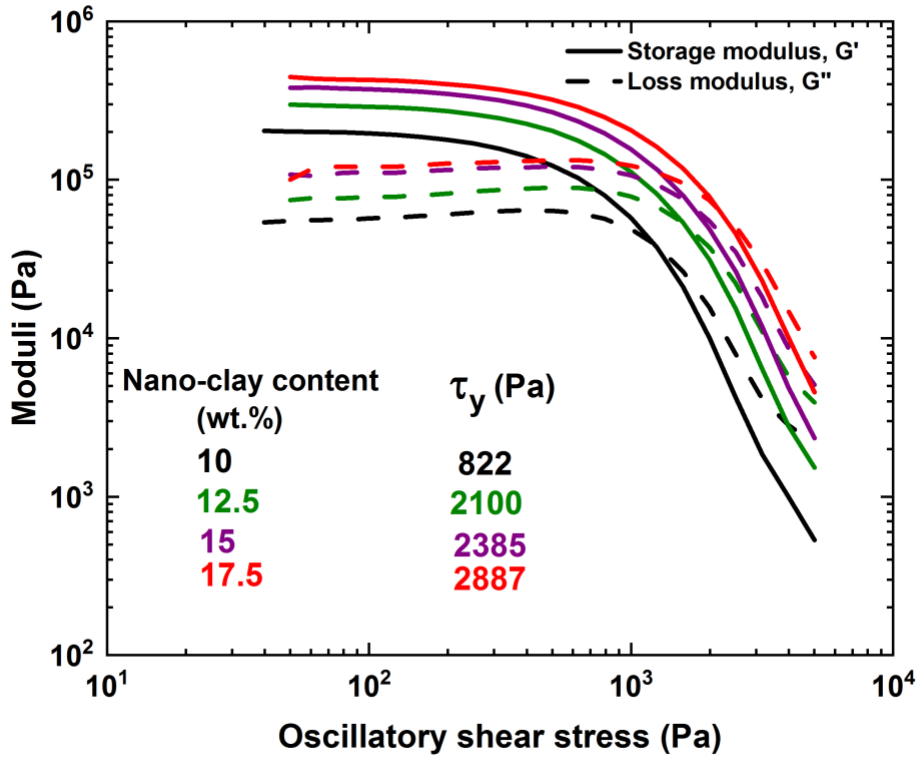


Figure 2.2. Log-log plots of G' and G" as a function of oscillatory shear stress for epoxy/nano-clay ink formulations along with experimentally determined τ_y values

Frequency Sweep

Frequency sweep tests were used to determine the variation of complex viscosity with angular frequency at the temperatures shown in Figures 2.3 and 2.4. The flow curves were fit to the power-law equation (Eqn. 2.5) to obtain n and C values. For both ABS and PLA, as the temperature decreases, the complex viscosity increases. However, their rheological profiles are quite different as described below.

ABS is shear thinning at all frequencies and temperatures (Fig. 2.3). The calculated n and C values for ABS are determined from a power-law fitting between 10 and 628 rad/s (Table 2.3). n increases with temperature while the consistency index, C, decreases with increase in temperature. This behavior has been observed in other polymer melts such as ethylene-vinyl acetate [73]. In contrast, PLA exhibits Newtonian behavior at angular frequencies less than 10 rad/s for lower temperatures and extending to ~100 rad/s at higher temperatures (Fig. 2.4). Regardless of temperature, PLA is shear-thinning above 100 rad/s and the n and C values are calculated by fitting the power-law in the region of 100 – 628 rad/s (Table 2.4). Like ABS, the power-law index, n, of PLA increases with deposition temperature while C decreases with increase in temperature.

The complex viscosity as a function of angular frequency for the three PPS grades at 370 °C in nitrogen are shown in Figure 2.5. n and C values were determined by fitting the power-law over the entire curve from 0.1 to 100 rad/s (Table 2.5). As the fiber content increases, the power-law exponent, n, becomes smaller, indicating that CF enhances the shear-thinning effect of the composite system. The complex viscosity of the PPS grades increases with subsequent increase in fiber content at all angular frequencies. At the lower angular frequencies (0.1 rad/s), complex viscosity of 60% wt.% CF-PPS is higher than that of 40% by 2 orders of magnitude. At 100 rad/s, the complex viscosity of 60% wt.% CF-PPS is 19x higher than that of 40% wt.% CF-PPS and 4x higher than that of 50% wt.% CF-PPS. The increase in viscosity creates a high torque condition during BAAM extrusion as the screw speed must be increased to match the desired flow rate. Similar complex viscosity patterns have been observed for 40% and 50% CF-PPS at temperatures between 300 °C and 345 °C in other studies [28,42].

Extrudability Trials

To demonstrate the effectiveness of the proposed pressure-driven extrusion model in predicting successful extrusion, three key variables were investigated. These variables are: (1) the role of viscosity modifiers on epoxy/nano-clay ink formulations used in DW, (2) the effect of varying extrusion temperature on FFF systems, and (3) how CF reinforcement impacts the torque of the BAAM system.

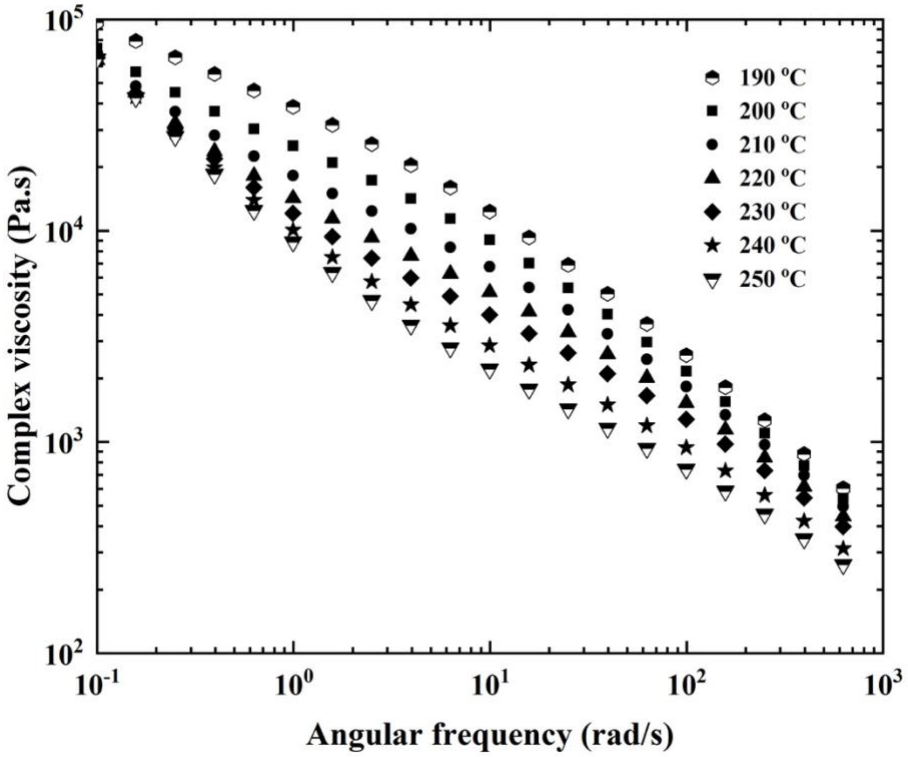


Figure 2.3. Complex viscosity plots of ABS as a function of angular frequency at various extrusion temperatures in air

Table 2.3. Experimentally calculated power-law n and C values for ABS

Temperature (°C)	n	C (Pa.s^n)
190	0.272	6.59 x 10^4
200	0.321	4.32 x 10^4
210	0.369	2.89 x 10^4
220	0.409	2.00 x 10^4
230	0.443	1.44 x 10^4
240	0.471	1.02 x 10^4
250	0.492	7.40 x 10^3

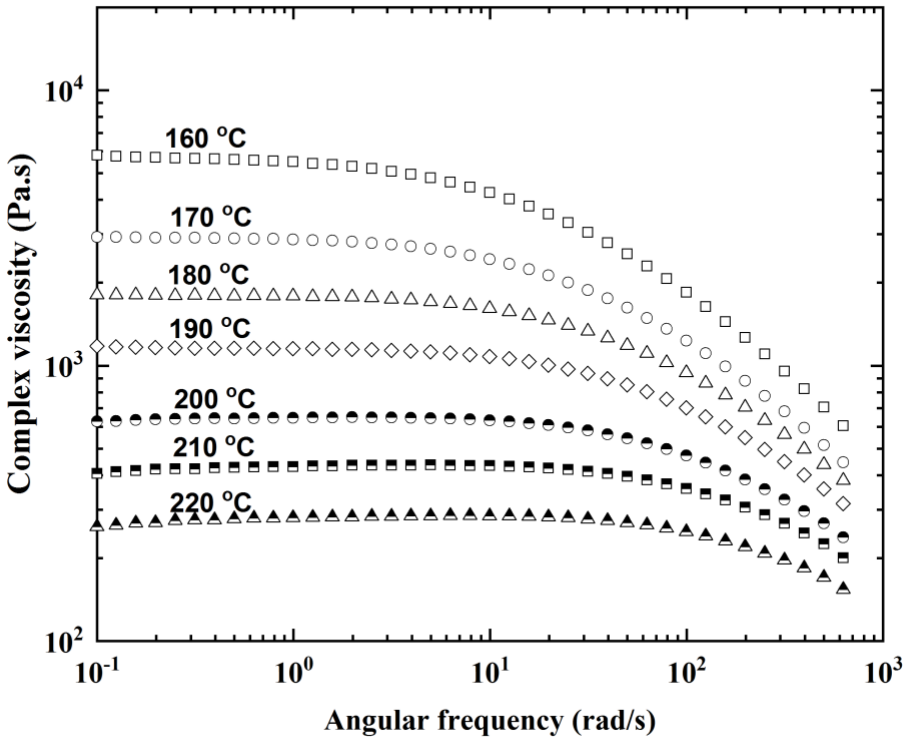


Figure 2.4. Complex viscosity plots of PLA as a function of angular frequency at various extrusion temperatures in air

Table 2.4. Experimentally calculated power-law n and C values for PLA

Temperature (°C)	n	C (Pa.Sn)
160	0.431	2.15 x 10^4
170	0.474	1.38 x 10^4
180	0.523	8.57 x 10^3
190	0.579	4.95 x 10^3
200	0.631	2.67 x 10^3
210	0.692	1.53 x 10^3
220	0.745	8.32 x 10^2

Table 2.5. Experimentally calculated power-law n and C values for CF-reinforced PPS

CF wt.%	n	C (Pa.sn)
40	0.31	19911
50	0.195	171825
60	0.18	849586

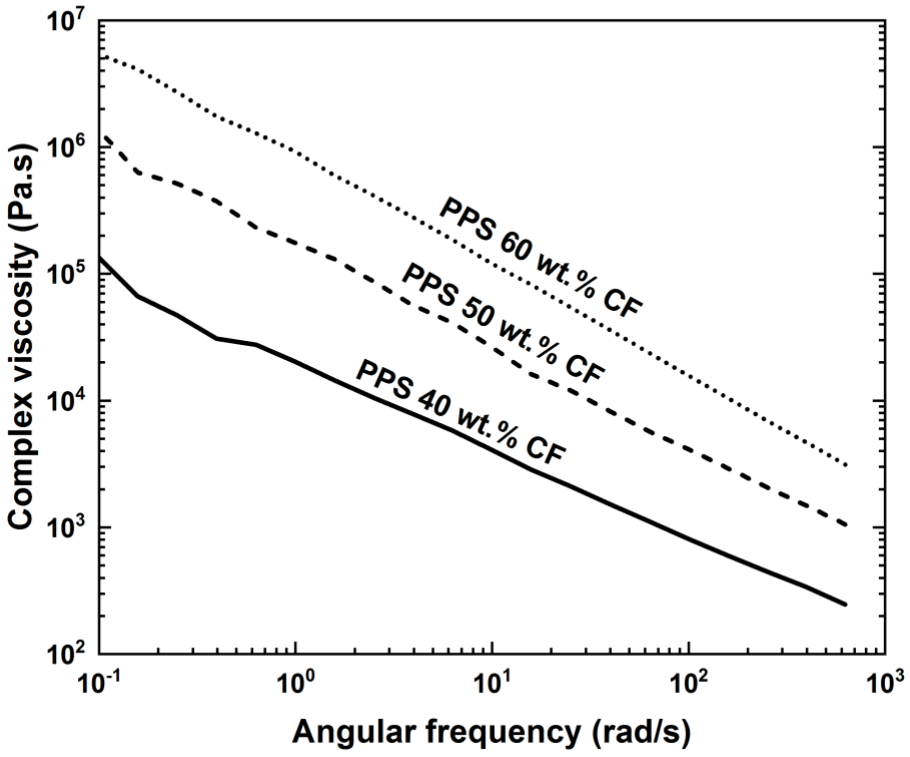


Figure 2.5.Complex viscosity plots of CF-reinforced PPS at 370 °C in nitrogen as a function of angular frequency

Effect of Viscosity Modifiers

Epoxy resins leverage the potential of AM to make lightweight composite structures through DW [21]. However, they behave predominantly as viscous liquids, in that their viscosity is independent of shear rate and their viscoelastic moduli (G' and G") are independent of applied shear stress [17,63]. Recent studies have shown that addition of small volume fractions of nano-clay filler materials and short fibers to the epoxy resin imparts the rheological properties such as shear-thinning and shear yield stress requirements needed for DW, enabling the fabrication of stable and fully dense structures with high mechanical properties [17,20,63,74,75]. The effect of viscosity modifiers on ink formulations is explored further in this model to determine the maximum nano-clay content beyond which extrusion on DW is not possible given the system limits.

To determine the pressure required to extrude viscoelastic inks on DW, the Benbow-Bridgewater equation (Eq. 2.3) for paste extrusion, discussed earlier in used. It treats the non-Newtonian behavior of the nano-clay ink formulations as Bingham plastics where flow occurs once τ_y is exceeded. Table 2.6 shows calculated pressure drop values for the four epoxy nano-clay formulations using the Benbow-Bridgewater equation and the yield stress values shown on Figure 2.2.

The model predicts that all ink formulations except epoxy/17.5 wt.% nano-clay "pass" and can be extruded on the DW system. Most of the pressure is concentrated in the die land region (ΔP_2) which is the narrowest part of the orifice. Results from a series of extrusion tests on DW using the same ink formulations further validate model predictions. The experimental values reported in Table 2.6 are in close agreement with predicted model results. During the trials, it was also not possible to extrude epoxy/17 wt.% nano-clay because the pressure required to deposit the ink formulation exceeded the system maximum and no material could be extruded using the 3-cc syringe and air pressure gauge. Generally, during the DW print trials, the pressure that is required to print a stable bead is manually controlled by varying the air pressure gauge. In these print trials, extrusion of the epoxy/17.5 wt.% nano-clay formulation using the 3-cc syringe was not possible because of the limitation posed by the air pressure gauge. The highest pressure that could be reached with this gauge was 4.34 MPa, which is below the pressure required to extrude epoxy/17.5 wt.% nano-clay formulation. However, it might be possible to extrude the epoxy/17 wt.% nano-clay formulation if a larger syringe and pressure gauge are used. The Benbow-Bridgewater paste extrusion equation is thus a good first approximation of the required extrusion pressure for inks used in DW provided the material properties and system parameters are known.

Table 2.6. Pressure drop predictions as well as experimental pressure values for epoxy/nano-clay ink formulations on DW system

EPON				
Nano-clay content (wt.%)	10	12.5	15	17.5
τ_y (MPa)	8.22 x 10-4	2.10 x 10-3	2.39 x 10-3	2.89 x 10-3
Maximum pressure (MPa)	4.34			
Model				
ΔP_1 (MPa)	0.02	0.02	0.02	0.03
ΔP_2 (MPa)	2.58	3.30	3.75	4.54
ΔP_{total} (MPa)	2.60	3.32	3.77	4.57
Print Criteria				
Is $\Delta P_{max} > \Delta P_{total}$	**PASS**	**PASS**	**PASS**	**FAIL**
Experimental pressure values (MPa)	2.41	3.36	3.60	-

Effect of Temperature

The liquefier in FFF systems is central to the extrusion process because it is where the solid filament is melted [49]. Successful extrusion through the nozzle requires that the filament is in the molten state. The force required for extrusion is highly dependent on material viscosity and nozzle geometry [49,58]. In FFF, the filament acts as both the piston driving the extrusion process and as the material being deposited [4]. It is fed through motorized rollers into a heated extrusion head where it is melted [49]. Above the rollers, the filament is under tensile stress and under compression between the rollers and the heater where it acts as a plunger [49]. It is this compressive force that becomes the force behind the extrusion process.

The force imposed on the filament by the two rollers is driven by a pair of motors whose torque (Γ) and power to each motor (P) required for extrusion are calculated using equations from Bellini [49]:

$$\Gamma = \frac{F}{2} \cdot R_r \tag{2.9}$$

$$P = \omega_r \cdot \Gamma \tag{2.10}$$

where R_r is the radius and ω_r is the angular velocity of a roller. The filament is assumed to be in constant contact with the rollers and the filament driving pressure (P_f) is calculated using Equation 2.11;

$$P_f = \frac{F_f}{A_f} \tag{2.11}$$

where F_f is the force of the filament (RT shear strength x shear area) and A_f is the cross-sectional area of the filament.

The most common failure mode for FFF systems tends to be filament buckling [50] and it occurs when the compression on the liquefier side of the feed rollers places a limit on the feed rate. To ensure that the filaments used in this study do not buckle, an approximate critical pressure of the filament is determined by Euler buckling analysis [8];

$$P_{cr} = \frac{\pi^2 E d_f^2}{16 L_f^2} \tag{2.12}$$

where E is the elastic modulus of the filament, d_f is the filament diameter and l_f is the filament length from the rollers to the entrance of the liquefier.

The theoretical limiting pressure for the FFF system is taken to be the material dependent P_f and maximum pressure drop permitted for extrusion of ABS and PLA used for this model is 2.65 MPA and 3.02 MPa, respectively (Table 2.7).

Table 2.7. Elastic modulus, tensile strength, and calculated pressures of ABS and PLA used to assess the pressure-driven model

	ABS	**PLA**
Elastic Modulus at RT (MPa)	2250	2690
Tensile strength at RT (MPa)	41.3	47
Buckling pressure (P_{cr})	45	48
Motor Driving Pressure (MPa)	4.79	
Filament Driving Pressure (P_f)	2.65	3.02
Limiting Critical Pressure (MPa)	2.65	3.02

The Hagen-Poiseuille equation (Eq. 2.4) is then used to determine the pressure required to extrude polymer melts on the FFF system using viscoelastic properties and experimentally determined Q values of ABS and PLA. The material is said to "pass" if the HP predicted pressured drop is less than the material dependent limiting critical pressure, P_f, used as P_{max} for the FFF system.

Rheological measurements were performed between 190 °C and 250 °C for ABS and 155 °C and 220 °C for PLA. From the melt flow curves (Fig. 2.3 & 2.4), a decrease in the deposition temperature results in an increase in the viscosity of the polymer which in turn, increases the pressure drop that the FFF system must overcome for extrusion to happen at the desired volumetric flow rate, Q at different print speeds.

From a predictive standpoint, the HP model predicts that ABS passes at all temperatures and print speeds at which extrusion was achieved except at 200 °C, 1.13 cm/s because the predicted ΔP of 2.7 MPa at this given temperature and print speed exceeds the 2.65 MPa material dependent limiting critical pressure (Table 2.8).

Given the extrusion orifice dimensions, the nozzle region has a low shear rate (~1 /s) and the resulting pressure drop in all cases is low based on the HP prediction. By contrast, the pressure drop in the exit region of the die is at least 4x greater than in the nozzle region for any given temperature and print speed (Table 2.8).

Table 2.8. Model predicted extrusion pressure values at various temperatures and print speeds along with Pass/Fail print criteria for ABS on the FFF system, P_{max} = 2.65 MPa

Print speed: 0.05 cm/s					
	Model (MPa)				**Experimental**
Temperature (°C)	**ΔP_{nozzle}**	**ΔP_{exit}**	**ΔP_{total}**	**PASS/FAIL**	**PASS/FAIL**
250	0.05	0.74	0.80	PASS	PASS
240	0.07	0.90	0.98	PASS	PASS
230	0.11	1.18	1.28	PASS	PASS
220	0.15	1.34	1.49	PASS	PASS
210	0.22	1.54	1.75	PASS	PASS
200	0.31	1.70	2.02	PASS	PASS

Print speed: 0.08 cm/s					
	Model (MPa)				**Experimental**
Temperature (°C)	**ΔP_{nozzle}**	**PASS/FAIL**	**ΔP_{total}**	**PASS/FAIL**	**PASS/FAIL**
250	0.07	0.97	1.04	PASS	PASS
240	0.09	1.14	1.24	PASS	PASS
230	0.14	1.47	1.60	PASS	PASS
220	0.18	1.65	1.83	PASS	PASS
210	0.26	1.83	2.09	PASS	FAIL
200	0.36	1.96	2.31	PASS	FAIL

Print speed: 1.13 cm/s					
	Model (MPa)				**Experimental**
Temperature (°C)	**ΔP_{nozzle}**	**ΔP_{exit}**	**ΔP_{total}**	**PASS/FAIL**	**PASS/FAIL**
250	0.09	1.21	1.30	PASS	PASS
240	0.12	1.42	1.53	PASS	PASS
230	0.17	1.83	1.99	PASS	PASS
220	0.22	1.99	2.22	PASS	FAIL
210	0.31	2.19	2.50	PASS	FAIL
200	0.42	2.28	2.70	FAIL	FAIL

Similarly, the HP model predicts that PLA can be extruded at all temperatures and print speeds because all total ΔP predictions are less than the 3.02 MPa maximum pressure (Table 2.9).

However, the HP ΔP predictions do not account for phase changes and non-isothermal conditions in the nozzle which result in deviation from the desired throughput, affecting print quality. From experimental data, failure to extrude manifests itself in the inability of the polymer melt to achieve the desired Q during deposition at higher deposition speeds (0.08 cm/s and 1.13 cm/s). Extrusion of ABS was attempted starting at a deposition temperature of 250 °C and lowering the temperature of the Lulzbot Taz 6 by 10 °C to the lowest temperature at which molten thermoplastic could be extruded. Experimentally, ABS material extrusion was achieved at all print speeds and temperatures above 200 °C. Q values are experimentally determined using the mass flow rate and material density values as described in experimental section and results plotted in Fig. 2.6 and 2.7.

From Fig. 2.6 and Fig. 2.7, it can be observed that as the print speed increases, so do Q values for both materials at all extrusion temperatures. However, material extrusion is not possible at certain temperatures and print speeds. For instance, ABS extrusion is not possible at 190 °C while PLA cannot be extruded below 170 °C. Melt flow is highly affected by material viscosity properties and the pressure drop required for extrusion increases with viscosity. When the temperature is low, viscosity of the melt is high and the pressure drop exceeds critical value resulting in filament buckling [58].

At the lowest print speed, 0.05 cm/s, Q values for ABS and PLA are very similar and are independent of extrusion temperature indicating that the desired throughput is achieved. At the intermediate print speed, 0.08 cm/s, the desired throughputs for ABS and PLA are achieved at 220 °C and 190 °C, respectively, well as at the highest print speed (1.13 cm/s), the desired throughputs are realized at even higher extrusion temperatures (230 °C for ABS and 200 °C for PLA).

Failure to achieve desired throughput at higher print speeds (0.08 cm/s and 1.13 cm/s) exhibited by a departure from the plateau is considered an experimental print “fail”. At high print speeds, the filament is not in the liquefier long enough for it to fully melt at the extrusion temperature and for deposition to occur at the desired throughput [58,60,61]. This results in an inhomogeneous temperature distribution within the FFF system which is attributable to heat transfer limitations. Therefore, although the gears in the FFF system continue to convey material forward, the phase change from solid to liquid does not occur fast enough [58,60,61]. This helps explain why ABS “fails” as early as 220 °C when printing at 1.13 cm/s, and 210 °C when printing at 0.08 cm/s. PLA on the other hand “fails” as early as 180 °C at the higher print speeds (0.08 cm/s and 1.13 cm/s).

Table 2.9. Model predicted extrusion pressure values at various temperatures and print speeds along with Pass/Fail print criteria for PLA on the FFF system, P_{max} = 3.02 MPa

Print speed: 0.05 cm/s					
	Model (MPa)				**Experimental**
Temperature (°C)	**ΔP_{nozzle}**	**ΔP_{exit}**	**ΔP_{total}**	**PASS/FAIL**	**PASS/FAIL**
220	0.01	0.34	0.35	PASS	PASS
210	0.01	0.48	0.49	PASS	PASS
200	0.02	0.61	0.63	PASS	PASS
190	0.04	0.87	0.90	PASS	PASS
180	0.06	1.09	1.16	PASS	PASS
170					

Print speed: 0.08 cm/s					
	Model (MPa)				**Experimental**
Temperature (°C)	**ΔP_{nozzle}**	**ΔP_{exit}**	**ΔP_{total}**	**PASS/FAIL**	**PASS/FAIL**
220	0.01	0.49	0.50	PASS	PASS
210	0.02	0.68	0.69	PASS	PASS
200	0.03	0.84	0.87	PASS	PASS
190	0.05	1.15	1.20	PASS	PASS
180	0.08	1.45	1.51	PASS	FAIL
170	0.13	1.69	1.82	PASS	FAIL

Print speed: 1.13 cm/s					
	Model (MPa)				**Experimental**
Temperature (°C)	**ΔP_{nozzle}**	**ΔP_{exit}**	**ΔP_{total}**	**PASS/FAIL**	**PASS/FAIL**
220	0.01	0.70	0.71	PASS	PASS
210	0.02	0.93	0.95	PASS	PASS
200	0.04	1.10	1.14	PASS	PASS
190	0.07	1.49	1.56	PASS	FAIL
180	0.11	1.79	1.90	PASS	FAIL
170	0.16	2.08	2.24	PASS	FAIL

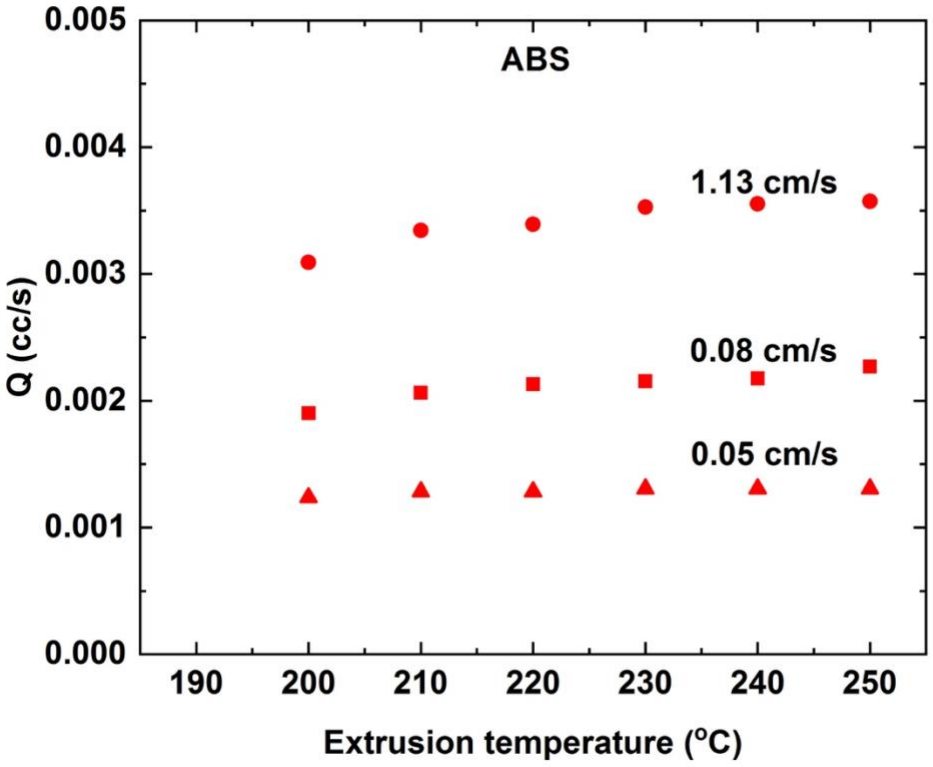


Figure 2.6. Volume flow rate (Q) values of ABS as a function of print speed and extrusion temperature on the Lulzbot TAZ6 FFF printer

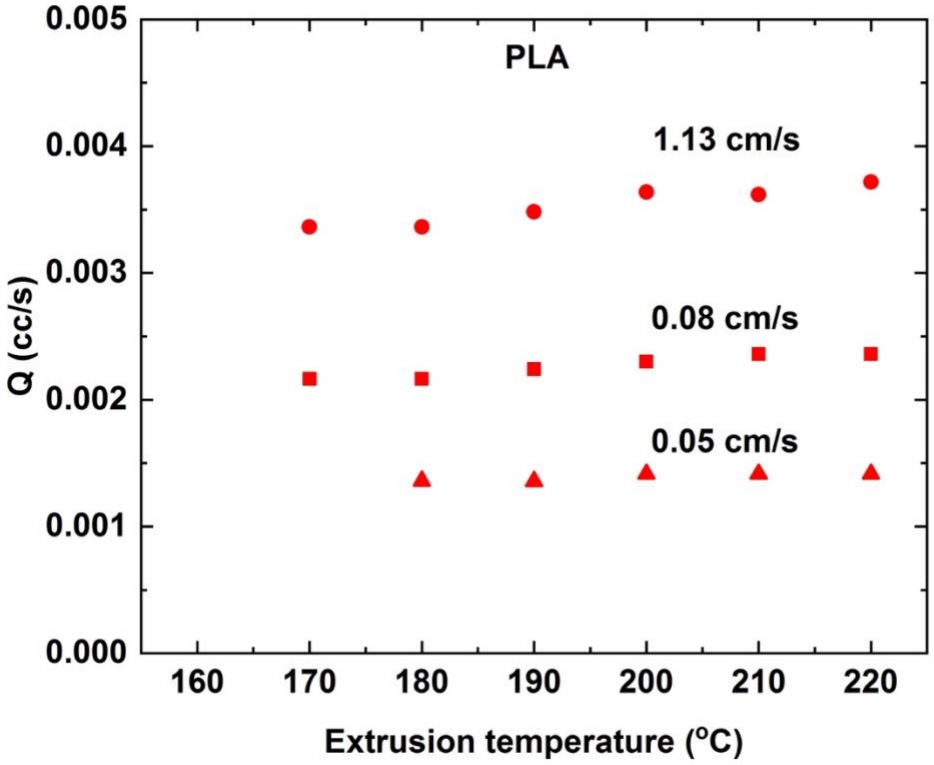


Figure 2.7. Volume flow rate (Q) values of PLA as a function of print speed and extrusion temperature on the Lulzbot TAZ6 FFF printer

Based on experimental observations, the true P_{max} for ABS is close to 2.05 MPa rather the material dependent critical limiting pressure of 2.65 MPa. This is further verified by literature findings where typical ΔP suitable for FFF processes are in the range of 1 – 2.1 MPa [58] and this is true for the scenarios in which ABS "passes" based on the HP ΔP calculations shown in Table 2.8.

ABS is deposited across a range of temperatures from 205 °C to 270 °C [15,26,76]. Higher melt temperatures foster better bonding between beads, too high leads to degradation and when the temperature is too low, the polymer melt within the liquefier is not uniform and pressure drop exceeds critical value which results in filament buckling.

From an experimental standpoint, PLA "fails" at temperatures and print speeds shown in Table 2.9, despite having P_{total} values that are less than material dependent critical limiting pressure, P_{max} (3.02 MPa). Like ABS, much of the pressure required to extrude PLA is concentrated in the shorter exit region of the die as depicted in Table 2.9. The shear rates in this exit region are much higher (~500 -1000 /s) due to the smaller diameter, resulting in higher pressures in this region than experienced in the nozzle region.

A few studies have modeled ΔP for flow of PLA in FFF nozzles using analytical equations and fluid flow simulations [58,59,61]. The range of predicted ΔP is between 0.5 and 5 MPa and the variation is due to inadequacy of analytical models in accommodating for the solid-fluid transition of material properties. From experimental data, the true P_{max} for PLA on the FFF system is 1.50 MPa (Table 2.9), and this value is half of the initial P_{max} of 3.02 MPa. More experimental studies need to be conducted to further validate these findings.

The use of the HP model to predict ΔP in FFF systems is based on a given system maximum. The model cannot be used to correctly predict system maximum but rather work within those limitations to predict extrudability. The HP model predictions are meant to serve as a guide for material extrudability at a given temperature and FFF system if material properties and desired flow rate are known.

Effect of Carbon Fiber Loadings

Filament feed issues have prevented the successful deposition of CF-reinforced PPS on FFF systems [42]. However, since BAAM eliminates the use of filaments and can extrude high loadings of fiber reinforced plastics [24], the effect of high fiber loading on extrusion is evaluated on the BAAM system using CF reinforced PPS grades as candidate materials.

Addition of carbon fiber to neat resins is preferred for BAAM 3D printed parts because it lowers the coefficient of thermal expansion by an order of magnitude which minimizes shrinkage as the part cools from deposition temperature to ambient temperatures [24]. However, modifying material composition by addition of fibers to the polymer matrix increases the viscosity and affects the ability to print successfully. The effect of adding carbon fiber to large scale AM feedstock such as PPSU, ABS, PEKK and PPS and the effect on processing conditions is well documented [30,31,42,77].

To determine the pressure required to extrude polymer melts on the BAAM system, the Hagen-Poiseuille equation (Eq. 2.4) was used. The model predicts that 40 wt.% and 50 wt.% CF-PPS could be extruded and therefore "pass" while 60 wt.% CF-PPS "fails" at all screw speeds because the pressure required to extrude the 60% CF-PPS composite exceeds the BAAM maximum system pressure of 6.89 MPa (Table 2.10).

Unlike FFF, much of the pressure that is required for extrusion to occur in BAAM is concentrated in the long nozzle region prior to the exit. The shear rates in the nozzle region are also much lower (80 – 122 s^{-1}) than those at the exit (190 – 289 s^{-1}) resulting in a higher viscosity in this region than that experienced at the exit. For instance, at 100 rad/s, the complex viscosity of PPS 60 wt.% CF is ~1800% higher than that of PPS 40 wt.% CF. This implies that a much higher ΔP is needed to extrude the melt under the same conditions: a 13x increase in ΔP_{total} is observed for PPS 60 wt.% CF compared to PPS 40 wt.% CF at 300 RPM.

ΔP predictions in Table 2.10 are supported by results from print trials on the BAAM system. For example, the model predicts that PPS 60 wt.% CF fails at 300 RPM and during deposition, the print failed as well because the desired throughput was not achieved [72]. During BAAM extrusion, the screw speed utilized controls the flow rate of the material out of the extruder and is selected based on the print geometry, layer time, and nozzle dimensions. For a given print, different screw speeds are often investigated and adjusted until the desired bead geometry (width and thickness) is attained. In all cases, as screw speed increases, so does the pressure required to extrude the material through the nozzle. In this work, the screw speed used for extrusion was 300 RPM and this is typical for parts made using CF-reinforced PPS on the BAAM. Such high ΔP values as predicted by the HP equation for the "fail" cases may also not be suitable for achieving smooth material flow and impact final print quality. Hassen et al. highlight some of the visual defects and processing challenges of extruding with 60 wt.% CF-PPS such as material irregularities due to drooling at the tip, cracks being initiated at the first few layers, and areas lacking material resulting in parts warping [72] supporting the model predictions. Key design variables that affect pressure drop such as nozzle diameter [58] are explored in the next

Table 2.10. Q values and Hagen-Poiseuille pressure drop predictions for CF-PPS at various screw speeds and an extrusion temperature of 370 °C

BAAM: P_{max} = 6.89 MPa, 100 RPM					
	Model (MPa)				**Print criteria**
PPS CF content (%)	**Q (cc/s)**	**ΔP_{nozzle}**	**ΔP_{exit}**	**ΔP_{total}**	**$P_{max} > \Delta P_{total}$**
40	1.76	0.89	0.21	1.10	PASS
50	1.97	4.35	0.93	5.28	PASS
60	2.18	14.50	2.94	17.44	FAIL
200 RPM					
PPS CF content (%)	**Q (cc/s)**	**ΔP_{nozzle}**	**ΔP_{exit}**	**ΔP_{total}**	**$P_{max} > \Delta P_{total}$**
40	3.78	1.13	0.27	1.40	PASS
50	4.15	5.03	1.07	6.10	PASS
60	4.53	16.04	3.25	19.29	FAIL
300 RPM					
PPS CF content (%)	**Q (cc/s**	**ΔP_{nozzle}**	**ΔP_{exit}**	**ΔP_{total}**	**$P_{max} > \Delta P_{total}$**
40	4.77	1.21	0.29	1.50	PASS
50	5.27	5.27	1.12	6.39	PASS
60	5.80	16.60	3.36	19.96	FAIL

chapter to investigate the impact of these properties on the pressure required for successful extrusion for the BAAM system.

Summary and Conclusions

This proposed approach presents a simple screening process for high-strength epoxy nano-clay composites and polymer melts as candidate feedstock for extrusion-based AM systems namely DW, FFF, and BAAM. Results from this chapter indicate that if viscoelastic properties such as shear yield stress, the shear thinning exponent, consistency index, and viscosity are known, the proposed pressure-driven models can successfully predict whether extrusion occurs although it may not be perfect. Extrusion trials of the candidate materials on the various AM platforms further validate model predictions in that, extrusion on the AM system is achieved in all instances where the model predicts it would and vice versa. This therefore, makes the proposed approach a useful tool for predicting successful material extrudability on DW, FFF and BAAM platforms, speeding up the process of material screening and selection. The model also indicates regions in the extrusion orifice where pressure is concentrated. For instance, in DW and FFF, much of the pressure required to extrude is in the exit region of the die while in BAAM, pressure is mostly built up in the long nozzle region. This proposed extrusion criterion is meant to serve as a first step to a more holistic approach of predicting successful extrusion on any extrusion-based AM platform that uses a shear-thinning material as feedstock. More work still needs to be done to address the challenge of modeling flow in extrusion-based AM systems such as determining the relationship between the variables encountered in AM including the material physical properties and rheology, flow rate, and nozzle geometry for improved process monitoring.

CHAPTER THREE

INVESTIGATING THE EFFECTS OF TRANSIENT START-UP PRESSURE DURING THE START/STOP PROCESS OF LARGE AREA ADDITIVE MANUFACTURING SYSTEMS

Introduction

Pressure transients play an important role in controlling the start-and-stop of extrusion in AM systems and impact final print quality. However, the occurrence of transients in AM has long been speculated but not studied or quantified [58,62,78]. Each time the extrusion process is started in AM, the system needs to overcome a pressure transient before steady-state driving pressure is achieved in a very short time [79–81]. The start-and-stop process is necessary for AM part fabrication because it is not feasible to generate tool paths with continuous extrusion profiles and if you do make a part without starts-and-stops, there are geometric limitations to what can be printed [78,82].

Transient behavior during AM extrusion processes impacts final print quality by creating weak points in areas where printing starts and stops and this is attributed to changes in flow behavior [58]. For example, visual observations of BAAM printed parts using carbon fiber reinforced composites show processing defects attributed to BAAM transient conditions and in particular, inconsistencies in bead geometry [72,78]. This is because at the start of extrusion, there is a lag before material starts to flow, and at the end, material continues to ooze out which leads to beads that are narrow at the start and wide at the end of the bead. For a large scale system such as BAAM, this causes significant geometric deviations in the printed part which limits the application of BAAM in composite tooling applications due to compromised structural integrity [72].

In BAAM, pellets are pushed by the screw through the feed section of the barrel into a transition section where the material is melted. The melted polymer travels through the metering section of the screw and out a die (deposition nozzle) under pressure [18]. Unlike other extrusion processes that use screw extruders, the BAAM extruder does not operate in steady-state conditions but rather, it starts and stops several times during extrusion. It is challenging to achieve a consistent bead profile during transient operation of the BAAM extruder due to the non-linear dynamics in the transient printing conditions that are present in the polymer extruder [78].

There is still a significant technical challenge of measuring the pressure inside AM nozzles. To date, several analytical and theoretical models are used to estimate the pressure drop in the AM nozzles [41,53,62,83,84] but these models fall short in their predictions because the assumptions used fail to capture the complexity of the liquefier dynamics, notably temperature and pressure. Of the studies where custom-design nozzles are used to measure pressure in the nozzle, pressure transients are not studied or quantified. Anderegg et al made in-situ temperature and pressure measurements of ABS in the FFF system using a custom-design nozzle during printing [62]. Their measurements showed an 11 °C decrease in temperature and a significant fluctuation in pressure during printing. Pressure readings from the nozzle sensor were higher than theoretical predictions suggesting that the assumptions used do not completely capture the dynamics in the FFF printer [62].

A few studies have characterized start-up pressure transients on the capillary rheometer using linear low-density polyethylene (LLDPE). In these studies, appearance of transient maximum peak is influenced by the volume of material in the barrel, isothermal compressibility, and die geometry [79,85]. Although useful, capillary rheometer measurements do not depict the true shear and thermal history that the materials undergo during BAAM processing using the single screw extruder. A more thorough understanding of the pressure conditions within the BAAM nozzle will improve predictions of the extrudability and printability of materials as well aid in optimizing process parameters.

To the author's knowledge, this is the first study aimed at investigating the transient and steady-state pressure profile in the BAAM nozzle during extrusion. The only available experimental pressure information on the BAAM is provided by a single transducer located at the end cap of the screw extruder [86]. No empirical data directly measured has been reported regarding pressure inside the BAAM nozzle.

In this chapter custom designed nozzles are used to measure pressure inside the BAAM nozzle, critical in ensuring that the polymer melt is flowing at the appropriate flow rate during the extrusion process. Testing is done using BAAM commonly utilized material, ABS 20 wt.% CF, and PPSU 25 wt.% CF, a high-performance composite used to manufacture in-autoclave tools and molds. Three custom nozzle sizes are fabricated: 0.508 cm, 0.762 cm, and 1.016 cm diameter nozzles and fitted with a sensor to monitor pressure. The results are compared to theoretical pressure predictions using the Hagen Poiseuille equation and numerical simulations using COMSOL Multiphysics Software laminar flow module. BAAM nozzle pressure measurements are also used to figure out how transient signals compare to steady-state pressures and analytical calculations are used to characterize the exponential pressure decay after extrusion stops.

Overall Objective

A more thorough understanding of the pressure conditions within BAAM nozzles to improve predictions of the extrudability and printability of materials as well as aid in the optimization of process parameters.

Primary Research Questions

i. How do the transient start-up pressures in the nozzle relate to steady-state pressures and influence extrudability?
ii. How do pressure predictions from analytical models and numerical simulations compare to experimentally measured nozzle pressures?

Numerical Modeling

It is of great significance to be able to accurately predict the pressure in the nozzle to optimize processing procedure of the material in AM. To do this, a computational fluids dynamic (CFD) based model is used to investigate the pressure and melt flow in the nozzle during extrusion of molten thermoplastics on AM systems. CFD-based approaches have been employed by other researchers to study various aspects of flow and heat transfer in extrusion and AM [87–90]. The numerical calculations for two-dimensional (2D) flow are performed with a finite element based CFD code COMSOL Multiphysics Software.

A 2D axisymmetric laminar flow model is considered in the numerical modeling of non-Newtonian flow of polymer melts in the BAAM nozzle. In the simulation, the polymer melt is treated as homogenous and isotropic with a uniform temperature, flowing continuously through a cylindrical die.

Laminar flow in the COMSOL Multiphysics module is governed by the Navier-Stokes equation:

$$\rho\left(\frac{\partial u}{\partial t} + (u \cdot \nabla)u\right) = -\nabla p + \nabla \cdot \left[\mu(\nabla u + (\nabla u)^T) - \frac{2}{3}(\nabla \cdot \mathrm{u})I\right] + F \tag{3.1}$$

The conservation of mass along with the Equation of state equations are also solved numerically using the finite element CFD code.

Conservation of mass

$$\frac{\partial \rho}{\partial t} + \nabla \cdot (\rho u) = 0 \tag{3.2}$$

Equation of state

$$\rho = \rho(p, T) \tag{3.3}$$

where ∇ is the Hamilton differential operator, u is the velocity vector, p is the pressure applied to the fluid, ρ is the density and μ is the dynamic viscosity. ρ and μ are material constants that define the specific fluid. The numerical solution treats the polymer melt as a power law fluid to model non-Newtonian flow behavior.

In the BAAM extruder, the thermoplastic starts melting as soon as glass transition temperature is reached before reaching the nozzle. Fluid flow is then simulated from this point on. Flow is forced by a pressure difference between the inlet and outlet at the tip of the nozzle. Considering the characteristics of the polymer melt flow in the die channel when steady extrusion is achieved, the following assumptions are made: 1) incompressible steady laminar flow, 2) no slip at the wall, and 3) the inertial and gravitational forces are assumed to be negligible. Flow is assumed to be laminar within the nozzle due to the low Reynolds-number caused by low diameter and high viscosity, respectively. Outlet pressure is set to a constant value of 1 atm (0.101 MPa).

Experimental Methods

Materials and Material Properties

Two composite systems are investigated: ABS 20 wt.% CF, a commonly used BAAM feedstock, as well as PPSU 25 wt.% CF, a high-performance amorphous thermoplastic. Both materials are compounded by Techmer PM (New Castle, DE) and come in pellet form. Prior to BAAM extrusion, ABS 20 wt.% CF is dried at 62.78 °C for 4-5 hours and PPSU 25 wt.% CF is dried at 137.78 °C for 3 hours. The model is fed with data generated from rheological experiments and literature (Table 3.1 and Table 3.2).

Capillary Rheometry Characteristic Decay Time Measurements

Variation of pressure over time during the extrusion of ABS 20 wt.% CF was studied using a Dynisco LCR 7001 capillary rheometer (Massachusetts, USA) at 250 °C. 10 g of pellets were loaded into the barrel and allowed to melt for 10 minutes once the barrel had equilibrated at the desired test temperature. The piston was lowered until molten material came out of the die. For uniformity in testing, the piston was lowered to 9.8 cm. A timer was set for 10 minutes to allow the plunger force to stabilize. At specified shear rates of 50, 100, 200, and 500 1/s, the polymer melt was extruded from the capillary rheometer until steady-state driving pressure was achieved. The change in pressure over time was

Table 3.1. Thermal and rheological parameters of ABS 20 wt.% CF and PPSU 25 wt.% CF used in the COMSOL simulation

	ABS 20 wt.% CF			**PPSU 25 wt.% CF**		
Test temperature (°C)	250			376		
Nozzle diameter (cm)	0.508	0.762	1.016	0.508	0.762	1.016
C	84019	53880	18506	37979	39488	12050
n	0.508	0.279	0.375	0.471	0.413	0.644
Melt density (g/cc)	0.97			1.29		

Table 3.2. Average mass flow rate of deposited ABS 20 wt.% CF and PPSU 25 wt.% CF beads

		Average mass flow rate (g/s)	
Nozzle diameter (cm)	**Screw speed (RPM)**	**ABS 20 wt.% CF**	**PPSU 25 wt.% CF**
0.508	50	1.56	1.04
	100	2.90	2.14
	150	3.83	2.95
0.762	50	1.70	1.16
	100	3.19	2.32
	150	4.29	3.38
	200	5.69	4.55
	250	7.06	5.39
	300	7.59	6.22
	350	8.51	7.43
1.016	50	1.75	1.21
	100	3.25	2.40
	150	4.92	3.61
	200	6.27	4.47
	250	7.74	5.74
	300	10.21	6.26
	350	12.63	5.70

monitored and recorded. Two dies with Two dies with varying length-to-diameter (L/D) ratios of 10 and 12 with a die diameter of 0.749 mm were used for these tests.

BAAM Extrusion

Four single layer beads (97 cm long) were deposited using ABS 20 wt.% CF and PPSU 25 wt.% CF at different screw speeds using a non-mixing screw. Extrusion was done using three nozzle diameters; 0.508 cm, 0.762 cm, and 1.016 cm nozzles. For the 0.508 cm nozzle, beads were extruded at 50, 100, and 150 revolutions per minute (RPM) well as for the 0.762 and 1.016 cm nozzles, extrusion was done at 50, 100, 150, 200, 250, 300, and 350 RPM. The BAAM extruder has five different zones and each zone is set to a different setting based on the material. For ABS 20 wt.% CF, the five zones were set at 175 °C, 209 °C, 249 °C, 249 °C, and 250 °C and temperature of the melt ranged from 255 – 260 °C due to shear heating. For PPSU 25 wt.% CF, the five zones were set at: 311 °C, 345 °C, 345 °C, 360 °C, 355 °C and temperature of the melt ranged from 360 – 375 °C. Prior to the test and after switching out material, a small amount of polymer was extruded to purge the system of impurities or leftover material. Bed temperature for both materials was kept at 110 °C to promote adhesion of the deposited bead to the BAAM print sheet. After deposition of each bead, the machine was rested for 60 seconds, and the nozzle cleaned of any residual material.

To measure pressure in the nozzle during BAAM extrusion, custom-designed nozzles with ports for a pressure transducer were fabricated (Figure 3.1). The nozzles were made using Ultra-Machinable 360 Brass Bars purchased from McMaster-Carr (Elmhurst, IL). The pressure transducer used, model number TPT4634-5M-3/18-SIL2 4, was purchased from Dynisco (Franklin, MA) and is an exact match to the one used to monitor pressure on the BAAM extruder. Figure 3.2 shows the BAAM extruder end cap fitted with two pressure sensors; one in the screw and the other in the nozzle. The transducer is connected to a data acquisition (DAQ) system and during extrusion, the pressure profile of the extruded bead is captured. The DAQ acquires 100 data points every second. The actual volumetric throughput, Q, of the deposited beads was determined by weighing the beads and dividing the mass by extrusion time to obtain mass flow rate. The mass flow rate was then divided by melt density to get Q. ABS melt density used is 0.97 g/cc from literature [69]. Melt density for PPSU 25 wt.% CF was determined experimentally to be 1.29 g/cc at 370 °C using a capillary rheometer as per ASTM D1238-13 guidelines for melt flow rates of thermoplastics [91].

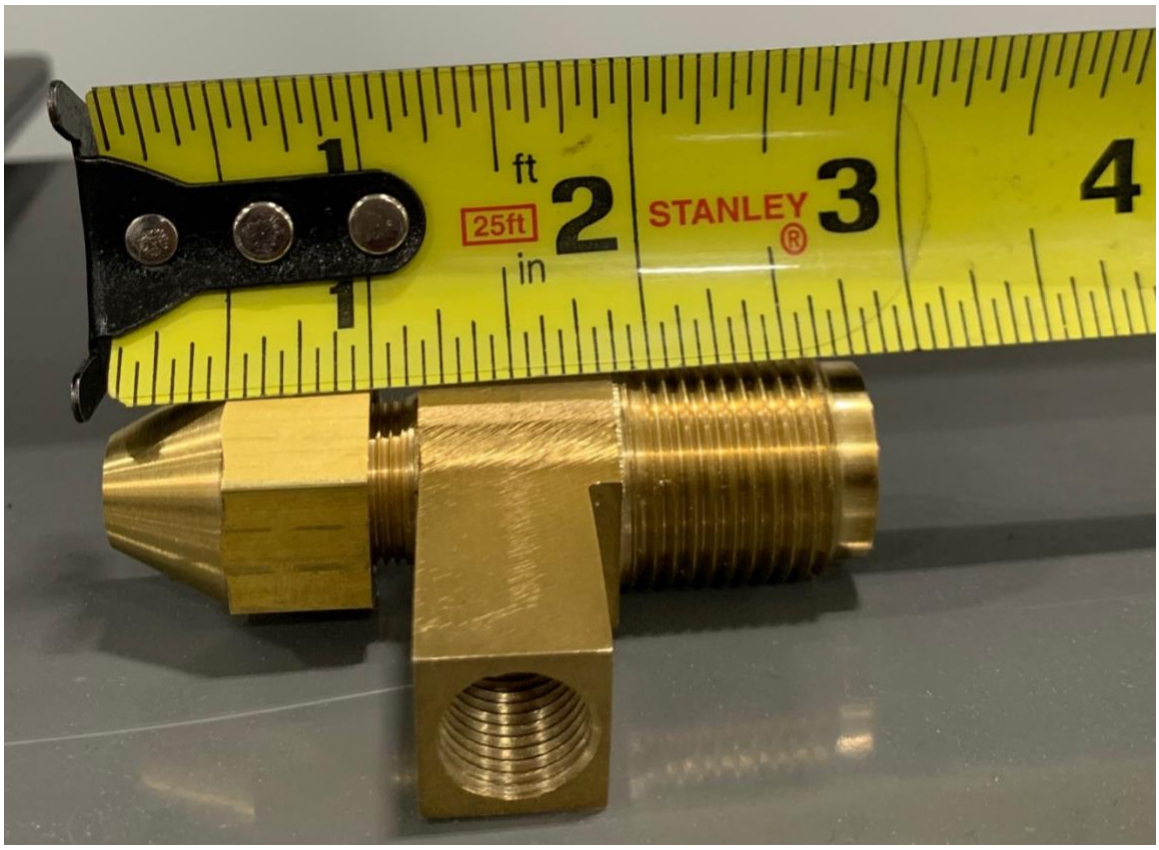


Figure 3.1. Custom designed BAAM nozzle with port for pressure transducer

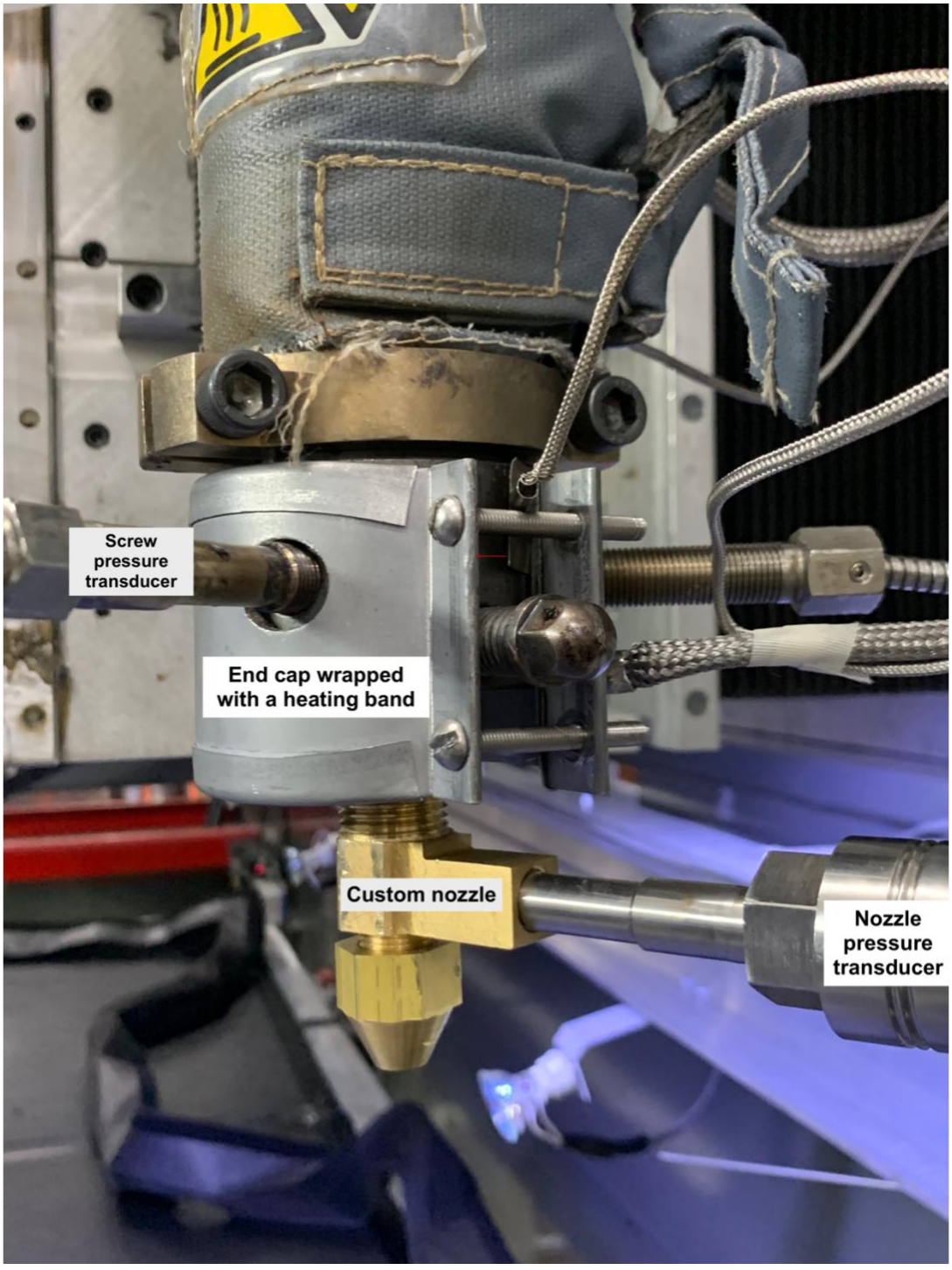


Figure 3.2. BAAM extruder end cap fitted with a custom designed 0.762 cm nozzle and pressure transducers

Results and Discussion

BAAM Extrusion: ABS 20 wt.% CF

Volumetric throughput Q of deposited beads was determined by dividing mass flow rate of each bead by melt density as described in the experimental methods section. For ABS 20 wt.% CF, there is a linear relationship between measured Q values and screw speed for all nozzle sizes (Figure 3.3). At low screw speeds (50 and 100 RPM), measured Q is independent of nozzle diameter. At 150 RPM, Q values deviate from this pattern and start to increase with increase in nozzle size. The largest nozzle (1.016 cm) has the highest Q values, while the 0.508 cm nozzle has the lowest.

Extrusion beyond 150 RPM with the 0.508 cm nozzle was not attempted to avoid damaging the BAAM extruder. Although the maximum barrel pressure is 68.9 MPa, caution is exercised to never reach this limit. As a result, safety measures are set in place: the rapture disk, designed as a one-time safety device that protects the extruder from over pressurization, has a limit of 34.47 MPa. To further mitigate damage to the rapture disc, the software stop limit is 24.13 MPa and “normal operating” pressure of the BAAM is set at 6.89 MPa. The normal operating pressure is thus used as the limit that should not be exceeded during extrusion to ensure minimal damage to the BAAM extruder.

In-situ monitoring of the extrusion process is captured and the resulting pressure change over bead deposition time is plotted in Figure 3.4 for the 1.016 cm nozzle for ABS 20 wt.% CF. Two characteristic areas are defined, transient start-up pressure and steady-state pressure. Transient start-up pressure is reached at the start-up of the extrusion process and steady-state pressure is reached when extrusion reaches steady flow. From Figure 3.4, it can be observed that as the screw speed increases, the start-up transient and steady-state pressures increase while the extrusion time decreases since screw speed controls the flow rate of the material out of the extruder.

BAAM Extrusion: PPSU 25 wt.% CF

One major challenge when extruding PPSU 25 wt.% CF on BAAM is failure to achieve the desired throughput. Unlike ABS 20 wt.% CF, Q appears to be independent of nozzle diameter as measured Q values are similar for all three nozzle diameters (Figure 3.5). During PPSU 25 wt.% CF extrusion, flow instabilities that impact final print quality such as irregular bead width, surface roughness, and instances of missing material in the deposited are observed at all screw speeds and across different nozzle sizes (Figure 3.6). These instabilities could be due to impacts on melt flow as a result of high melt viscosity properties of the fiber reinforced composite.

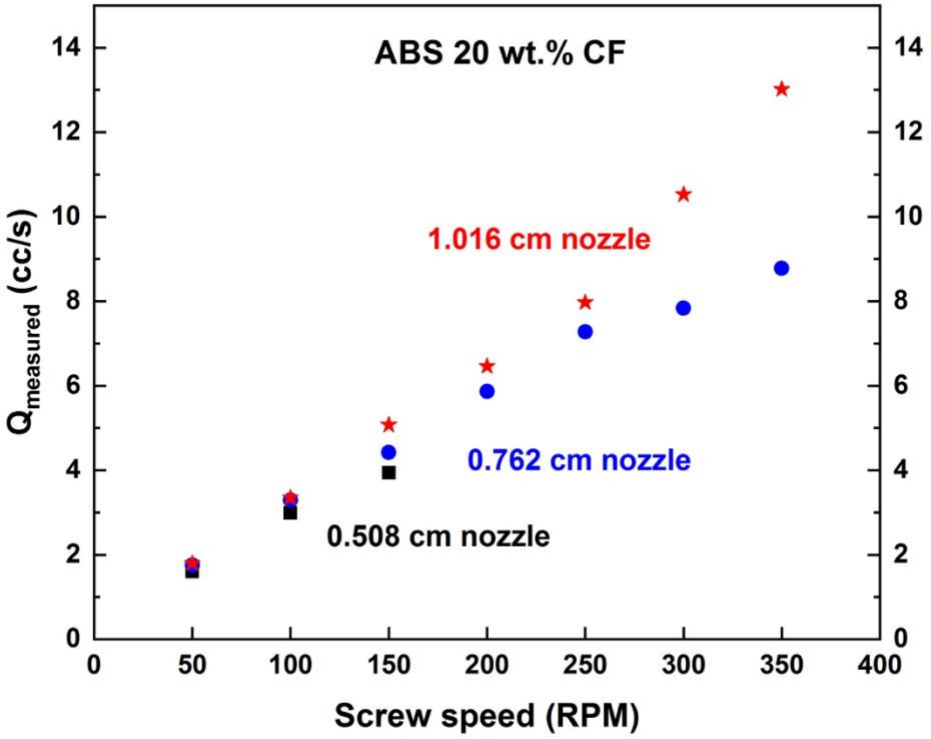


Figure 3.3. Measured volumetric flow rate vs screw speed for ABS 20 wt.% CF

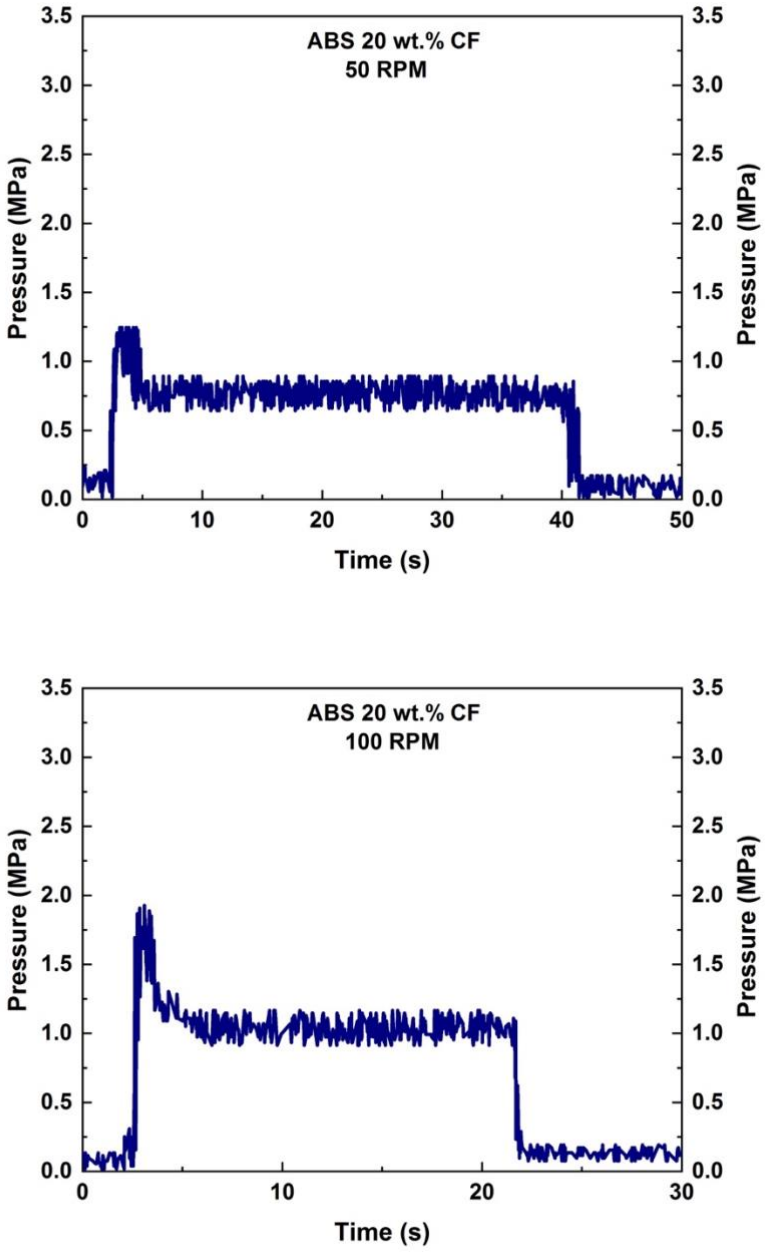
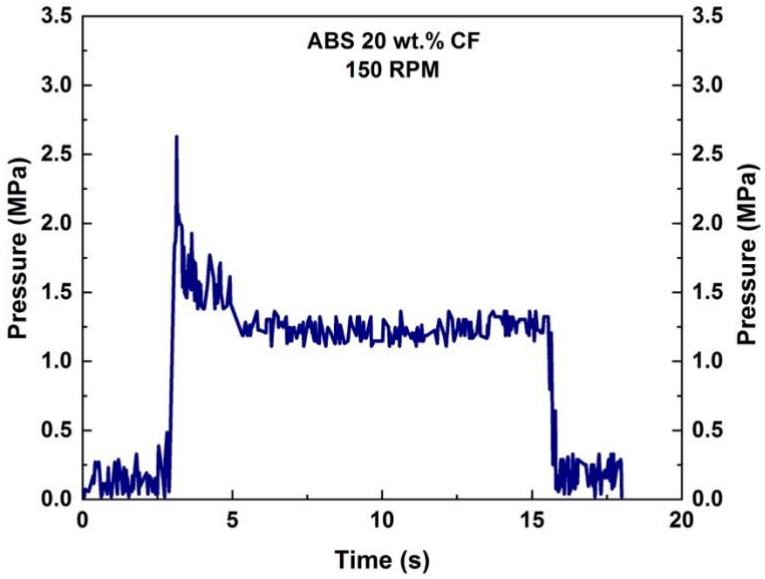


Figure 3.4. BAAM transient and steady-state pressure in the nozzle during ABS 20 wt.% CF extrusion at different screw speeds using the 1.016 cm nozzle



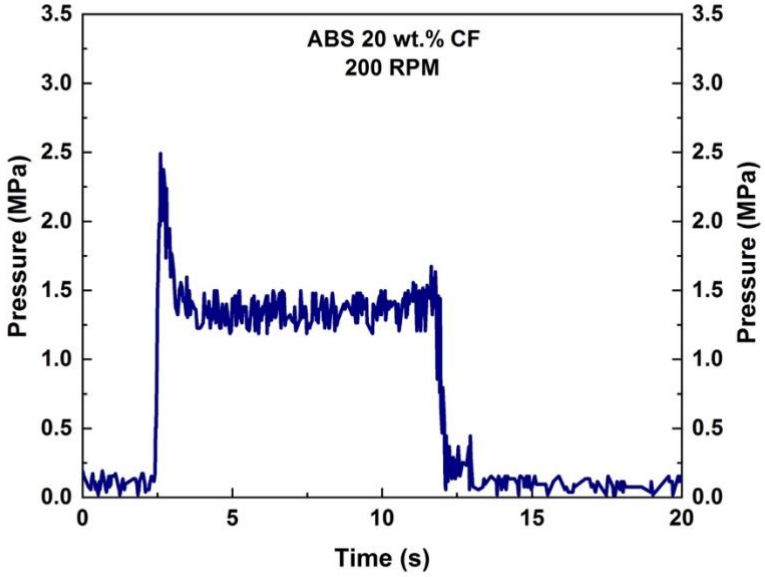
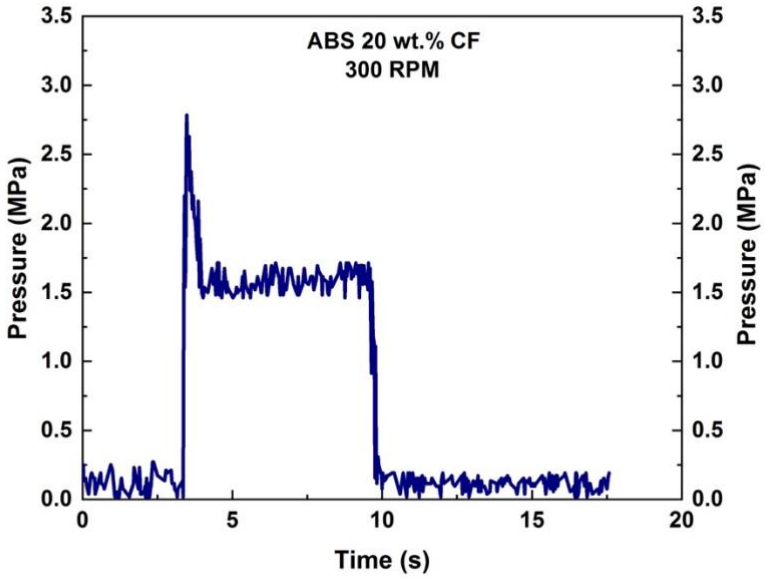


Figure 3.4. (Continued)



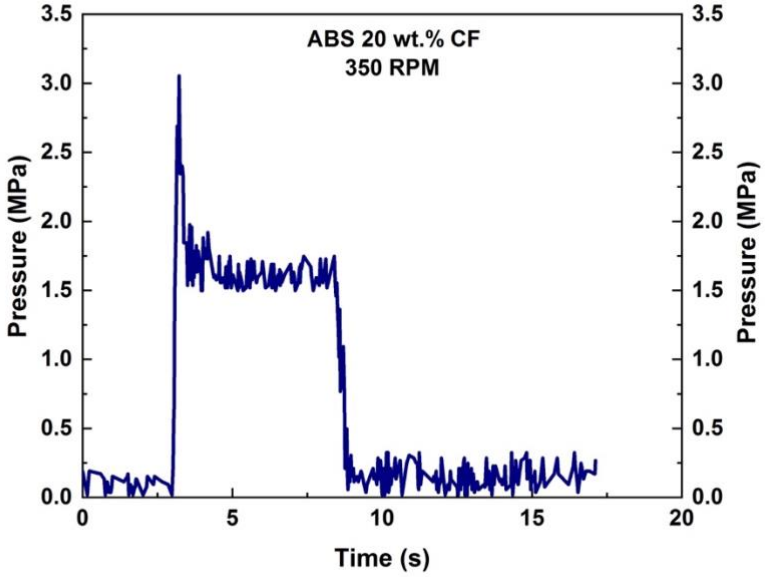


Figure 3.4. (Continued)

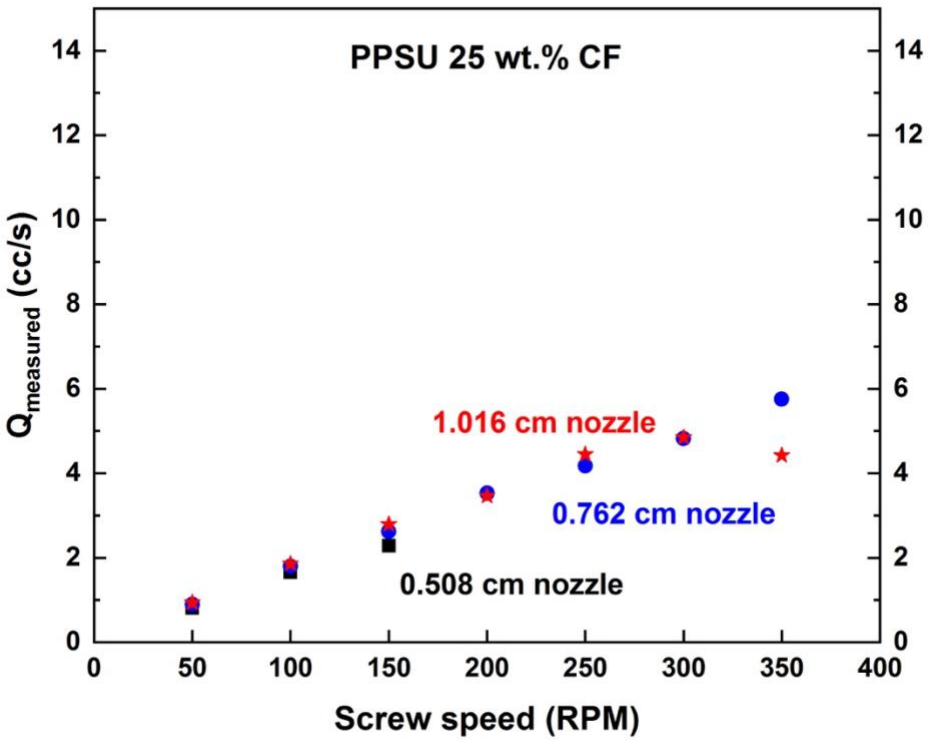


Figure 3.5. Measured volumetric flow rate vs screw speed for PPSU 25 wt.% CF

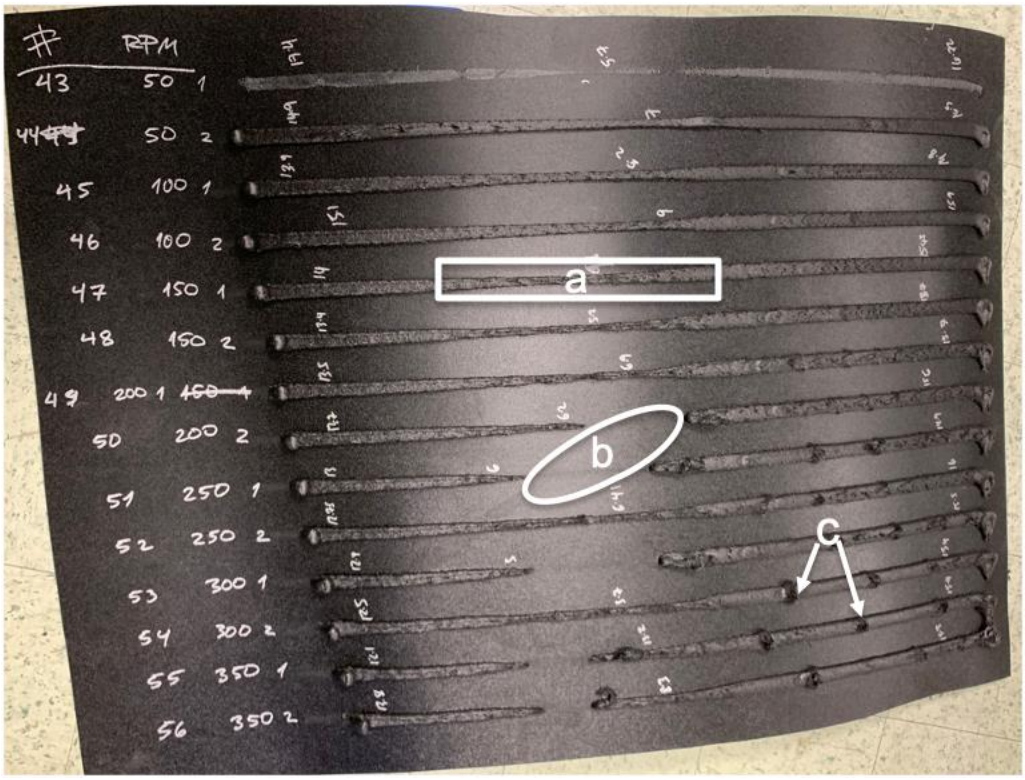


Figure 3.6. BAAM build sheet showing three kinds of flow instabilities (a) irregular bead width, (b) lack of material, and (c) surface roughness on PPSU 25 wt.% CF deposited beads using a 1.016 cm diameter nozzle at all screw speeds

These flow instabilities are captured in the BAAM nozzle pressure profile during extrusion. For example, pressure in the nozzle drops below steady-state when bead width is irregular at 100 and 150 RPM (Figure 3.7) whereas in instances where material is missing at screw speeds of 250 – 350 RPM, the pressure drops to the "holding" pressure (~0.345 MPa). Insufficient material during BAAM extrusion at 200 RPM resulting in print part defects has also been reported in PPS 50 wt.% CF, another high-performance composite [72].

The BAAM steady-state pressures for ABS 20 wt.% CF and PPSU 25 wt.% CF are presented in Figure 3.8. From the figure, it can be seen that the steady-state pressures for PPSU 25 wt.% CF are higher than those of ABS 20 wt.% CF for all nozzle sizes and Q values. For the 0.762 cm and 1.016 cm nozzle diameters, steady-state pressures increase with increase in Q at lower throughputs, but the values plateau at higher Q values. All steady-state pressures based on the BAAM nozzle measurements fall under the normal operating pressure of 6.89 MPa, represented by the dotted line in Figure 3.8. The BAAM steady-state pressures are compared to the Hagen-Poiseuille pressure drop predictions as well as computational fluids dynamics simulations using COMSOL Multiphysics software. Power-law fit n and C values were experimentally determined from parallel-plate rotational rheometry measurements. Frequency sweep tests for ABS 20 wt.% CF and PPSU 25 wt.% CF were performed at 250 ºC and 376 ºC, respectively. Frequency sweep tests for the neat resins were done for comparison and show the effect of adding carbon on the viscosity. Logarithmic plots of complex viscosity (η^*) as a function of angular frequency (ω) for ABS 20 wt.% CF and PPSU 25 wt.% CF materials are shown in figures 3.9 and 3.10, respectively.

Compared to PPSU, ABS is more shear thinning across the range of frequencies at which the tests were performed. This is reflected in the n and C values, with ABS having n values that are smaller, denoting more shear thinning behavior (Table 3.3). Results of the BAAM steady-state pressures, HP predicted pressure drop predictions along with COMSOL simulated pressures using parallel-plate n and C values in Table 3.3 are presented in Figures 3.11 and 3.12 for ABS 20 wt.% CF and PPSU 25 wt.% CF, respectively. For ABS 20 wt.% CF (Figure 3.11), HP predictions for the 1.016 cm nozzle are within 5-10% of BAAM steady-state nozzle pressures whereas COMSOL simulated pressure drop values are higher than both HP and BAAM steady-state pressures. For the 0.762 cm nozzle, HP predicted pressure drop values are 5-25% lower than BAAM steady state pressures while COMSOL predictions are 5-20% higher. For the 0.508 cm nozzle, HP and COMOSL underpredict pressures in the nozzle for ABS 20 wt.% CF. In the case of HP, pressure drop values are 68-90% lower than BAAM steady state pressures while COMSOL pressure drop predictions are 30-40% lower. Nozzle geometry and non-isothermal conditions in the extruder impose

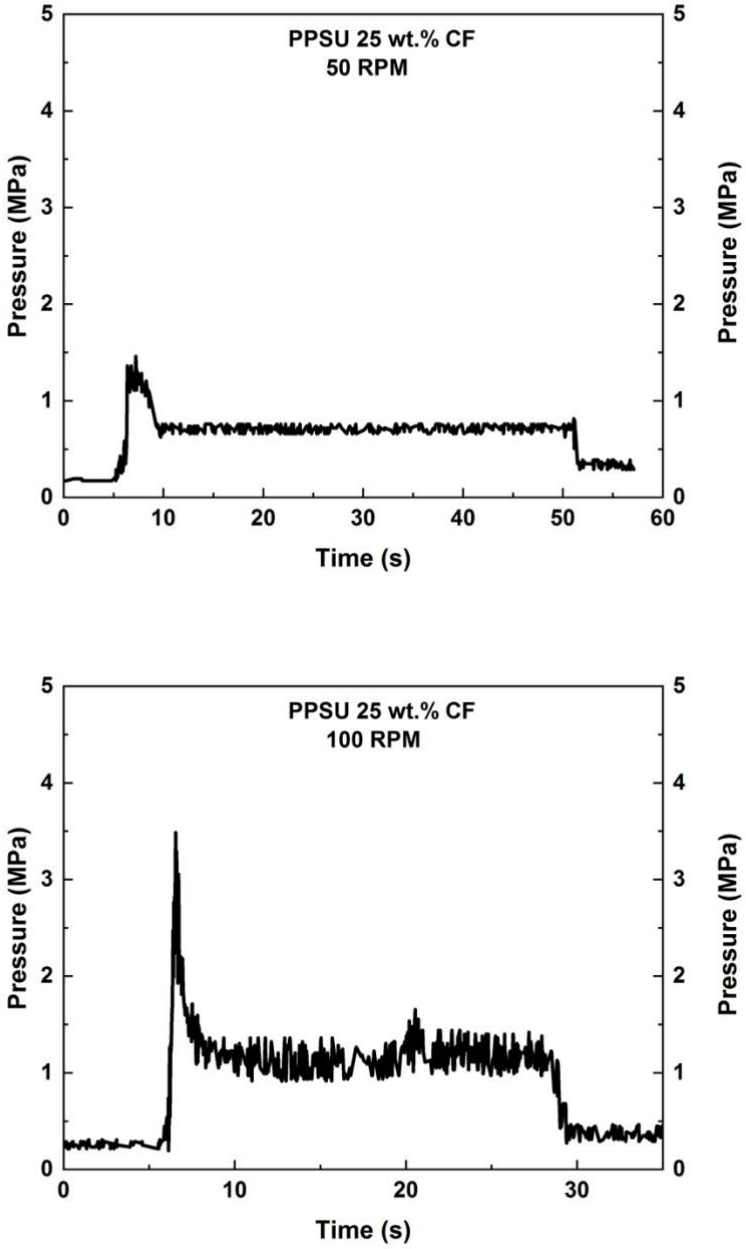
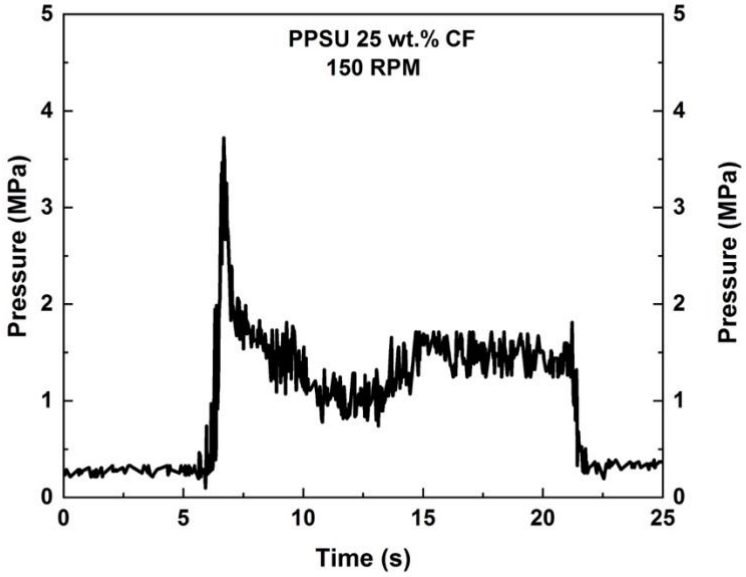


Figure 3.7. BAAM transient and steady-state pressure in the nozzle during PPSU 25 wt.% CF extrusion at different screw speeds using the 1.016 cm nozzle



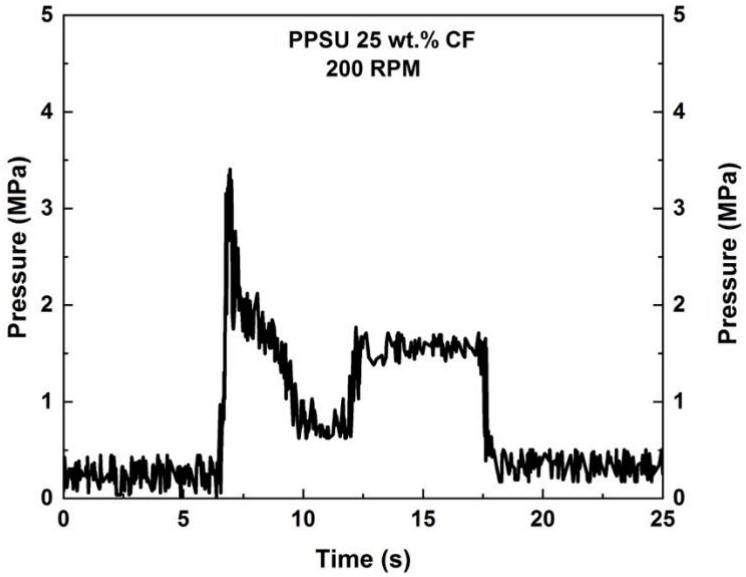
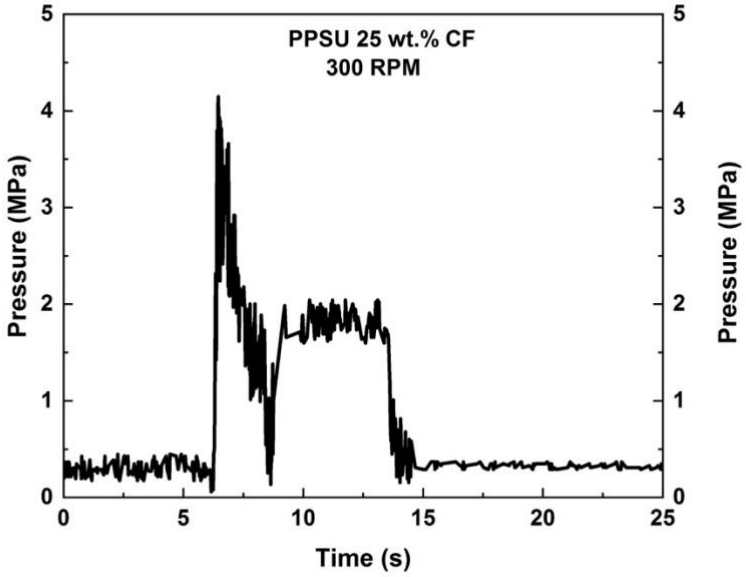


Figure 3.7. (Continued)



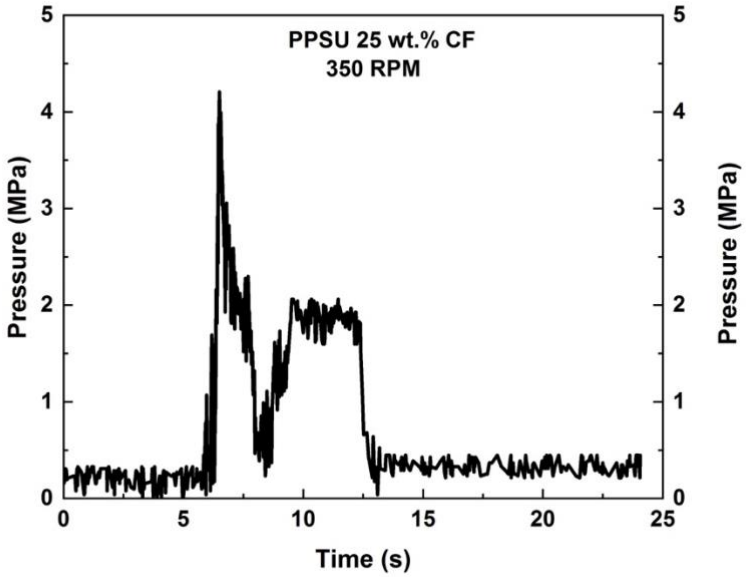


Figure 3.7. (Continued)

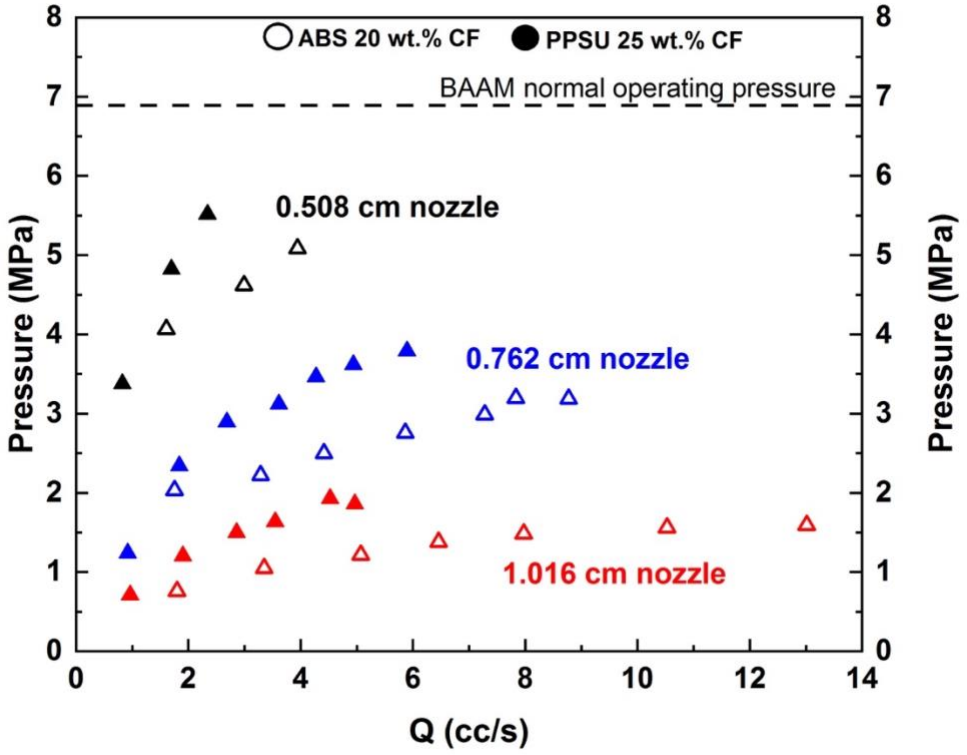


Figure 3.8. BAAM steady-state pressures vs volume flow rate (Q) for ABS 20 wt.% CF and PPSU 25 wt.% CF for different nozzle sizes

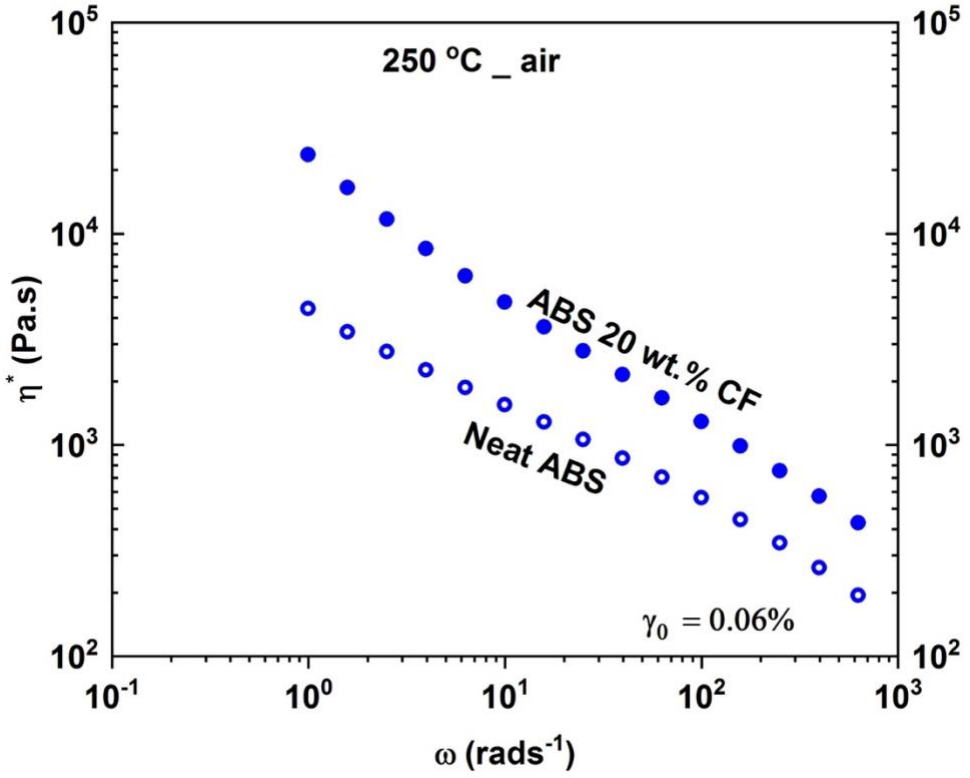


Figure 3.9. Complex viscosity vs angular frequency for neat and ABS 20 wt.% CF at 250 ºC in air

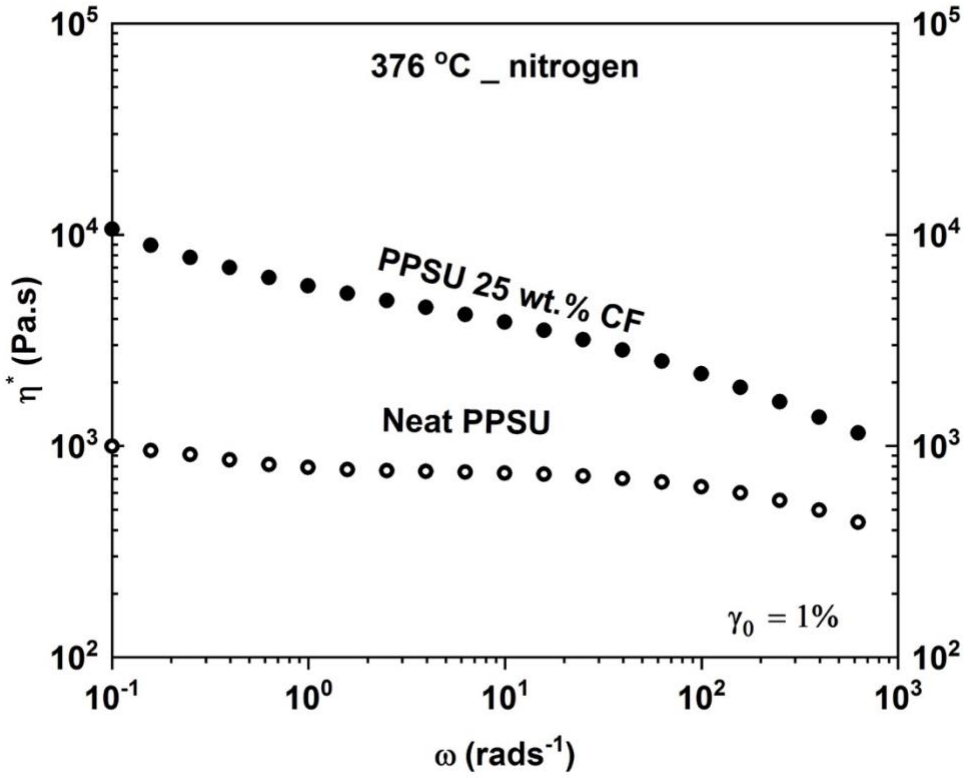


Figure 3.10. Complex viscosity vs angular frequency for neat and PPSU 25 wt.% CF at 376 ºC in nitrogen

Table 3.3. Parallel-plate rheological parameters of ABS 20 wt.% CF and PPSU 25 wt.% CF used in the COMSOL simulation

Test temperature (°C)	250		376	
Material	ABS	ABS 20 wt.% CF	PPSU	PPSU 25 wt.% CF
C	4455.9	20499	835.7	6031
n	0.536	0.396	0.928	0.77
Melt density (g/cc)	0.97		1.29	

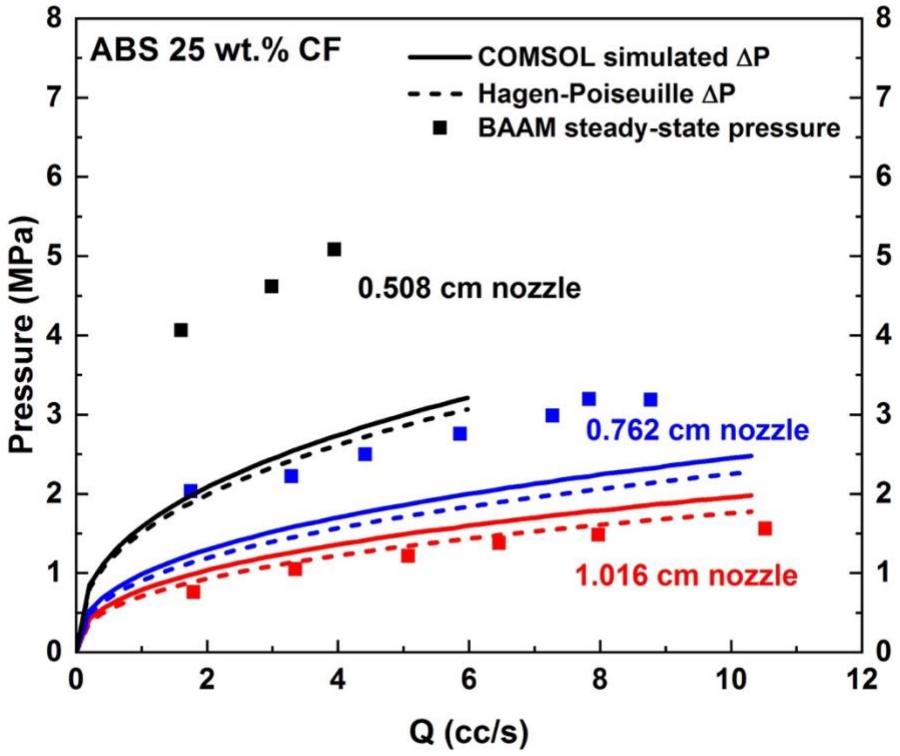


Figure 3.11. ABS 20 wt.% CF BAAM steady-state pressures, Hagen-Poiseuille predicted pressure drop, and COMSOL simulated nozzle pressures as a function of volume flow rate (Q)

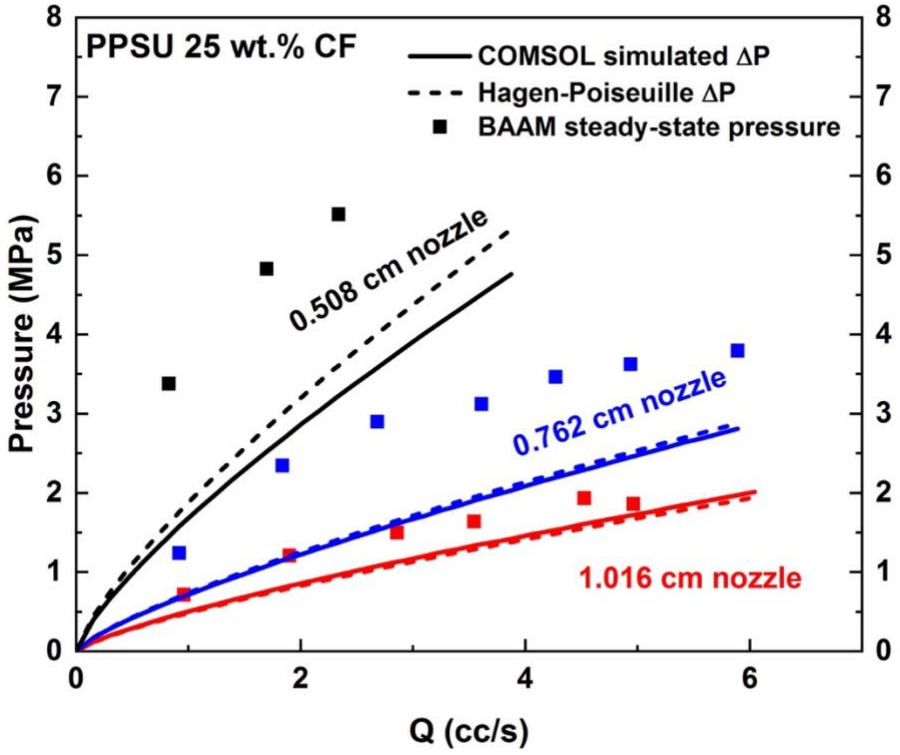


Figure 3.12. PPSU 25 wt.% CF BAAM steady-state pressures, Hagen-Poiseuille predicted pressure drop, and COMSOL simulated nozzle pressures as a function of volume flow rate (Q)

limits on the use of HP and COMSOL to predict BAAM pressures for the 0.508 cm and 0.762 cm nozzle diameters.

The results for PPSU 25 wt.% CF (Figure 3.12) are very similar to those of ABS 20 wt.% CF where the analytical and numerical models are able to predict within acceptable reason, the pressure in the 1.016 cm nozzle, but underpredict for the 0.508 cm and 0.762 cm nozzle diameters. These initial results prompted the use of the BAAM steady-state pressures to calculate n and C inputs for the HP model and COMSOL CFD simulations. Using the BAAM as a capillary rheometer, viscosity and shear rate values are calculated as detailed in the Appendix and tabulated in Table 3.1.

Measured steady-state pressures for ABS 20 wt.% CF are compared to predicted pressure drop (ΔP) calculations in the BAAM nozzle. BAAM steady-state pressures are used to numerically solve for the power-law coefficient C and the shear thinning exponent, n. These n and C values are then used as inputs for the Hagen-Poiseuille pressure drop model as well as COMSOL simulated pressure drops (Table 3.1). For details on how the BAAM is adapted and used as a rheometer, please refer to the Appendix section, “BAAM as a Rheometer” for more details. Theoretical ΔP values based on measured flow rate are calculated using the HP Equation and the power law model and numerical simulations of pressure in the BAAM nozzle using COMSOL Multiphysics software simulated predicted ΔP values are plotted as a function of measured BAAM Q for all nozzle diameters (Figure 3.13 and Figure 3.14). HP predictions are in close agreement with measured BAAM steady-state nozzle pressures while COMSOL simulated ΔP are higher than BAAM steady-state pressures by 10-15 % and 2-10% for 0.762-cm and 1.016-cm nozzle diameters, respectively for ABS 20 wt.% CF. For PPSU 25 wt.% CF, HP predicted and COMSOL simulated values using BAAM n and C inputs accurately predict pressure values in the nozzle.

The transient pressures for all three nozzle diameters are plotted as a function of screw speed. It is observed that at 150 RPM, ABS 20 wt.% CF (Figure 3.15) start-up transient pressure exceeds normal BAAM operating pressure of 6.89 MPa. Assuming that transient pressures in the 0.508 cm nozzle follow the same pattern as the 0.762 cm and 1.016 cm nozzles, and pressures increase with increase in screw speed, extrusion beyond 150 RPM for the 0.508 cm would cause BAAM operation to be outside the preferred operational zone and most likely put it out of commission.

Like ABS, transient start-up pressures in the nozzle increase with increase in screw speed (Fig. 3.16). Extrusion was not attempted above 150 RPM with the 0.508 cm nozzle as well due to the high pressures in the nozzle and screw that can damage the BAAM extruder and put it out of commission. From Figure 3.16,

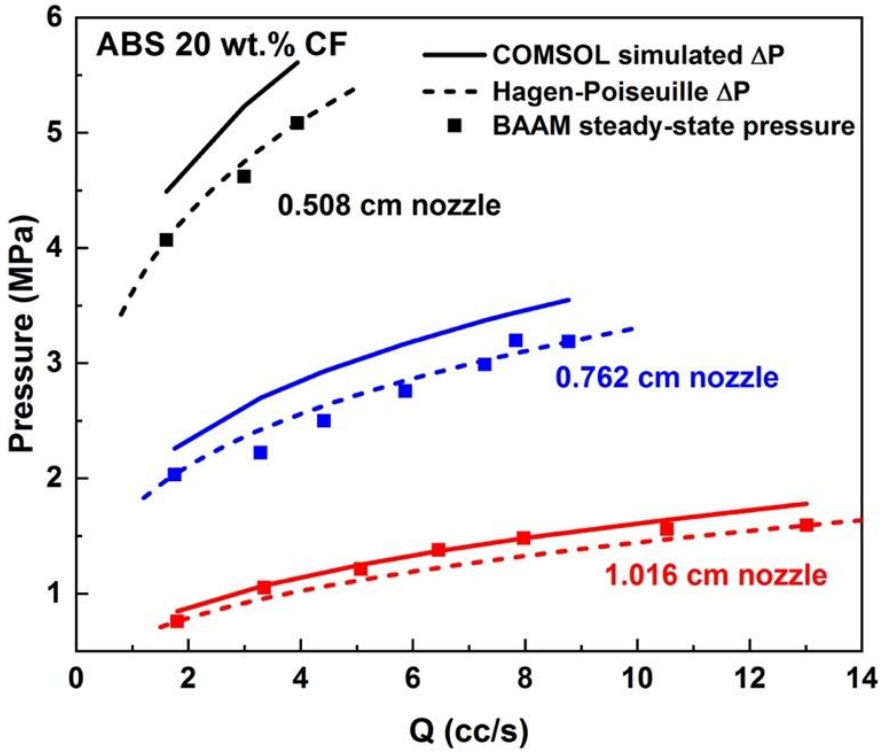


Figure 3.13. Theoretical and experimental ΔP for ABS 25 wt.% CF as a function of measured volumetric flow rate (Q)

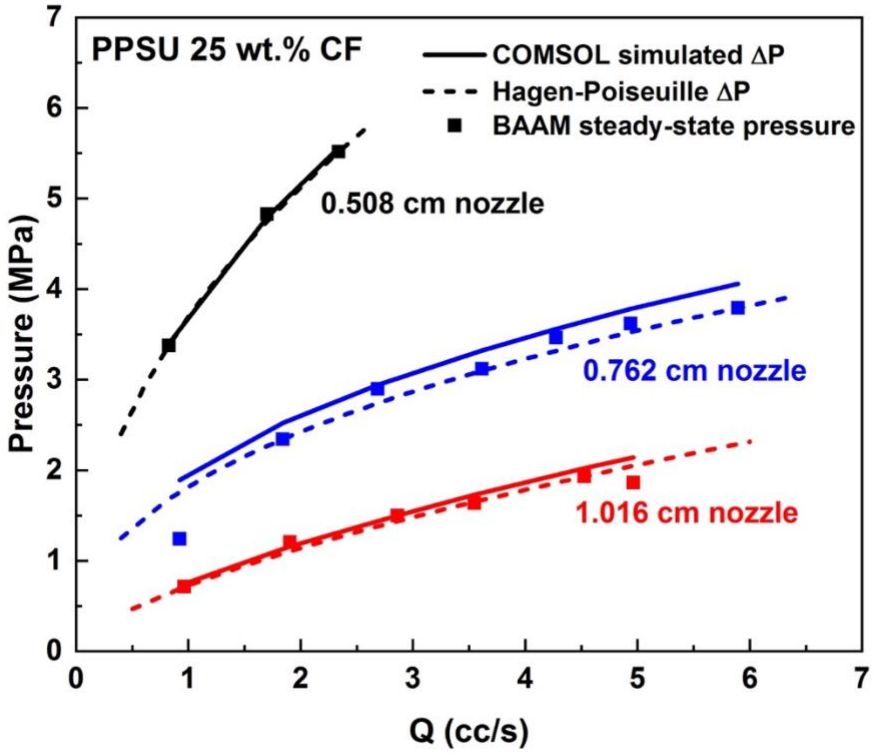


Figure 3.14. Theoretical and experimental ΔP for PPSU 25 wt.% CF as a function of measured volumetric flow rate (Q)

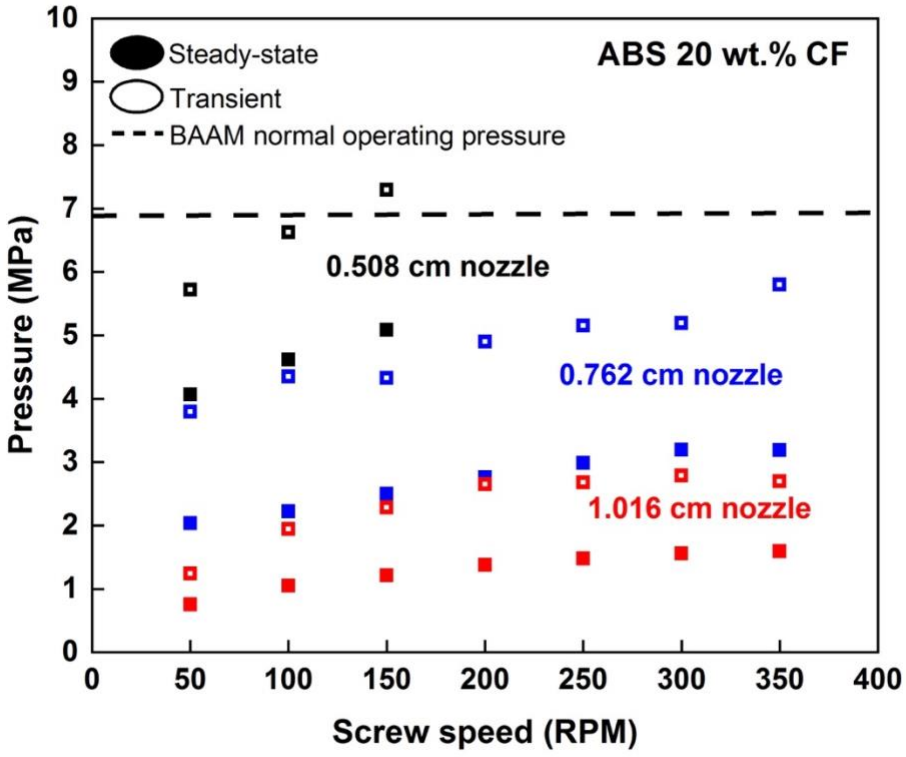


Figure 3.15. Transient and steady-state pressures during BAAM extrusion of ABS 20 wt.% CF beads at all screw speeds and different nozzle sizes (Deposition temperature: 250 °C)

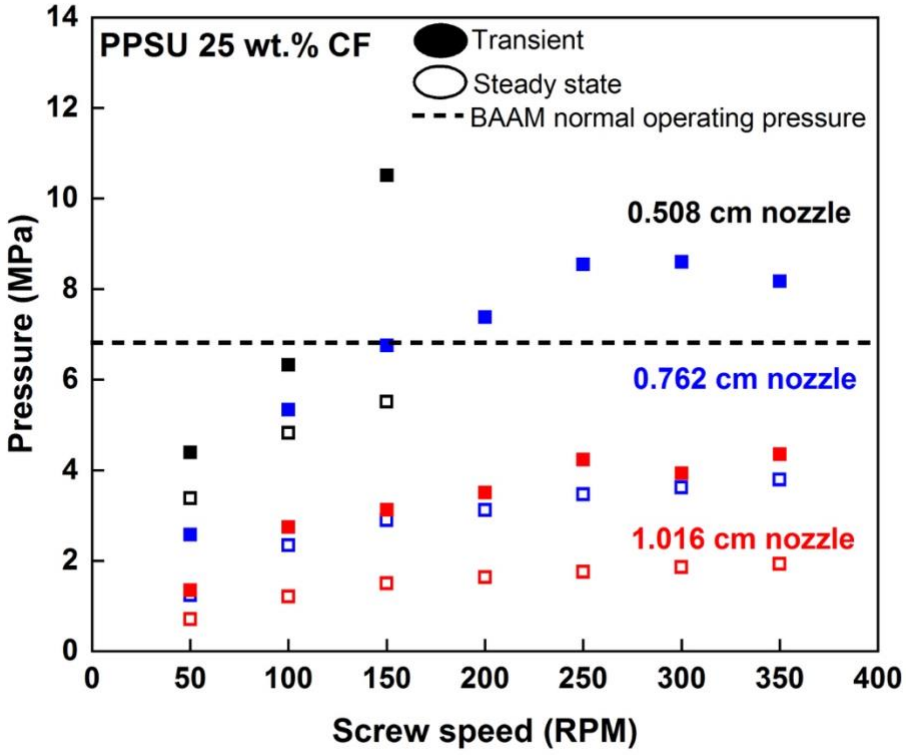


Figure 3.16. Transient and steady-state pressures during BAAM extrusion of PPSU 25 wt.% CF beads at all screw speeds and different nozzle sizes (Deposition temperature: 355 °C)

transient pressures for 0.762 cm nozzle also exceed the “normal operating” pressure of the BAAM set at 6.89 MPa. Although the steady-state pressures are well below the normal operating limit, deposition of PPSU 25 wt.% CF would still pose a challenge at screw speeds greater than 150 RPM because of the strain that the system would be under. These measurements are an indication of the importance of studying the transient effects during starts-and-stops.

Relationship Between Transient Start-up and Steady-State Pressures

Pressure drop predictions using analytical methods such as the Hagen-Poiseuille equation predict the steady-state pressure. They do not account for the transient start-up pressure which is likely to exceed the system operating pressure preventing extrusion. Based on BAAM pressure readings in the nozzle during extrusion, we can define a relationship between transient start-up pressures and steady-state pressures. In ABS 20 wt.% the transient pressure is 1.4x – 2x higher than steady-state pressure while for PPSU 25 wt.% CF, transient pressure ranges between 1.2x – 2.5x higher than steady-state pressures for the 0.508 cm and 1.016 cm nozzles respectively. Therefore, if steady-state pressure is correctly predicted using any of the analytical equations, the transient pressure can be determined and used to decide if extrudability is possible or not given material properties of the candidate feedstock. Transients during BAAM starts-and-stops also indicate screw speeds and nozzle geometries that could put the BAAM system out of commission, a costly process. For both ABS 20 wt.% CF and PPSU 25 wt.%, extrusion above 150 RPM using the 0.508-cm nozzle exceeds normal operating pressure limits of the BAAM. In the case of PPSU 25 wt.% CF, screw speeds above 150 RPM for the 0.762-cm nozzle also result in transient start-up pressures that are above the operating limit.

Stress Relaxation

When a polymeric material is subjected to a step increase in strain, the stress relaxes in an exponential fashion. The stress relaxation is converted to a relaxation modulus, G(t):

$$G(t) = \frac{\tau(t)}{\gamma} \tag{3.4}$$

$G(t)$ can be measured directly, and the function is an exponential decay using the Maxwell Model Governing Equation:

$$G(t) = G_0 e^{-t/\tau} \tag{3.5}$$

where τ is the relaxation time and G_0 is the relaxation modulus at t = 0.

Stress relaxation [92], transient rheology tests, are often used to investigate the elastic responses on longer time scales and show how the structure relaxes. There are 4 distinct regions during the relaxation behavior of most polymeric materials [44,93]. In the glassy region, the material is hard and brittle, hard to measure given instrument limitation. In the transition region, short range molecular motions come into play, this is where the relaxation of stress occurs without interference from entanglements. In the plateau region, further relaxation is inhibited by entanglements, the value of G(t) in this region is the plateau modulus, and eventually the molecule can escape its entanglements through reptation and begin to flow in the terminal zone. In the case of rubbery materials, they cannot flow because of chemical crosslinks and relax by means of Brownian motion in the longer times [44,93].

Stress relaxation tests are time and temperature dependent especially around the glass transition temperature. Tests performed at lower temperatures are used to record the initial relaxation, while tests performed at higher temperatures capture the end of the relaxation of the rapidly decaying stresses [93]. High temperatures lead to short molecular relaxation times and low temperatures lead to materials with long relaxation times. This is due to the fact that at low temperatures the free volume is larger and the molecules can move with more ease. Hence, when changing temperature, the shape of creep or relaxation test results remain the same except that they are horizontally shifted to the left or right, which represent shorter or longer response times, respectively [93]. The time-temperature equivalence seen in stress-relaxation test results can be used to reduce the data at various temperatures to one general master curve for a reference temperature, using the time-temperature superposition principle. To generate a master curve, the curves are shifter by a horizontal shift factor, a_T. Williams, Landel and Ferry (WLF) chose a reference temperature of 243 K which holds true for nearly all polymers if the chosen reference temperature is 45 K above the glass transition temperature [93].

The stress relaxation tests in this work were performed at 230 ºC and 340 ºC for ABS 20 wt.% CF and PPSU 25 wt.% CF, respectively. These temperatures are within the BAAM deposition range for both materials and they are 110 ºC above their respective glass transition temperatures [43]. The time-dependent relaxation modulus curves of ABS 20 wt.% CF and PPSU 25 wt.% CF are plotted against time in Figure 3.17. ABS 20 wt.% CF and PPSU 25 wt.% CF exhibit distinct relaxation dynamics. ABS 20 wt.% CF is more elastic than PPSU 25 wt.% CF and has a high plateau modulus of ~10_4 Pa that is maintained over a longer time scale. The high plateau modulus of ABS 20 wt.% CF contributes to the good processability of the composite on BAAM. The high plateau modulus also contributes to retention of the bead shape during solidification. PPSU 25 wt.% CF composite takes a long time to reach its plateau modulus of ~400 Pa. Having a lower elasticity than ABS 20 wt.% CF contributes to the printability

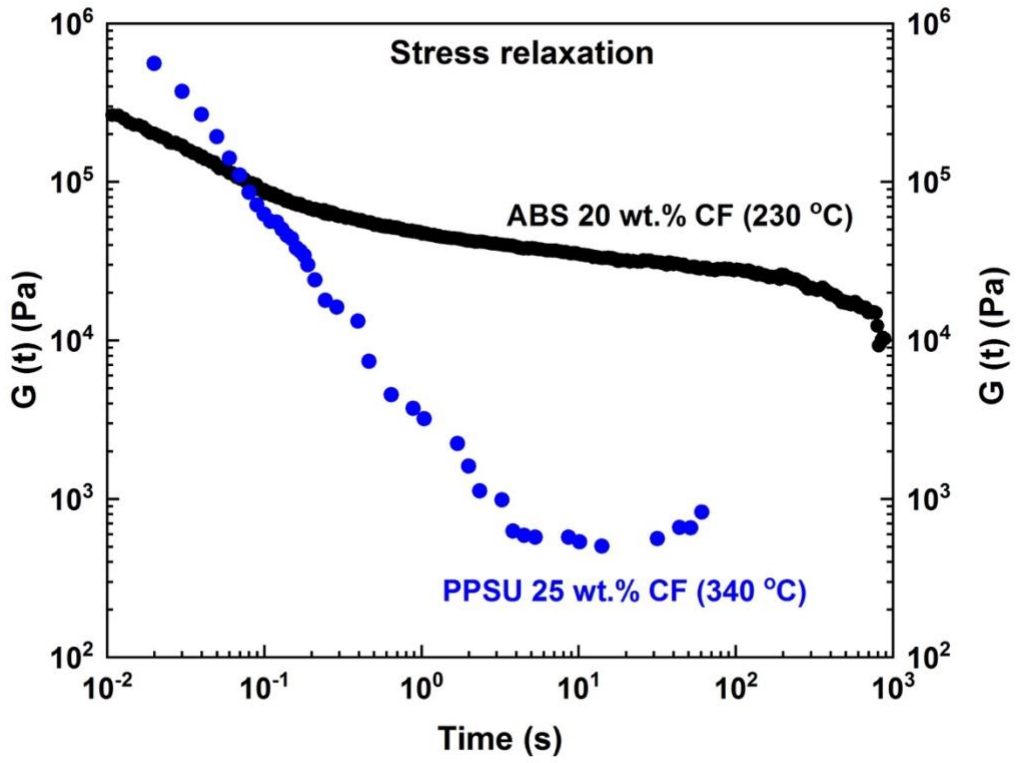


Figure 3.17. Relaxation modulus of ABS 20 wt.% CF at 230 ºC, strain = 0.06% and PPSU 25 wt.% CF at 340 ºC, strain = 1%

issues that researchers have faced when depositing PPSU 25 wt.% CF on the BAAM [72]. The relaxation time, τ, is taken to be the time it takes the initial relaxation G_0 to relax to 1/e (36.7%). For ABS 20 wt.% CF, $\tau = 0.07s$, and for PPSU 25 wt.% CF, $\tau = 0.05s$. The relaxation time described herein captures the instantaneous material response when the imposed strain is removed (usually t < 0.1 s). Since higher temperatures promote faster relaxation, PPSU 25 wt.% CF relaxes 0.02s faster than ABS 20 wt.% CF. However, the macroscopic relaxation times for high molecular weight polymeric systems such as ABS 20 wt.% CF and PPSU 25 wt.% CF are not due to the slow dynamics on the monomer scale but arise from the chain connectivity and the restriction that the backbones cannot cross which happen over longer time scales [94]. Data collected from the BAAM system and capillary rheometer during extrusion are on these longer time scales and the relaxation dynamics are not be accurately captured by rotational rheometry measurements. To describe the pressure decay of AM feedstock during extrusion, a characteristic decay time, which is a function of nozzle geometry, is defined.

Stress relaxation tests are commonly employed to observe the timescales at which polymer chains relax through short-range and long-range thermal motions [44]. When entanglements hinder chain relaxation, a stress plateau or rubbery regime is observed, for which the plateau modulus is defined. The magnitude of this plateau modulus is related to the molecular weight of polymer segments between entanglements; a property unique to the structure of the polymer chain [45]. Beyond the plateau regime, with sufficient time, terminal relaxation results in a total stress reduction. For neat resins, an increase in molecular weight prolongs the stress relaxation to longer time scales. Since time and temperature are proportional, the terminal region may be entered with higher processing temperatures [46]. The added complexity of filler reinforcement can lead to networks which must first be destroyed to sufficiently reduce the stress. However, the buildup of a filler network after flow cessation is much quicker than the buildup of entanglement networks [47]. By controlling temperature, molecular weight, and filler concentration, a polymer can exhibit significant shear thinning behavior from filler network breakdown to allow extrusion through the nozzle, high zero-shear viscosity within extruder torque limits, and fast filler network buildup to maintain the shape of the deposited bead.

Characteristic Decay Time

Capillary Rheometer

The pressure required to extrude ABS 20 wt.% CF from the capillary rheometer increases with increase in shear rate and L/D ratio (Figure 3.18). This behavior

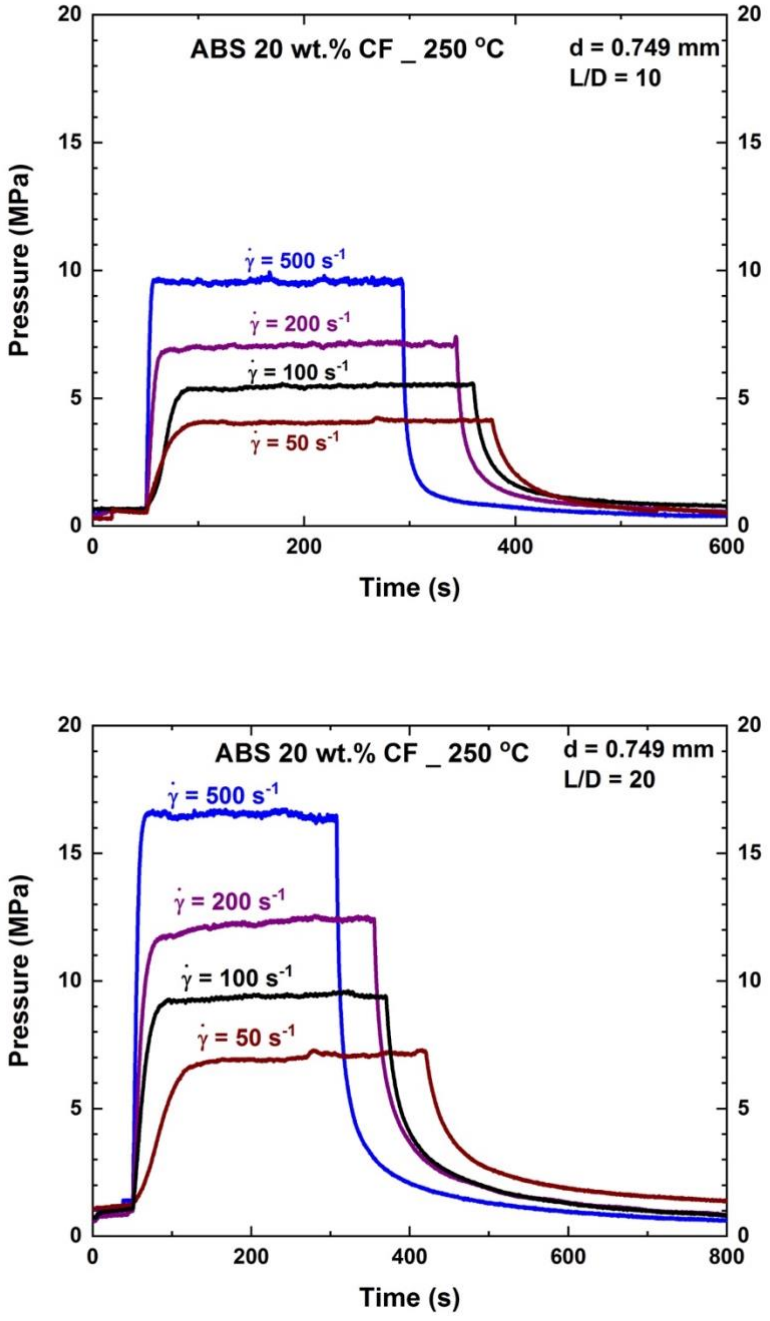


Figure 3.18. Transient and steady-state pressure of ABS 20 wt.% CF extrusion at different shear rates and L/D ratios in the capillary rheometer

is similar to what has been observed in literature for linear low density polyethylene [79]. However, the appearance of a pressure maxima at start-up is not distinct at all shear rates.

The pressure drop decay profile of ABS 20 wt.% CF following cessation of flow follows an exponential decay pattern. To characterize this relaxation behavior, the Maxwell Model is adapted:

$$P(t) = (P_{SS} - P_H)e^{-\frac{t}{\lambda}} + P_H \tag{3.6}$$

where λ is the characteristic decay time, P_{SS} is the steady-state pressure, and P_H is the holding pressure. The characteristic decay time is defined as the time it takes the reach 36.7% (1/e) of the steady-state pressure (P_{SS}). In the capillary rheometer, this characteristic decay time decreases with increase in shear rate and is smaller for smaller L/D ratios (Figure 3.19). These trends are similar to what has been observed in literature for drilling fluids [95]. However, Reynolds et. al. did not find a clear dependence of the characteristic decay time of polystyrene with shear rate [96]. More work needs to be done to understand how shear rate influences the characteristic decay time for AM feedstock.

BAAM

The characteristic decay time for BAAM feedstock was quantified. Similar to capillary rheometry measurements, the pressure decay profile once extrusion stopped was monitored and the time taken to reach 36.7% of BAAM steady-state pressure was calculated. To observe the impact of nozzle diameter on the characteristic decay time, the pressure extrusion profiles of ABS 20 wt.% CF at 150 RPM for the 0.508 cm, 0.762 cm, and 1.016 cm nozzles were plotted as a function of deposition time (Figure 3.20). From the figure, the largest nozzle diameter has the shortest characteristic decay time because of the larger size of the orifice which promotes faster relaxation. At 150 RPM, the characteristic decay times for the 0.508 cm, 0.762 cm, and 1.016 cm nozzle sizes are 0.24s, 0.13s, and 0.11s, respectively.

The characteristic decay times for both ABS 20 wt.% CF and PPSU 25 wt.% CF as a function of screw speed and varying nozzle sizes were analyzed and plotted in Figure 3.21. It can be observed that when using a similar nozzle diameter to extrude, the characteristic decay time decreases with increase in screw speed and beings to plateau at 250 RPM for both materials. At low screw speeds (less than 250 RPM), material properties such as elasticity influence how quickly the pressure decays once extrusion stops. For instance, in Figure 3.21, the characteristic decay times for PPSU 25 wt.% CF are higher than ABS 20 wt.% CF for all nozzle diameters at these screw speeds. Compared to PPSU 25 wt.%

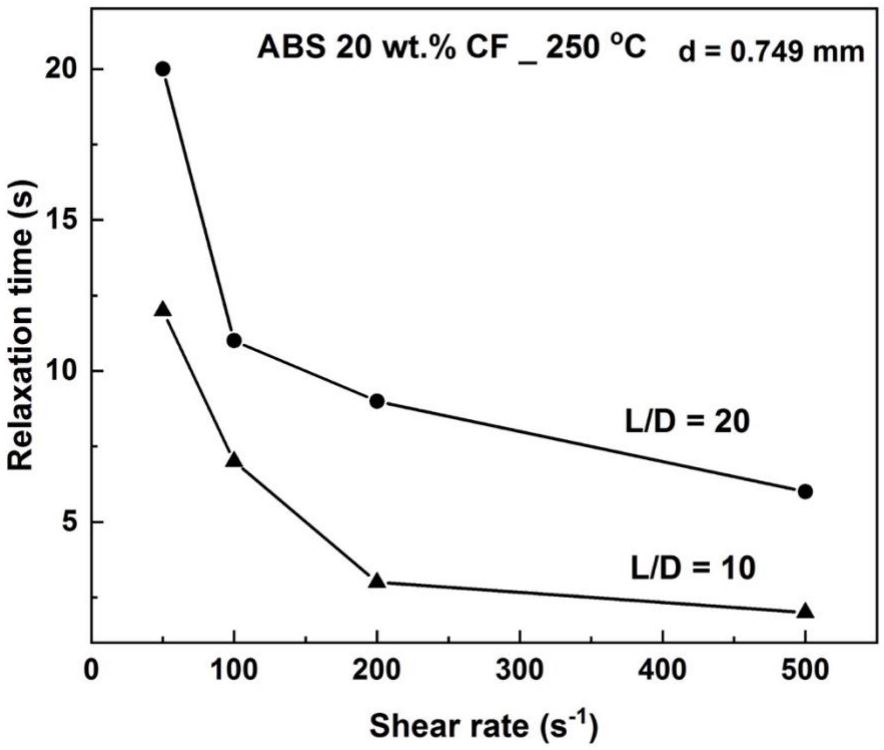


Figure 3.19. Characteristic decay time for ABS 20 wt.% CF on the capillary rheometer as a function of shear rate for varying L/D ratios and die diameter = 0.749 mm (Test temperature = 250 ºC)

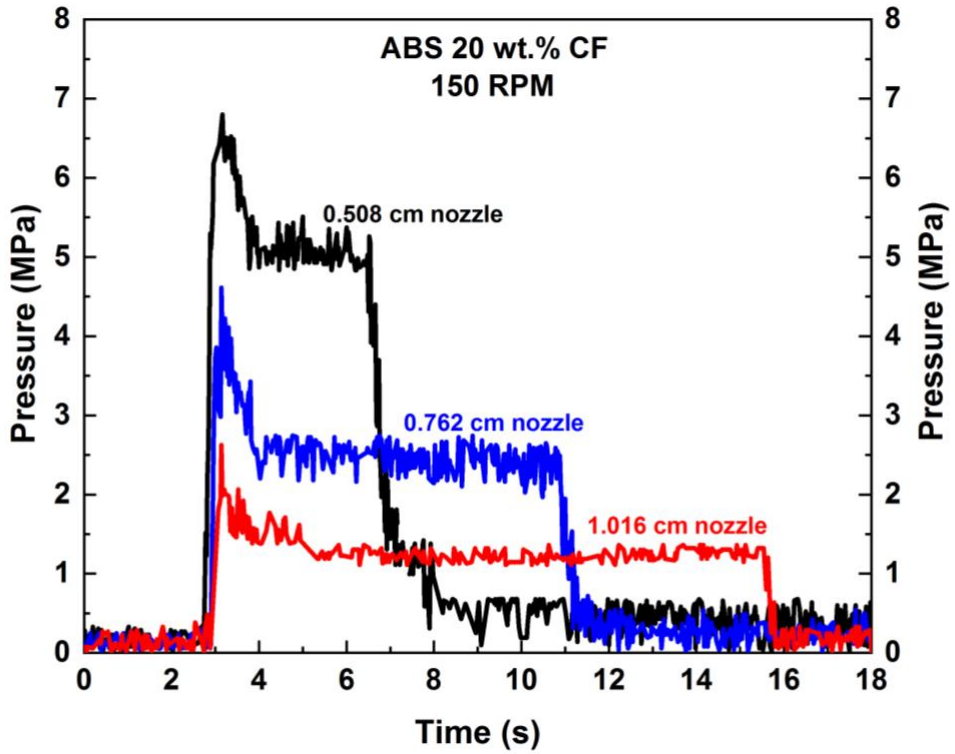


Figure 3.20. Transient and steady-state pressure profile of ABS 20 wt.% CF at 150 RPM deposited at 250 ºC

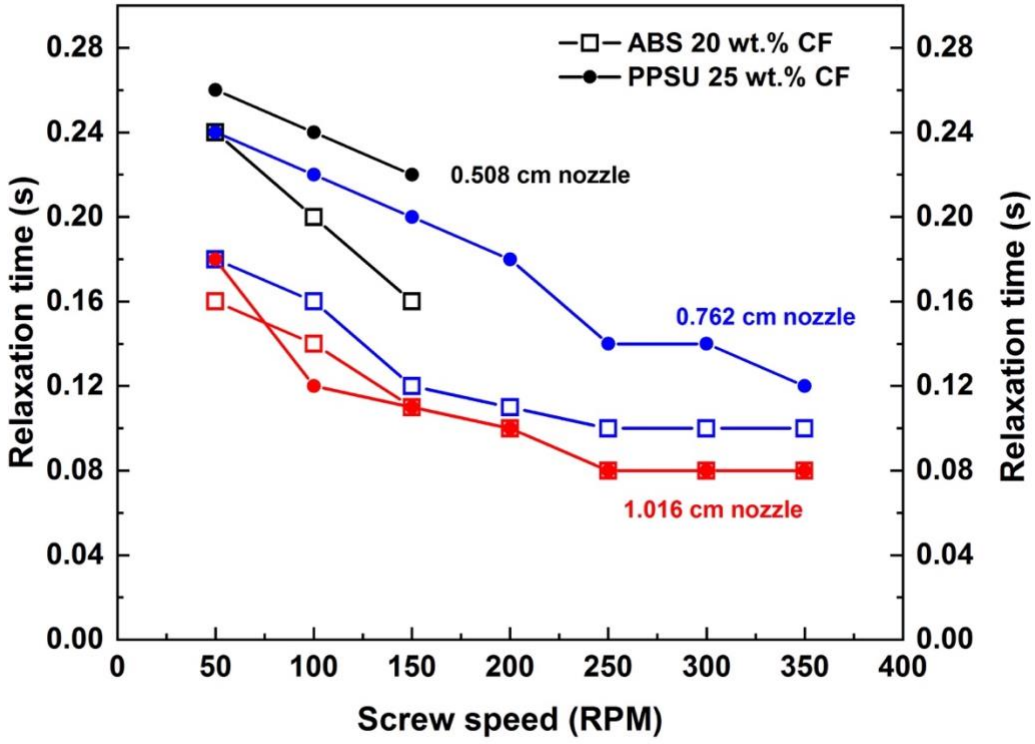


Figure 3.21. BAAM characteristic decay times for ABS 20 wt.% CF and PPSU 25 wt.% CF as a function of screw speed for nozzle diameters (ABS 20 wt.% CF was deposited at 250 ºC, PPSU 25 wt.% CF was deposited at 355 ºC)

CF, ABS 20 wt.% CF has a higher elasticity and lower entanglement density hence faster characteristic decay times [94]. At screw speeds greater than 250 RPM, characteristic decay times plateau for the 0.762 cm and 1.016 cm nozzles. At these screw speeds, the volume of the system along with the cross-sectional area of the nozzle play a bigger role in influencing the characteristic decay time. The largest nozzle size (1.016 cm) has the shortest characteristic decay times for both materials because the cross-sectional area for pressure release is larger compared to the 0.762 cm nozzle. However, as the nozzle diameter size decreases, the characteristic decay time is higher due to compressibility effects. During deformation, there is a pressure build up before the contraction in the geometry which causes some compression of the polymer before the geometry. When extrusion stops, the polymer continues to flow to recover the change in density, as well as relaxing stress via polymer motion [96].

Material compressibility plays a big role in the characteristic pressure decay times for polymer melts and composite systems [79,80]. In the case of incompressible flow, there is a very fast decrease in characteristic decay time towards the holding pressure. Compressibility not delays the reaching of the holding pressure, and the higher it is the longer the time it takes to achieve the holding pressure. The material compressibility factors for ABS 20 wt.% CF and PPSU 25 wt.% CF were not measured. Future work will need to characterize the compressibility to support these assertions.

Influence of Characteristic Decay Time on BAAM Processing Conditions

Material ooze during BAAM extrusion is an issue that impacts print quality because of seam defects during the frequent starts and stops of the BAAM process [78]. This challenge is magnified in large-scale components which limits the applicability of BAAM parts in tooling applications [72]. Oozing from the nozzle does not happen in a fraction of a section, but rather, material comes out very slowly over a long period of time. From a practical standpoint, the characteristic decay times can be used to inform BAAM processing conditions such as screw speed and nozzle geometry for different composites used. When extruding PPSU 25 wt.% CF on the BAAM, use of a large diameter nozzle (1.016 cm) and screw speeds greater than 250 RPM is recommended due to shorter characteristic decay times. Shorter characteristic decay times for AM feedstock are preferred for improved print conditions because it makes it manageable to keep the “mess” in one spot during deposition and avoid stringing it along the whole printed part. Similarly, larger nozzle diameters are preferred because material oozes out faster ensuring that the “mess” is contained in one area of the print. The viscoelastic behavior of AM feedstock also influences the characteristic decay time. ABS 20 wt.% CF has a higher plateau modulus and is more elastic than PPSU 25 wt.% CF. This contributes to the ease with which ABS 20 wt.% CF can be processed and deposited on the BAAM. Although the relaxation time of PPSU 25 wt.% CF is 0.02s faster than that of ABS 20 wt.% CF, this relaxation time does not account for

the duration of time it takes for PPSU 25 wt.% CF to reach its low plateau modulus of 400 Pa. Such a low plateau modulus leads to poor bead formation since the chains take a long time to entangle after deposition occurs, thus poor print quality. For a more detailed discussion of the influence of viscoelastic properties on BAAM processing conditions, please refer to Chapter Four of this dissertation.

Summary and Conclusions

Custom-designed nozzles capable of measuring and recording pressure distribution were designed and tested on the BAAM extruder system during extrusion of ABS 20 wt.% CF and PPSU 25 wt.% CF. This design enables process monitoring which is of interest to the AM community for quality control purposes such as changes in the flow rate which lead to inconsistent extrusion and print defects when depositing PPSU 25 wt.% CF. Transient start-up pressures in BAAM were also quantified for the first time and inform BAAM operations. In both ABS 20 wt.% CF and PPSU 25 wt.% CF, extrusion above 150 RPM is not recommended for 0.508 cm nozzle because transient pressures at and above this screw speed exceed the normal operating pressure of 6.89 MPa and there is a risk of putting the BAAM out of commission, a process that is costly. For PPSU 25 wt.% CF, although steady-state pressures are below normal operating pressure for the 0.762 cm nozzle, transient start-up pressures above 150 RPM exceed the 6.89 MPa and requires that BAAM processing conditions such as deposition temperature be adjusted if deposition of large-scale parts is to be done. In-situ steady-state pressure measurements were in agreement with the Hagen-Poiseuille pressure-driven analytical model and were within 10% of COMSOL simulated pressure drop predictions for ABS 20 wt.% CF. In the case of PPSU, there is agreement among the experimental steady-state readings, analytical, and simulated pressure drop predictions. Further work needs to be done to determine the relationship between the variables encountered in BAAM including material physical properties, flow rate, nozzle geometry, but this chapter is a step towards system pressure measurements to improve our knowledge.

CHAPTER FOUR

DETERMINATION OF MELT PROCESSING CONDITIONS FOR HIGH-PERFORMANCE AMORPHOUS THERMOPLASTICS FOR BIG AREA ADDITIVE MANUFACTURING

Introduction

One of the potential applications for BAAM is high-temperature tooling for autoclave operations [1,23,72,97]. Currently, tooling for composite material processing involves long lead times and high costs. Switching from traditional tooling methods to BAAM is estimated to reduce the cost of tooling by 10 - 100 times and can reduce the lead time by an order of magnitude [24,72]. However, there are currently very few high-performance polymers that can be printed that satisfy autoclave mold requirements, such as exposure to elevated temperature (175 °C) and pressure (0.6 MPa) while maintaining dimensional accuracy. In-autoclave tools made from CF reinforced PPS and PPSU composites have been demonstrated using BAAM [23,72]. As the application space for large-scale 3D printed components continues to grow, it is necessary to identify appropriate processing conditions for high-performance thermoplastics on large-scale AM systems such as BAAM. However, studies on the melt dynamics and processing conditions of these thermoplastics in BAAM are limited.

When evaluating potential BAAM feedstock, understanding the melt dynamics is crucial for identifying inherent material properties that are necessary for potential AM feedstock [40]. Rheological characterization of polymers can provide screening methodologies that prevent a costly trial-and-error approach to evaluating potential feedstock materials. This chapter provides a protocol for using thermal and rheological characteristics when selecting candidate materials suitable for the BAAM system and in developing processing bounds to achieve required material properties for applications such as high temperature tooling and composite structures.

The use of fiber reinforced composites is preferred for BAAM applications as fibers lower the coefficient of thermal expansion by an order of magnitude [8]. This in turn minimizes shrinkage in printed parts as they cool from deposition temperature to ambient temperature [24]. However, the presence of fibers in the polymer matrix presents a processing challenge due to fiber orientation during flow and modified rheology of the polymer system. The mechanical properties of the parts made with fiber reinforced composites are also dependent on the

orientation of the fibers during material processing from the molten state to the solidification process. Given the anisotropy of the composites, maximum reinforcement is attained when fibers are properly oriented [98–102]. Rheological studies of short glass fiber reinforced polystyrene showed that the complex viscosity of the fiber reinforced polymer is lower when the fibers are oriented parallel along the flow direction than when the fibers are randomly oriented in the matrix [103]. The authors of that study also observed a change in the complex viscosity, loss modulus, and storage modulus for fiber reinforced polymers with repeat measurements during oscillatory shearing. It is therefore, useful to have some insight into the change of fiber orientation during flow and to find a relationship between fiber orientations and macroscopically observable rheological properties such as viscosity. However, the scope of this work does not include the effect of fiber orientation and distribution.

The high-performance materials investigated include CF reinforced PEI and PPSU composite systems. The rheological behavior of CF reinforced ABS is also investigated since ABS tends to be the most utilized base feedstock for BAAM [14,24,27]. It is also important to note that ABS, PEI, and PPSU have distinct structural properties that influence their rheological behavior. This rheological characterization is not intended to compare these polymer systems but instead to use the well-studied rheological behavior of ABS [104–110] to inform the processing conditions of PEI and PPSU on BAAM. Analysis of the unfilled material for all the systems is incorporated along to highlight the effect that addition of reinforcing fillers have on the neat resin.

Approach

Rheological properties are routinely used in the polymer processing industry to evaluate melt state properties and identify appropriate processing conditions [39]. The approach presented here is followed to select candidate processing temperatures for ABS, PEI, and PPSU composites on the BAAM system. The lower bound for processing temperature is the glass transition temperature (T_g) (Fig. 4.1) obtained from a differential scanning calorimetry (DSC), and the upper bound is the decomposition onset temperature (DOT) defined as the temperature demonstrating 1% weight loss during thermogravimetric analysis (TGA) [111]. At the lower bound, the polymer tends not to be sufficiently fluid enough and so the candidate processing temperatures are selected to be at least 120 °C above T_g. The higher processing temperature ensures that the polymer melt forms a continuous stream and passes through the nozzle and also facilitates the interlayer bonding of the printed parts on BAAM [11,13,112].

The melt flow properties of the thermoplastics are then studied across a range of candidate processing temperatures. During the BAAM extrusion process, the

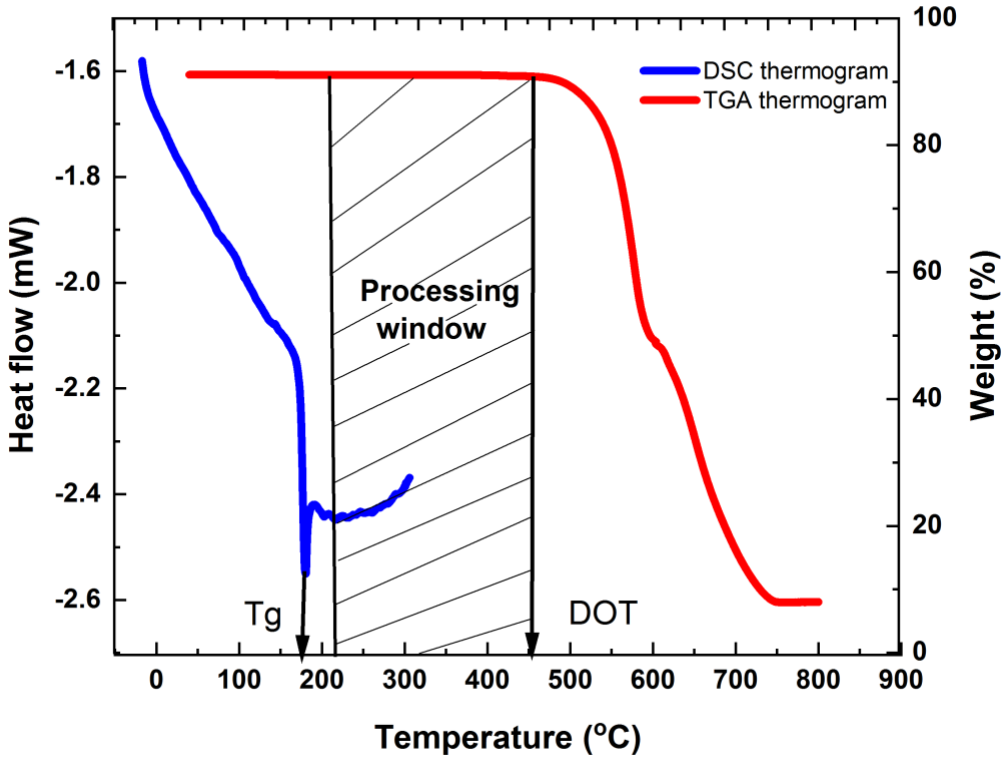


Figure 4.1. Determination of the BAAM processing temperature window using DSC and TGA thermograms. DOT is the decomposition onset temperature.

polymer melt is subject to shearing flow over a wide range of temperatures and shear rates. Knowledge of the rheological behavior of the melt at various temperatures, shear rates, and with reinforcing fillers is essential for an assessment of the material processability, process design/optimization and trouble shooting. Since neat ABS, PEI, and PPSU have been successfully extruded on FFF systems, the temperatures selected for rheological characterization are also informed by these extrusion temperatures to a great extent. In addition to understanding the rheological behavior of the polymer systems under investigation, another reason for characterizing the flow properties is to try and relate the rheological properties of the ABS, PPSU, and PEI polymer systems to the BAAM extrusion process. Comprehension of the flow properties of polymer melts during extrusion on the BAAM system is crucial in assessing the impact of adjusting the temperature or process parameters such as the screw speed for a successful print.

Overall Objective

Determining the appropriate processing conditions of neat and CF reinforced amorphous thermoplastics (ABS, PEI, and PPSU) on BAAM using thermal characterization and dynamic oscillatory rheological measurements.

Primary Research Questions

i. Can thermal and rheological properties be used to identify suitable processing windows for amorphous thermoplastics on BAAM?
ii. How are key BAAM processing parameters such as screw speed and deposition temperature influenced by a material's melt flow behavior?

Experimental Methods

Materials

The resin systems used include neat as well as CF reinforced ABS, PPSU, and PEI (Fig. 4.2). The neat ABS resin used was a Lustran 433 grade, obtained from INEOS, the ULTEM 1000™ neat resin was supplied by SABIC , while the ULTRASON P 3010 neat PPSU resin was supplied by BASF. The carbon reinforced composites of ABS and PPSU were compounded by TECHMER ES with varying weight percentages (wt.%); ABS 20 wt.% CF, PPSU 25 wt.% CF, as well as PPSU 35 wt.% CF. Two different CF wt.% of PEI (20% and 30%) were compounded by SABIC. All the CF composites are commercially available as 3D printing grades. The diameter of the CF used during compounding is 7 µm. The starting fiber length is approximately 6350 µm, however, the compounding

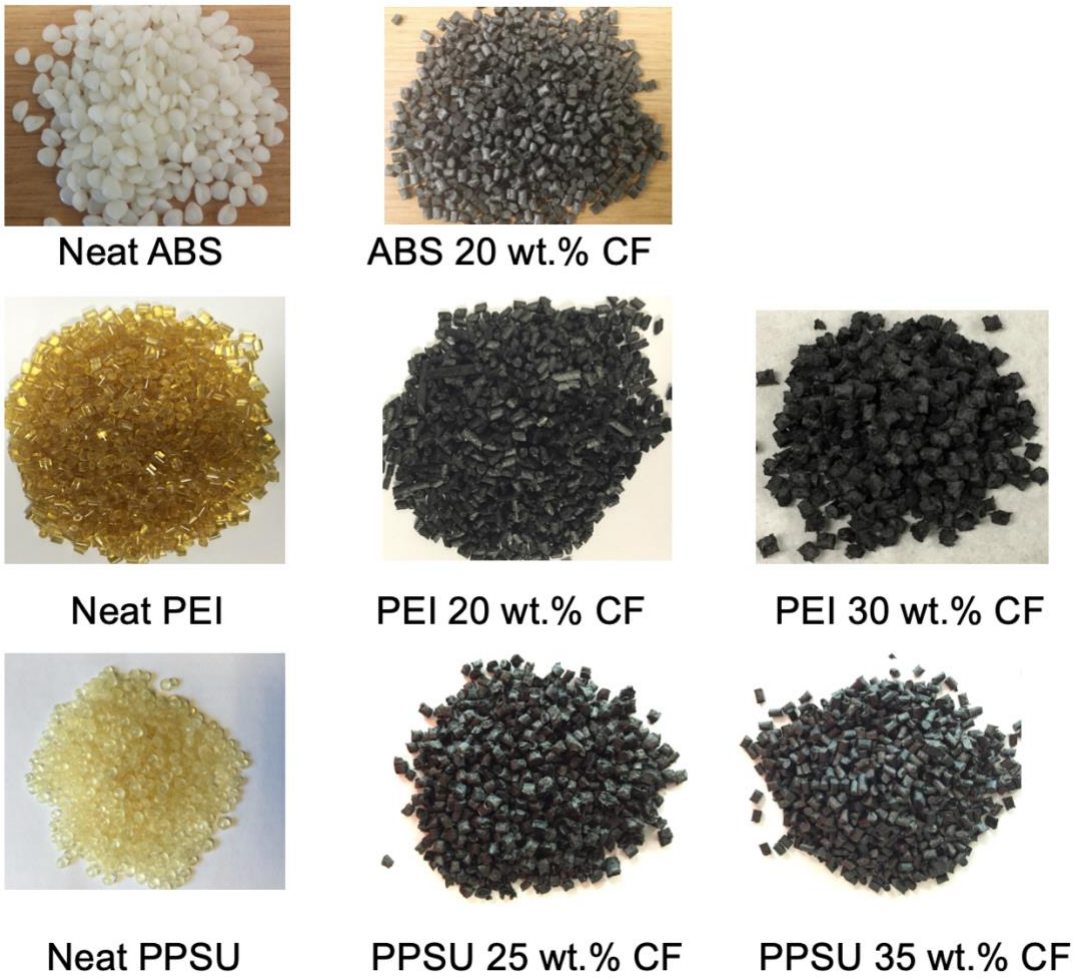


Figure 4.2. Neat and CF-reinforced ABS, PEI, and PPSU used for thermal and rheological characterization

process causes fiber breakage and reduced length. The final fiber length distribution in the pellets is between 50 µm and 1000 µm.

Thermal Analysis

A differential scanning calorimeter (DSC Q2000, TA Instruments) was used for thermal characterization to measure thermal transitions of the resin systems. About 9 - 10 mg of the sample material was placed in an aluminum pan and was first heated from 25 °C to 450 °C at 5 °C/min to eliminate any thermal history. After the first scan, the samples were quenched at a rate of 5 °C/min to 25 °C, and reheated as the second run. The ABS and PEI samples were scanned in air while the PPSU samples were scanned under a nitrogen environment, to mimic the environment in which they are printed on the BAAM. To determine the phase transitions, the area under the relevant peak in the curve was analyzed. The thermal stability of the samples was observed using thermogravimetric analysis (TGA Q500, TA Instruments). The heating rate for all samples was 10 °C/min from 25 °C to 800 °C except for ABS samples which were heated up to 600 °C.

Dynamic Rheological Characterization

Dynamic rheological properties of the neat and CF reinforced composites were measured on a Discovery Hybrid Rheometer-2 (DHR-2, TA instruments) fitted with a 25-mm parallel-plate geometry (Fig. 4.3). First, an oscillation strain sweep was performed on the samples at the candidate test temperatures (Table 4.1) to determine the linear viscoelastic (LVE) region, a region in which the sample structure is intact. The applied strain amplitude (γ_o), expressed as a % was varied from 0.01% to 100% at a fixed angular frequency (ω) of 10 rad/s. The applied γ_o utilized for further dynamic tests on the DHR-2 was 0.06% for ABS and PEI and 1% for PPSU. The plate gap was maintained between 1.5 and 1.8 mm during testing which is within the recommended range for testing short fiber reinforced composites [113]. This recommended gap in the rheometer must be between three to ten times larger than the fiber length to minimize the boundary effect of the rheometer on the fibers. Pelletized samples of ABS, PEI, and PPSU were used for the small amplitude oscillatory tests and directly melted on the plates using melt rings. Since, the linear viscoelastic properties of fiber reinforced composites can change with repeat measurements due to fiber orientation during oscillatory shearing [114].

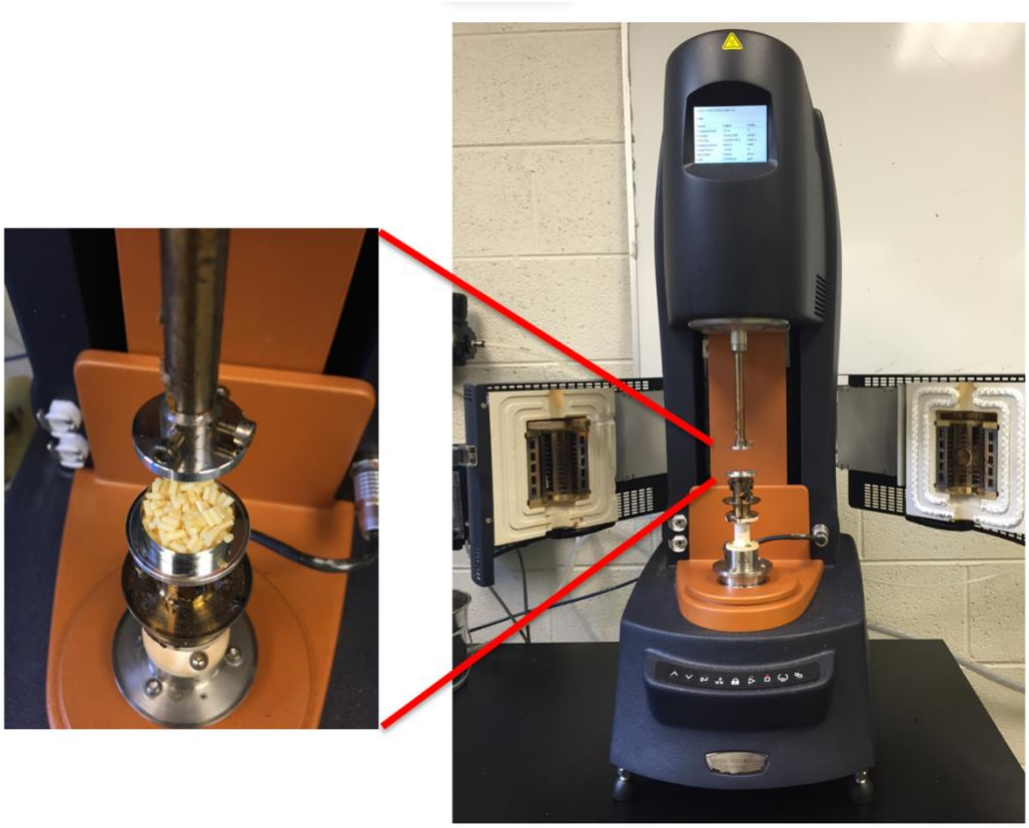


Figure 4.3. TA Instruments' DHR-2 fitted with 25-mm disposable parallel-plate fixture used for SAOS measurements

Results and Discussion

Thermal Analysis

The results of the DSC scans (second heating cycle) of neat and CF reinforced ABS, PEI and PPSU are shown in Fig. 4.4. The DSC data show that the T_g for ABS is 105 °C, while that of PEI and PPSU is 215 °C and 225 °C, respectively. Note that the addition of CF to the polymer matrix does not affect the base properties of the polymer. The reinforcing fiber instead tends to be much more efficient in enhancing key mechanical properties such as the tensile and flexural strengths which are out of scope for this work [38]. The high T_g values for PEI and PPSU render both polymer systems suitable for high temperature use. T_g is used to set the lower processing temperature, informed in part by the injection molding and polymer extrusion industries that set their processing temperatures at least 120 °C above T_g for melt processability. With this in mind, the lowest temperature for processing ABS, PEI, and PPSU on the BAAM system would be 225 °C, 320 °C, and 340 °C respectively. In addition, setting the lower processing temperature limit above T_g is crucial in AM because interlayer bonding is thermally driven to create strong interlayer bonds [11].

Figure 4.5 shows the TGA thermograms for the neat and CF reinforced ABS, PEI, and PPSU. The TGA degradation profile is used to inform the upper processing temperature limit for these composites. The decomposition onset temperature (DOT), described as the temperature at which 1% weight loss is observed is used to set the upper processing temperature for these materials on the BAAM. For ABS, DOT is around 310 °C, while PEI and PPSU's DOT is around 480 °C. For printing purposes on the BAAM, the processing temperature for these materials should not exceed the DOT because the matrix material starts to degrade and this could compromise the integrity of the BAAM part by reducing stiffness. Similar to DSC, reinforcing the neat resin with CF does not affect the DOT. The only difference is the residual weight loss. For instance, at 370 °C for ABS 20 wt.% CF, 20% of the sample does not fully decompose compared to the neat resin due to the 20 wt.% CF in the polymer composite.

Dynamic Rheological Characterization

Strain Sweep

SAOS measurements assume that the material response is in the linear region, and therefore, material functions such as the storage modulus (G') and loss modulus (G") fully describe the material response. Linear viscoelasticity is useful

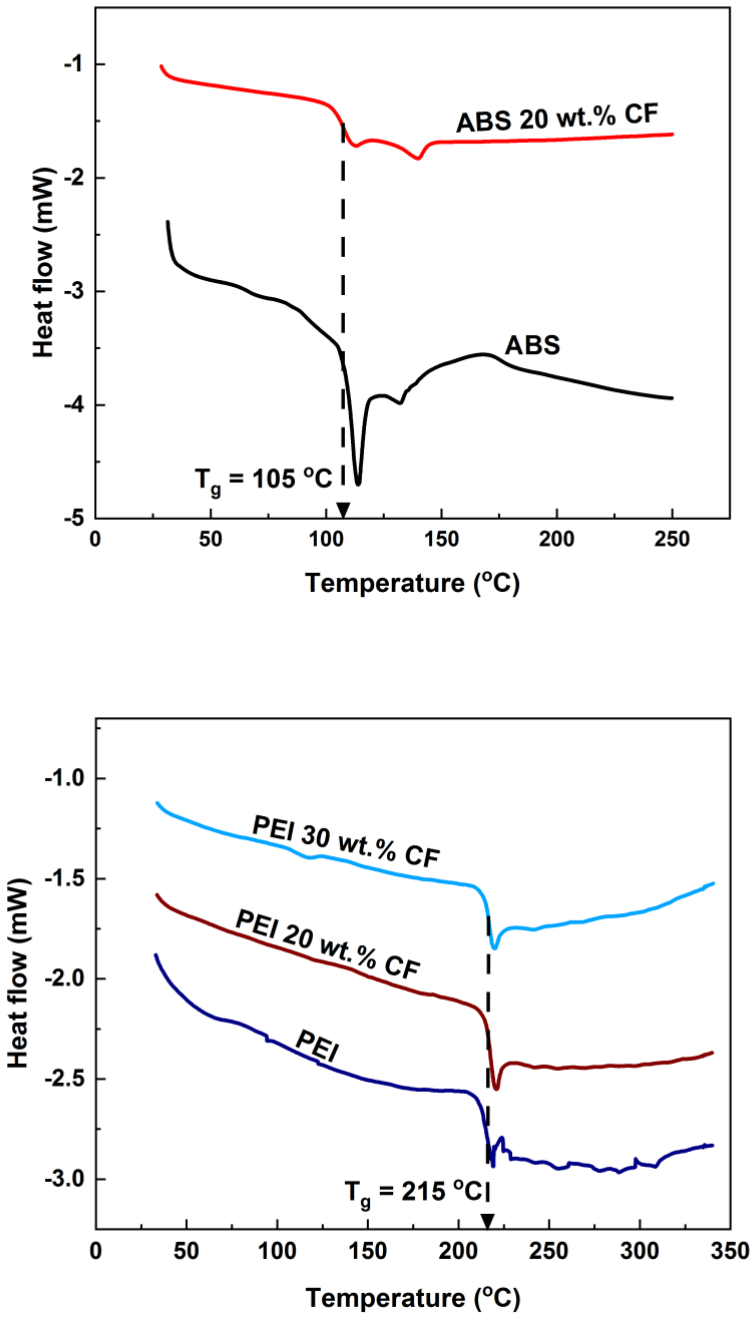


Figure 4.4. DSC Thermograms for ABS, PEI, and PPSU as well as their CF reinforced composites

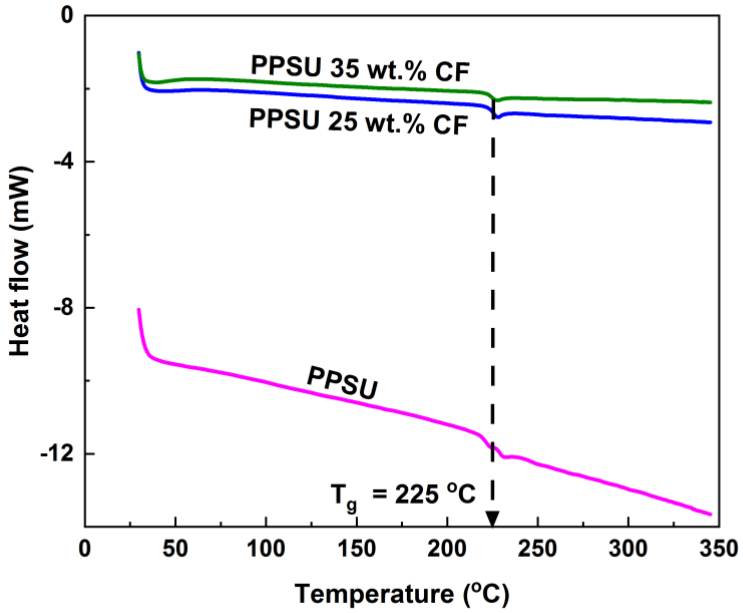


Figure 4.4 (Continued)

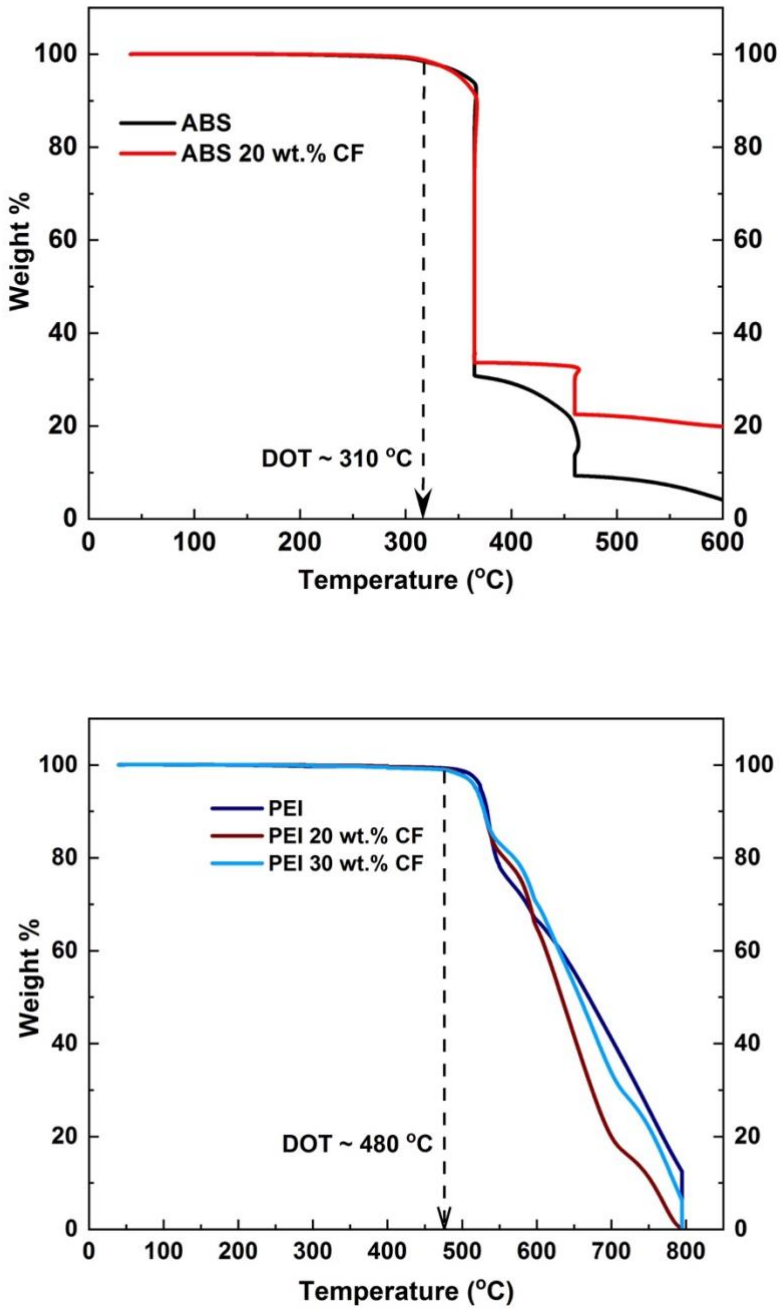


Figure 4.5. TGA Thermograms for ABS, PEI, and PPSU as well as their CF reinforced composites

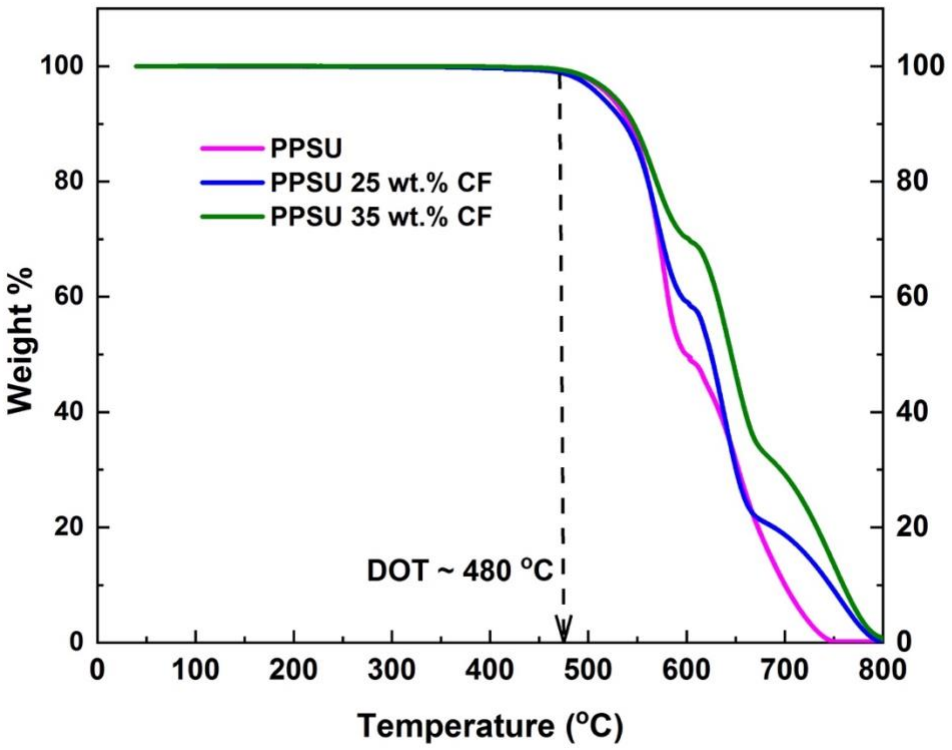


Figure 4.5 (Continued)

for understanding the relationship between the microstructure of a polymer and its rheological properties. A strain sweep can characterize the linearity and level of homogeneity in the polymer system or composite. Rheological properties of viscoelastic materials are independent of the amount of strain up to a critical strain, beyond which the material's behavior is nonlinear. To evaluate the relationship between the molecular structure of ABS, PEI, and PPSU composites and the viscoelastic behavior, rheological experiments were first conducted in the LVE region. Strain sweep tests covering four orders of magnitude of strain were performed to assess the internal structure of the polymer systems.

During the strain sweep tests, G' and G" were plotted against percentage oscillation strain at a low frequency of 10 rad/s (Fig. 4.6). A decrease in G' with increase in percentage strain may indicate structural breakdown of the polymer [115]. In the neat resins, (Fig. 4.6), G' and G" were independent of applied γ_o over the range observed. However, the addition of fillers reduced the critical strain level below which the dynamic response was unaffected (Fig. 4.6). For instance, for the PEI 20 wt.% CF and 30 wt.% CF, the critical γ_o were 1% and 0.09% respectively. The reduced critical strain level in the fiber reinforced composites required that the dynamic viscoelastic properties were investigated at a strain that was below the threshold that affected the material response [116]. Below the critical γ_o, the composites were highly structured and behaved in a viscous-like manner, where G" is larger than G'. Beyond the critical γ_o, the material structure was disrupted and G' declined. The γ_o used in subsequent tests was selected to be below the critical strain percentage for the all composites. For ABS and PEI composites, the γ_o used was 0.06% while for PPSU, the γ_o used was 1%.

Storage modulus, loss modulus, and tan δ

After defining the linear viscoelastic region, dynamic frequency sweeps were conducted over a range of oscillation frequencies (628 - 0.1 rad/s) at a constant oscillation amplitude within the LVE region.

As demonstrated in Fig. 4.7, G' and G" of ABS increases with ω and the moduli are higher in both instances for CF reinforced materials. It is notable that at low ω, G' seems to plateau for both neat and CF-ABS and the effect of temperature is less substantial. At high ω, the effect of temperature is more noticeable and G' is dependent on ω. The appearance of a plateau at low frequencies has been observed by others and was attributed to the degree of grafting of the rubber particles in ABS [104,117]. Comparison of G' and G" for both material sets in Fig. 3.7 shows that G' exceeds G" across all ω. Therefore, ABS and CF-reinforced ABS behave more like an elastic solid than a viscous liquid across the range of ω and temperatures investigated. Figure 4.7 also includes tan δ values for neat and CF-ABS. It can be observed that addition of CF to the matrix lowers

the tan δ value considerably in the intermediate ω. Tan δ values for CF-reinforced ABS are less than unity (more elastic) across all ω and independent of temperature.

Tan δ, a ratio of G" and G', provides a useful measure of the relative magnitude of energy storage and dissipation of energy. Tan δ values of less than unity signify a more elastic like behavior while values greater than unity exhibit a more viscous dominant behavior in the material.

For all PEI materials investigated, the viscous component, G", was more dominant than G' across the entire frequency range tested (Fig. 4.8). The addition of fillers to the neat PEI resin produced composite systems with greater dynamic moduli than the neat matrix. This effect was greater at the lower frequencies (< 1 rad/s) compared to the higher frequencies (> 10 rad/s). This behavior has also been observed by others and it is attributed to the fact that at higher frequencies, fibers contribute very little to the viscoelastic properties of a composite because they become aligned [101,114,118]. For instance, at 400 °C, G' and G" of the CF-reinforced PEI composites respectively increased by as much as 100x and 10x at lower ω when compared to the neat resin. At the higher ω (> 10 rad/s), G' and G" increased by approximately 20x and 4x, respectively (see Fig. 4.8). Having a greater G" than G' indicates that the viscous component of the material dominates the elastic component across all ω.

Polymer melts with very low viscosities may be extruded from the nozzle, but would fail to retain their shape during the printing process. Therefore, it is important to investigate the relative viscoelastic moduli of candidate polymer systems to identify which of the components (G' or G") is dominant during BAAM processing. Since the neat PEI resin and its CF-PEI composites have a more dominant viscous component, it is important to allow for longer relaxation times after melt deposition to form a stable bead during printing.

Fig. 4.9 similarly shows G',G", and tan δ of PPSU as well as the CF-reinforced blends. G' increases with increasing CF content across all ω with a more pronounced effect at lower frequencies. The reinforced blends of PPSU have a higher modulus (both G' and G") than the neat PPSU resin. In contrast to the ABS materials, G' of neat PPSU is higher than G" especially at the lower ω, meaning that it behaves more like a viscous liquid under these conditions. The addition of CF makes the two moduli more equivalent, which provides more of a viscoelastic behavior. All of the PPSU tan δ values at all ω, temperatures and fiber loading are greater than unity (more viscous) and are generally higher than those of ABS.

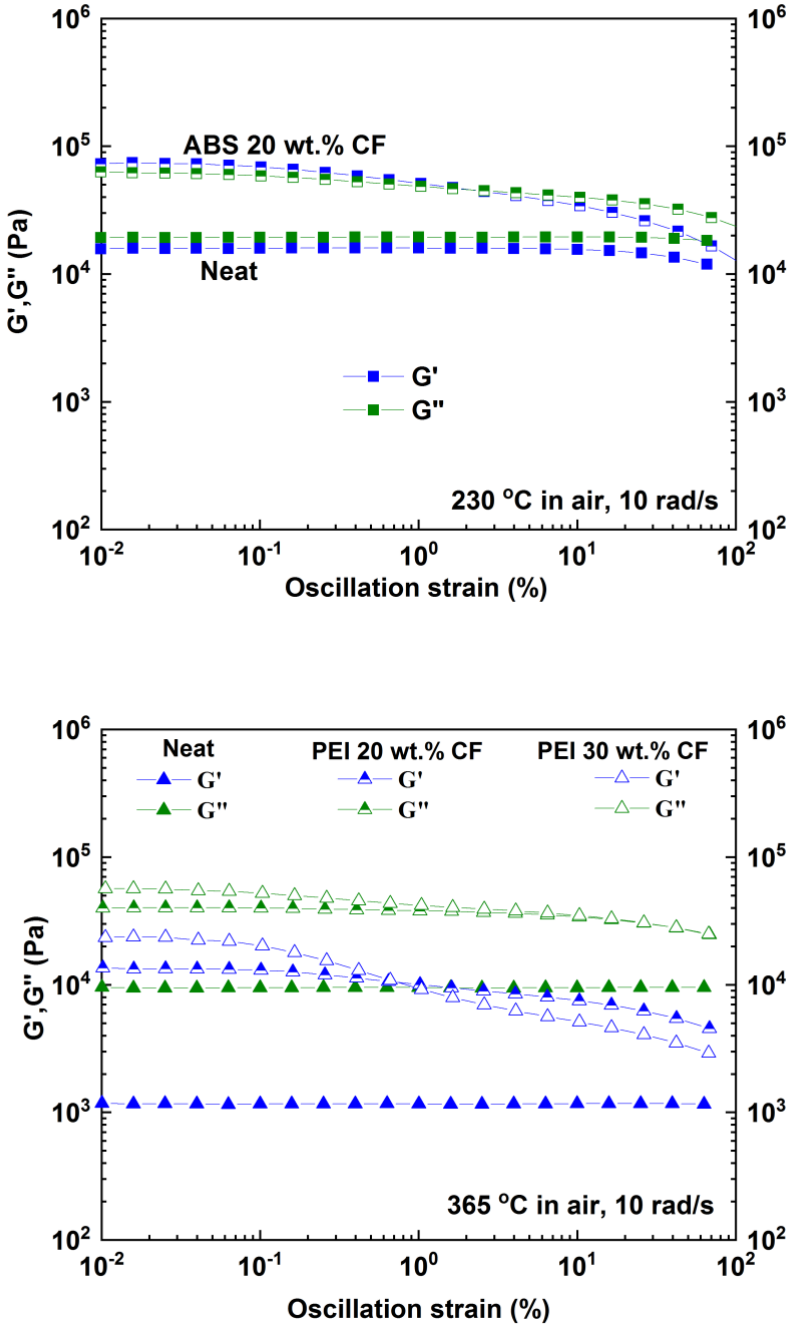


Figure 4.6. Strain sweeps for ABS, PEI, and P as well as their CF reinforced composites

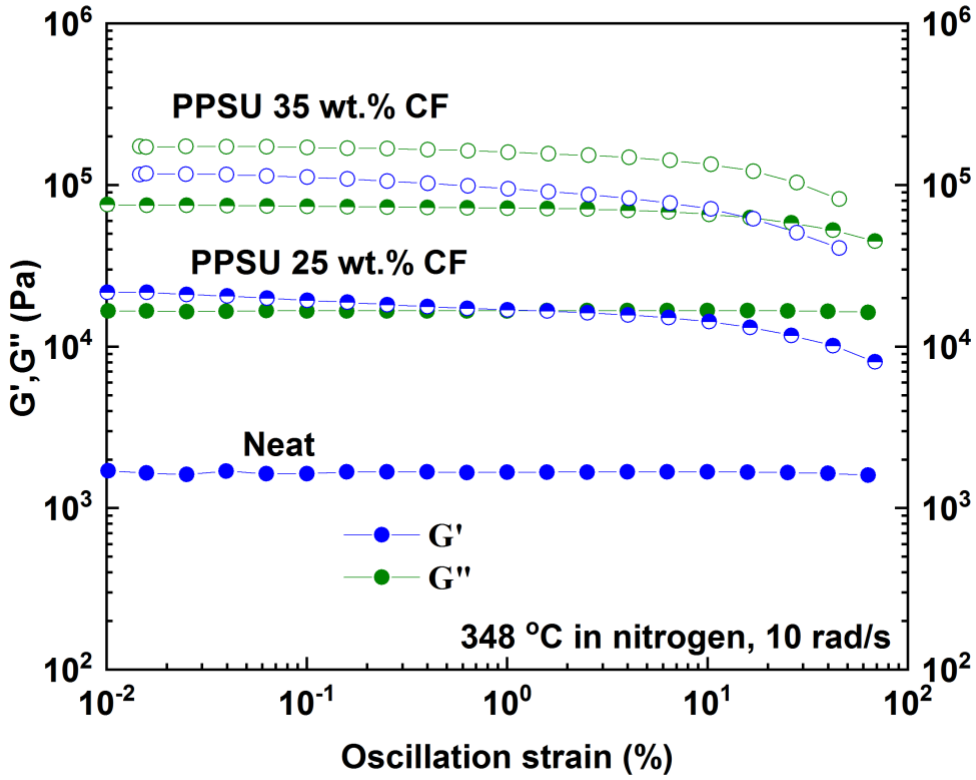


Figure 4.6 (Continued)

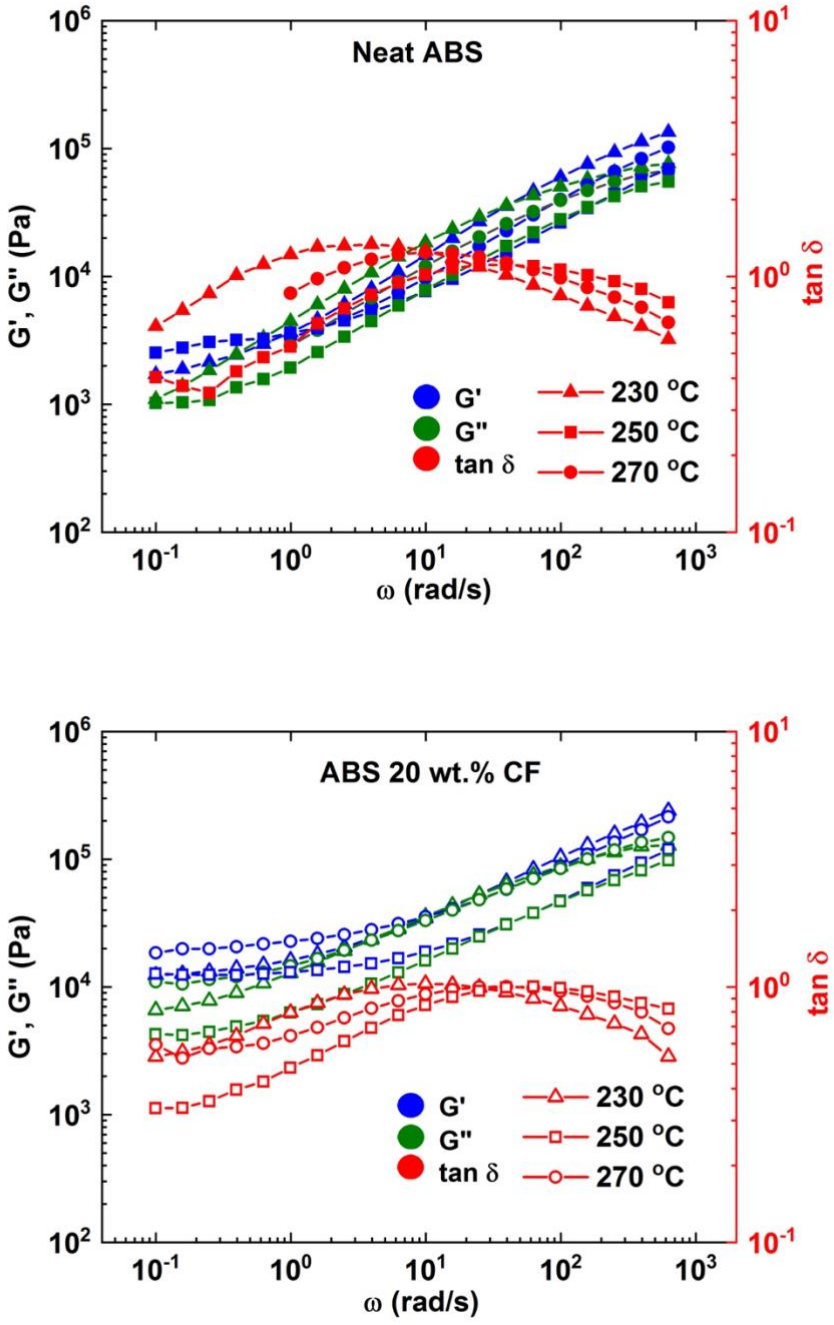


Figure 4.7. G', G", and tan δ vs angular frequency at various temperatures for neat and CF reinforced ABS in air

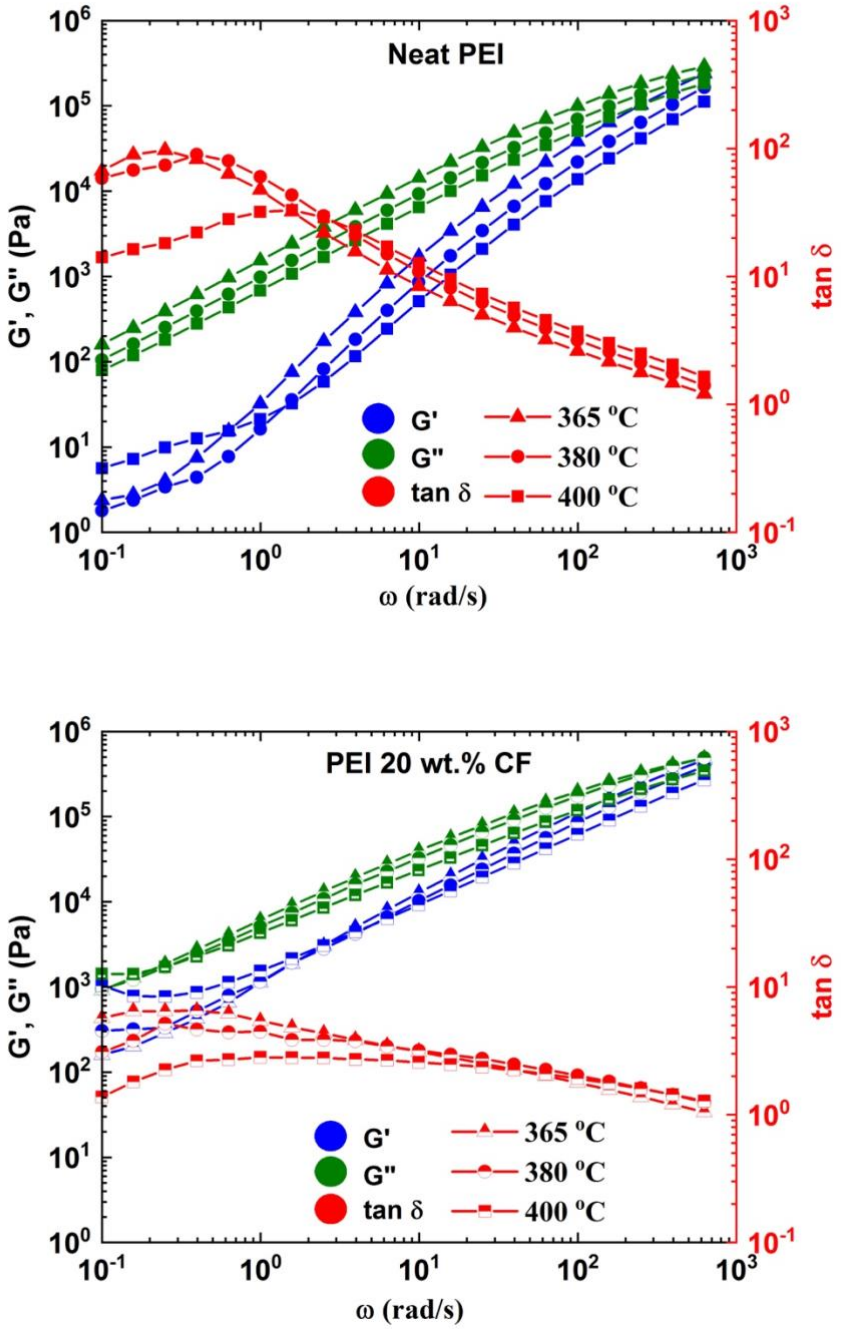


Figure 4.8. G', G", and tan δ vs angular frequency at various temperatures for neat and CF reinforced PEI in air

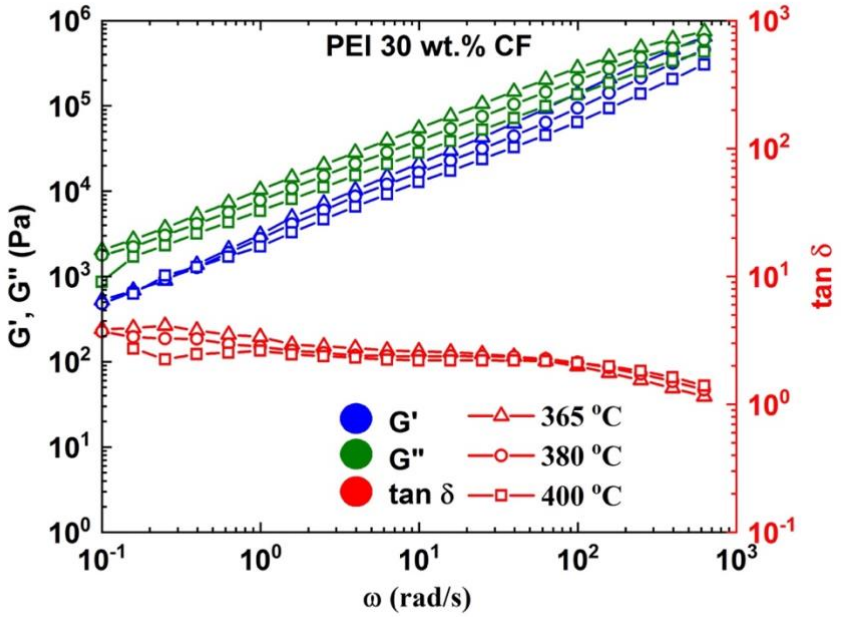


Figure 4.8 (Continued)

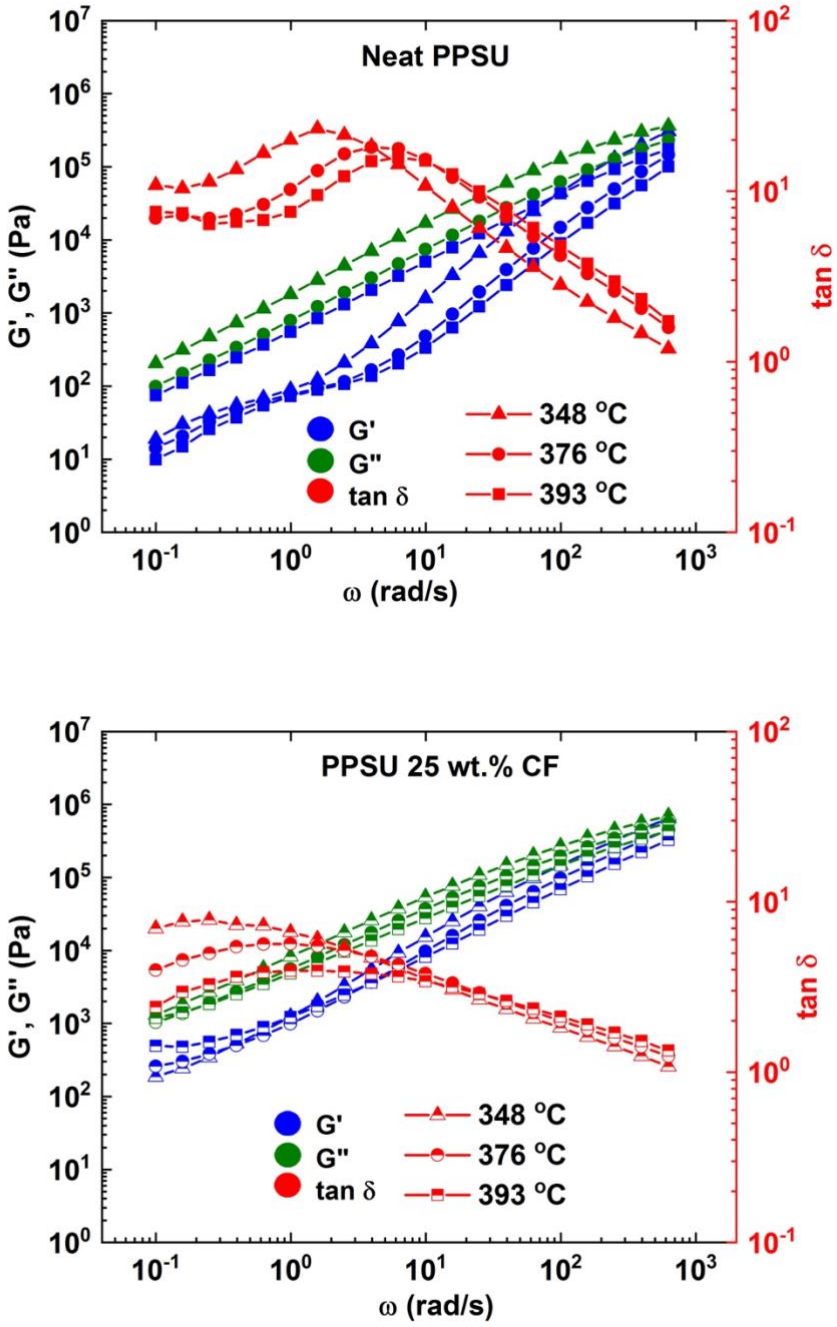


Figure 4.9. G', G", and tan δ vs angular frequency at various temperatures for neat and CF reinforced PPSU in nitrogen

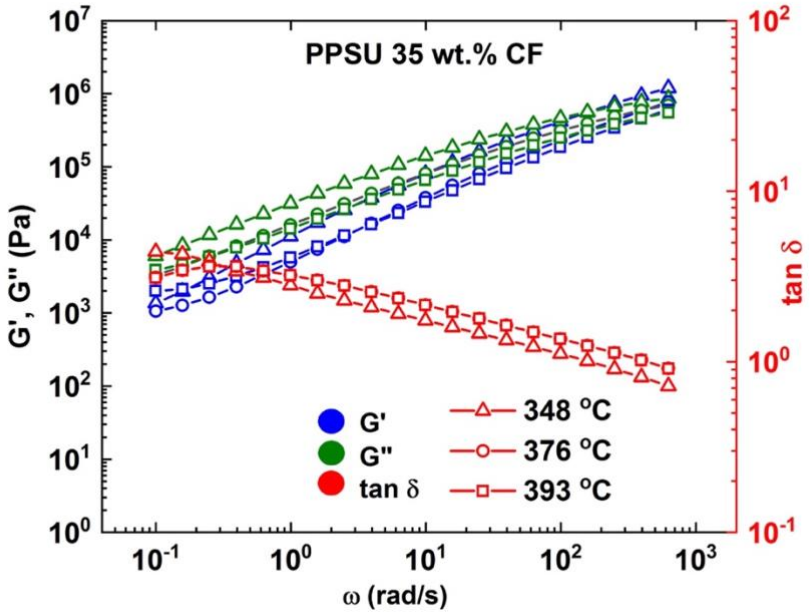


Figure 4.9 (Continued)

Complex Viscosity

The complex viscosity (η*) of neat and CF reinforced ABS, PEI, and PPSU are presented in Figs. 4.10, 4.11, and 4.12 respectively, as a function of ω. ABS is shear thinning, at all temperatures and angular frequencies. However, the addition of CF enhances the shear thinning effect of ABS and increases the η* by 4-10% over the neat resin.

The η* of neat PEI exhibited relatively Newtonian behavior at the lower a ω (< 10 rad/s) and was shear thinning at the higher ω (> 10 rad/s) (Fig. 4.11). The trend and η* values as a function of ω for neat PEI are in agreement with those reported by other researchers [37,119–122]. Reinforcing PEI with carbon fiber not only increased the viscosity, but it also significantly enhanced the shear thinning effect. Neat PPSU (Fig. 4.12) demonstrates a uniform Newtonian-like viscosity across the majority of ω observed. However, the addition of fiber reinforcement makes PPSU exhibit a moderate shear thinning behavior at all ω and temperatures. Accurate measurements of viscosity as a function of shear rate provide useful information about a material during the printing process, since the shear rate could vary by several orders of magnitude at different points in the process. Within the nozzle just prior to extrusion, the shear rate is considered to be approximately 100 s^{-1}. To relate the η values obtained with the rotational rheometer to the viscosity at relevant BAAM shear rates, the Cox-Merz Rule [Eq. 4.1] was applied [123].

$$\eta(\dot{\gamma}) = \eta^*(\omega) \; for \; \dot{\gamma} = \omega \tag{4.1}$$

The Cox-Merz principle was applied to one of the material systems; neat and ABS 20 wt.% CF and was found to hold true (Fig. 4.13). The applicability of the Cox-Merz rule to the fiber-filled PEI composites in this study is an initial approximation. Previous studies on glass fiber-filled LLDPE showed that the dynamic viscosity measurements were higher than the steady- state viscosity measurements [124]. In PPS 40 wt.% CF, a high-performance thermoplastic, the Cox-Merz rule did not apply and the shear viscosity values measured on the capillary rheometer were at least 7x lower than the complex viscosity values from the rotational rheometer [29]. The reduction in steady- state viscosity was attributed to fiber alignment along the flow direction, which is a condition more likely encountered during printing [17,33,102,125]. Therefore, the measured viscosity values may be slightly elevated, but the relative impact on viscosity due to changes in material composition and processing conditions (temperature and shear rate) can be quantified (Table 4.1).

As shown in Table 4.1, an increase in processing temperature for all materials decreases the η* at 100 rad/s. As the temperature increases from 230 to 270 °C,
As shown in Table 4.1, an increase in processing temperature for all materials decreases the η* at 100 rad/s. As the temperature increases from 230 to 270 °C,

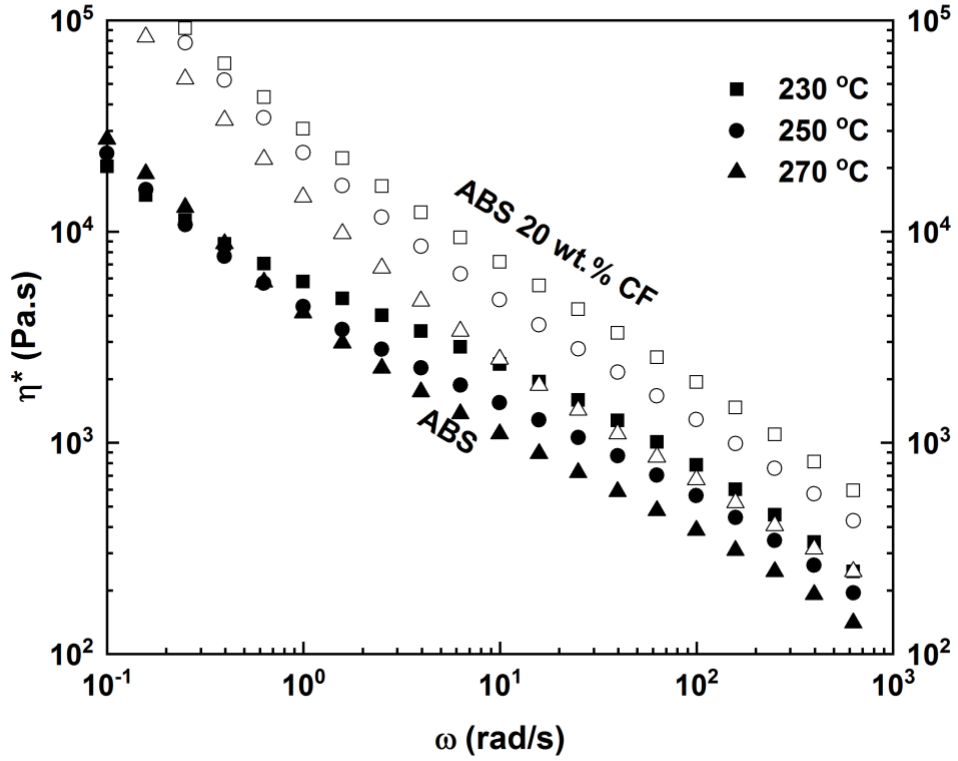


Figure 4.10. Complex viscosity vs angular frequency at various temperatures for neat and CF reinforced ABS in air

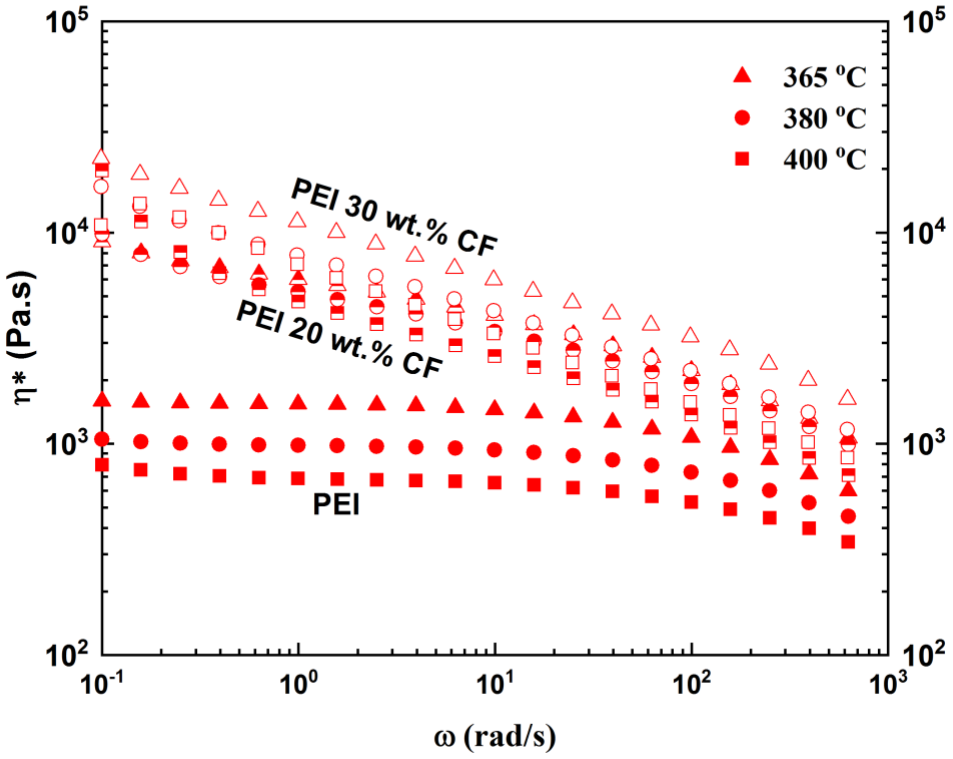


Figure 4.11. Complex viscosity vs angular frequency at various temperatures for neat and CF reinforced PEI in air

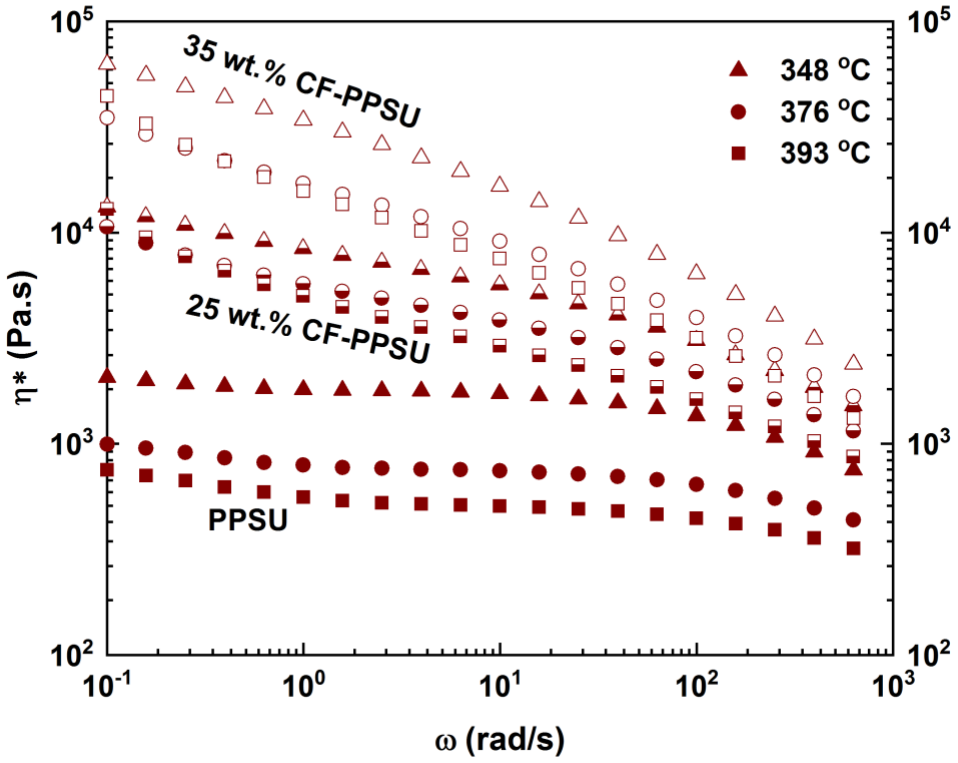


Figure 4.12. Complex viscosity vs angular frequency at various temperatures for neat and CF reinforced PPSU in nitrogen

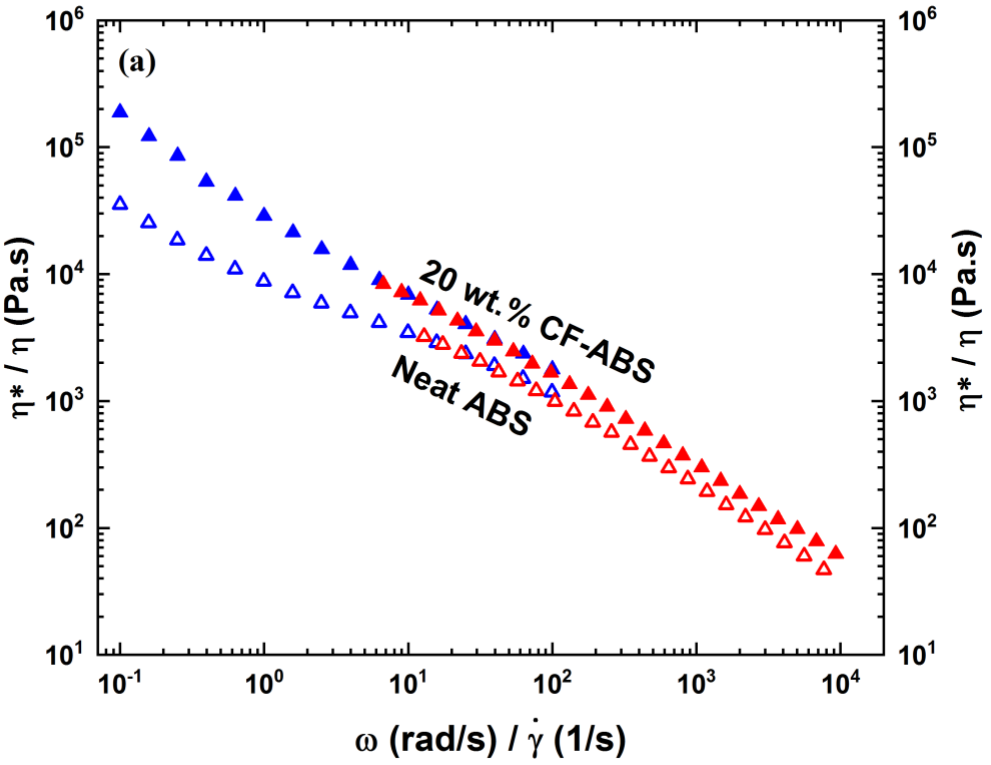


Figure 4.13. Complex viscosity and shear viscosity curves of neat (unfilled symbols) and carbon fiber reinforced (filled symbols) ABS at 230 C°

Table 4.1. Effect of temperature, carbon fiber loading, and frequency on the complex viscosity of ABS, PEI, and PPSU

	Effect on complex viscosity (%)			
Temperature increase		ABS	ABS 20 wt.% CF	
	230 – 270 °C	-55	-51	
		PEI	PEI 20 wt.% CF	PEI 30 wt.% CF
	365 – 400 °C	-51	-47	-53
		PPSU	PPSU 25 wt.% CF	PPSU 35 wt.% CF
	348 – 393 °C	-65	-35	-50
Addition of CF		ABS	ABS 20 wt.% CF	
	250 °C		+230	
		PEI	PEI 20 wt.% CF	PEI 30 wt.% CF
	400 °C		+155	+200
		PPSU	PPSU 25 wt.% CF	PPSU 35 wt.% CF
	376 °C		+240	+500
Frequency increase (10 – 100 rad/s)		ABS	ABS 20 wt.% CF	
	250 °C	-65	-75	
		PEI	PEI 20 wt.% CF	PEI 30 wt.% CF
	400 °C	-19	-46	-54
		PPSU	PPSU 25 wt.% CF	PPSU 35 wt.% CF
	376 °C	-10	-40	-55

the η* of ABS decreases by 55%, while that of the CF reinforced ABS decreases by 51%. Neat PEI resin on the other hand, demonstrated a sensitivity to changes in temperature (Fig. 4.11), such that increasing the processing temperature from 365 °C to 400 °C reduced the η* at 100 rad/s frequency by 51%. By contrast, the decrease in viscosity as temperature increases from 348 °C to 393 °C for neat PPSU is greater than that of CF reinforced PPSU (35% to 50%).

Likewise, Table 4.1 indicates that the addition of CF to the neat resins significantly increases the η* and enhances the shear thinning effect. At 250 °C, the η* of ABS increases by 230% when 20% by weight CF is added. Similarly, for PPSU at a processing temperature of 376 °C, the addition of 25% by weight CF results in a 240% increase in η* while adding 35% by weight CF increases viscosity by 500%. At 400 °C, the η* of the neat PEI resin increased by 155% and 200% with the addition of 20% CF and 30% CF, respectively (Table 4.1). The η* of polymer composites can be very important when determining appropriate screw speed on BAAM systems. An increase in melt viscosity due to the addition of fiber reinforcement can increase the torque on the extrusion screw. The load on the screw can be varied by changing the extrusion temperature. The carbon fiber reinforced composites are shear thinning at all frequencies, which provides a wide processing window on BAAM by adjusting the flow rate.

Another processing aspect to consider when printing materials on BAAM is the volumetric throughput, which directly changes the shear rate/ω during extrusion and deposition. For shear thinning materials (most amorphous polymers), an increase in ω results in a marked decrease in η*. This effect is much greater in the CF reinforced blends compared to the neat resins (Table 4.1). For example, the η* of neat ABS and CF reinforced ABS decreases by 65% and 75%, respectively, when ω increases from 10 rad/s to 100 rad/s. However, the neat PEI resin is relatively insensitive to changes in ω (< 20% change) compared to the CF-reinforced composites. A similar pattern is observed in PPSU where a similar increase in ω results in a decrease in η* of 10% in neat PPSU and by 40-50% when CF is added to the neat PPSU resin. This is because the addition of fiber reinforcements can dramatically increase the local shear experienced by the matrix between rigid fibers compared to the apparent shear experienced by the overall sample [98]. Therefore, this shows that during the BAAM process, the viscosity of the neat ABS, PEI, and PPSU resins would most effectively be controlled by changing the extrusion temperature.

However, as observed in Table 4.1, it is possible to reduce the viscosity of fiber reinforced materials by increasing the processing temperature. For example,

increasing the temperature of the CF-reinforced PEI composites from 365 °C to 400 °C, reduces the η* by 47% and 53% for the 20% CF-PEI and 30% CF-PEI, respectively.

Dynamic oscillatory measurements can be useful for relating material properties to structure in the LVE region and identifying the effect of BAAM processing conditions, such as screw speed and processing temperature. However, polymer melts can experience shear rates as high as 5000 s^{-1} during the shear-melting phase within the BAAM single-screw extruder. These shear rates greatly exceed the LVE region for ABS, PEI, and PPSU composites, which limits the scope and interpretation of linear viscoelastic measurements obtained from rotational rheometers.

Summary and Conclusions

Successfully printing high performance thermoplastics on BAAM demands the identification of appropriate processing conditions to insure the end part is robust and possesses the desired properties. Thermal characterization techniques such as DSC and TGA are useful for identifying the boundary processing conditions, namely, the glass transition and onset of decomposition temperatures. These bounds allow for an educated judgement to be made when choosing candidate processing temperatures. The ability to process high performance thermoplastics such as PEI and PPSU composites on BAAM is also highly dependent on the rheological properties. The rheological behavior of these materials can help to identify the effects of BAAM extrusion parameters, such as the extrusion temperature, screw speed, and fiber reinforcement. The rheological behavior of the three thermoplastics studied: ABS, PEI, and PPSU, was found to vary significantly as a function of various processing conditions. The viscosity of unreinforced ABS and PPSU decreased by more than 50% with an increase in temperature. The addition of CF drastically increased the viscosity of ABS (over 4x for 20% by weight CF), PEI (by 2.5x for 20% CF and 3x for 30% CF), and PPSU (~5x for 35% by weight CF). Fiber reinforcement also increased the shear thinning effect of both thermoplastics, showing a potential variation of 2–3x over the range of expected shear rates: 10–100/s (assuming Cox-Merz rule holds). The strong impact of various process parameters on the viscosity of high performance thermoplastics highlights the value of understanding the rheological behavior of candidate materials for printing with large-scale extrusion AM systems and similar extrusion systems. Future work will need to entail evaluating the viscosity of carbon fiber reinforced ABS and PPSU composites at high apparent shear rates using a capillary rheometer. Also, the degree and effect of fiber orientation on dynamic and apparent viscosity in AM feedstock needs to be investigated.

CHAPTER FIVE

CONCLUSIONS AND FUTURE OUTLOOK

Summary of Research Work

This dissertation was motivated by the need to expand the current selection of AM feedstock to accommodate the growth in the application space for 3D printed components because there was not a formal process for designing, screening, and evaluating the extrudability and printability of various materials on AM systems. The AM platforms discussed include DW, FFF, and BAAM and the material systems used include viscoelastic ink formulations, neat and fiber reinforced ABS, PEI, and PPSU composites.

Predicting Material Extrudability

Research Questions

i. Can a simple pressure-driven flow model be used to predict extrudability on various extrusion-based AM platforms?
ii. Can you relate experimental laboratory based measurements to real life AM processes? This work was discussed in chapter 2.

Overall Conclusions

i. The proposed pressure-driven flow model is a useful tool for predicting successful material extrudability on DW, FFF and BAAM platforms, speeding up the process of material screening and selection.
ii. If viscoelastic properties such as shear yield stress, the shear thinning exponent, consistency index, and viscosity are known, the proposed pressure-driven model can successfully predict whether extrusion occurs although it may not be perfect.
iii. Extrusion trials of the candidate materials on the various AM platforms further validate model predictions in that, extrusion on the AM system is achieved in all instances where the model predicts it would and vice versa.
iv. The model also indicates regions in the extrusion orifice where pressure is concentrated. For instance, in DW and FFF, much of the pressure required to extrude is in the exit region of the die while in BAAM, pressure is mostly built up in the long nozzle region.

BAAM System Pressure Monitoring in the Nozzle

Research Questions

i. BAAM system pressure monitoring in the nozzle: How do the transient start-up pressures in the nozzle relate to steady-state pressures and influence extrudability?
ii. How do pressure predictions from analytical models and numerical simulations predictions compare to experimentally measured nozzle pressures? This work was discussed in Chapter 3.

Overall Conclusions

i. Custom-designed nozzles capable of measuring and recording pressure distribution were designed and tested on the BAAM extruder system at the Manufacturing Demonstration Facility, Oak Ridge National Laboratory during extrusion of ABS 20 wt.% CF and PPSU 25 wt.% CF.
ii. This design enables process monitoring which is of interest to the AM community for quality control purposes such as changes in the flow rate which lead to inconsistent extrusion and print defects when depositing PPSU 25 wt.% CF.
iii. Transient start-up pressures in BAAM were also quantified for the first time and inform BAAM operations. In both ABS 20 wt.% CF and PPSU 25 wt.% CF, extrusion above 150 RPM is not recommended for 0.508 cm nozzle because transient pressures at and above this screw speed exceed the normal operating pressure of 6.89 MPa and there is a risk of putting the BAAM out of commission, a process that is costly.
iv. In-situ steady-state pressure measurements were in agreement with the Hagen-Poiseuille pressure-driven analytical model and were within 10% of COMSOL simulated pressure drop predictions for ABS 20 wt.% CF. In the case of PPSU, there is agreement among the experimental steady-state readings, analytical, and simulated pressure drop predictions.
v. In ABS 20 wt.% the transient pressure is 1.4x – 2x higher than steady-state pressure while for PPSU 25 wt.% CF, transient pressure ranges between 1.2x – 2.5x higher than steady-state pressures for the 0.508 cm and 1.016 cm nozzles respectively. Therefore, if steady-state pressure is correctly predicted using any of the analytical equations, the transient pressure can be determined.

Determining Melt Processing Conditions

Research Questions

i. Can thermal and rheological properties be used to identify suitable processing windows for amorphous thermoplastics on BAAM?
ii. How are key BAAM processing parameters such as screw speed and deposition temperature influenced by a material's melt flow behavior? This work was discussed in Chapter 4.

Overall Conclusions

i. Thermal characterization techniques such as DSC and TGA are useful for identifying the boundary processing conditions, that allow for an educated judgement to be made when choosing candidate processing temperatures.
ii. The ability to process high performance thermoplastics such as PEI and PPSU composites on BAAM is highly dependent on the rheological properties.
iii. The viscosity of unreinforced ABS and PPSU decreased by more than 50% with an increase in temperature.
iv. The addition of CF drastically increased the viscosity of ABS (over 4x for 20% by weight CF), PEI (by 2.5x for 20% CF and 3x for 30% CF), and PPSU (~5x for 35% by weight CF).
v. Fiber reinforcement also increased the shear thinning effect of both thermoplastics, showing a potential variation of 2–3x over the range of expected shear rates: 10–100/s (assuming Cox-Merz rule holds).
vi. The strong impact of various process parameters on the viscosity of high performance thermoplastics highlights the value of understanding the rheological behavior of candidate materials for printing with BAAM and similar extrusion systems.

Practical Printing Application

Material ooze during BAAM extrusion is an issue that has long been observed but not been quantified or studied. Material ooze impacts final print quality because of the defects that are caused at the seams during deposition on the BAAM [78]. In this dissertation, key observations and recommendations are made that contribute to the knowledge of the occurrence of material ooze during deposition and how to minimize it when using the BAAM system. Oozing from the nozzle does not happen in a fraction of a section, but rather, material comes out very slowly over a long period of time. From a practical standpoint, the characteristic decay times can be used to inform BAAM

processing conditions such as screw speed and nozzle geometry for different composites used. To minimize ooze when depositing, it is recommended that a larger extrusion orifice be used. In Chapter Three, it was observed that the 1.016 cm nozzle, had the shortest characteristic decay times for both ABS 20 wt.% CF and PPSU 25 wt.% CF. Shorter characteristic decay times for AM feedstock are preferred for improved print conditions because it makes it manageable to keep the "mess" in one spot during deposition and avoid stringing it along the whole printed part. Similarly, larger nozzle diameters are preferred because material oozes out faster ensuring that the "mess" is contained in one area of the print. Faster characteristic decay times are observed at screw speeds that are greater than 250 RPM. This informs BAAM operations in that, in order to get a good quality print, deposition for BAAM materials needs to happen at higher screw speeds to minimize die ooze and promote good print quality. The viscoelastic behavior of AM feedstock also influences the characteristic decay time. ABS 20 wt.% CF which is more shinning and has a higher plateau modulus than PPSU 25 wt.% CF, also has smaller characteristic decay times which informs us that these are material traits that are desired in other potential AM feedstock. These material can be enhanced to minimize die ooze for instance by increasing their shear thinning ability through higher fiber loading to promote faster relaxation dynamics after deposition on the BAAM extruder at the Manufacturing Demonstration Facility, Oak Ridge National Laboratory.

List of Publications

Portions of this dissertation have been drawn from the following publications.

i. Ajinjeru, C.; Kishore, V.; Chen, X.; Hershey, C.; Lindahl, J.; Kunnc, V.; Hassen, A. H.; Duty, C., Rheological survey of carbon fiber-reinforced high-temperature thermoplastics for big area additive manufacturing tooling applications. *Journal of Thermoplastic Composite Materials 1- 19,* 2019.

ii. Ajinjeru, C.; Kishore, V.; Lindahl, J.; Sudbury, Z.; Hassen, A. A.; Kunc, V.; Post, B.; Love, L.; Duty, C., The influence of dynamic rheological properties on carbon fiber-reinforced polyetherimide for large-scale extrusion-based additive manufacturing. *The International Journal of Advanced Manufacturing Technology*, *99, 411 – 418,* 2018.

iii. Ajinjeru, C.; Kishore, V.; Peng, L.; Lindahl, J.; Hassen, A. A.; Kunc, V.; Post, B.; Love, L.; Duty, C., Determination of melt processing conditions for high performance amorphous thermoplastics for large format additive manufacturing. *Additive Manufacturing 21, 125 – 132,* 2018.

iv. Ajinjeru, C.; Kishore, V.; Peng, L.; Lindahl, J.; Hassen, A. A.; Kunc, V.; Duty, C., Rheological evaluation of high temperature polymers to identify successful extrusion parameters. In *proceedings of the 28th Annual Solid Freeform Fabrication Symposium. Austin, TX* 2017.

v. Ajinjeru, C.; Kishore, V.; Sudbury, Z.; Lindahl, J.; Hassen, A. A.; Post, B.; Love, L.; Kunc, V.; Duty, C., The influence of rheology on melt processing conditions of carbon fiber reinforced polyetherimide for big area additive manufacturing (BAAM). In *SAMPE Conference Proceedings. Seattle, WA* 2017.

vi. Ajinjeru, C.; Kishore, V.; Chen, X.; Lindahl, J.; Sudbury, Z.; Kunc, V.; Post, B.; Love, L.; Duty, C., The influence of rheology on melt processing conditions of amorphous thermoplastics for big area additive manufacturing (BAAM). In *proceedings of the 27th Annual Solid Freeform Fabrication Symposium. Austin, TX* 2016.

LIST OF REFERENCES

[1] A.A. Hassen, R. Springfield, J. Lindahl, B. Post, L. Love, C. Duty, U. Vaidya, V. Kunc, R.B. Pipes, The durability of large-scale additive manufacturing composite molds, 3rd Annu. Compos. Adv. Mater. Expo, CAMX 2016. (2016) 1–10. https://www.scopus.com/inward/record.uri?eid=2-s2.0-85010064672&partnerID=40&md5=64f76124304346e2a4b748fbeceaffc4.

[2] S. Singh, S. Ramakrishna, R. Singh, Review Material issues in additive manufacturing: A review, J. Manuf. Process. 25 (2017) 185–200. doi:10.1016/j.jmapro.2016.11.006.

[3] S.L.N. Ford, Additive Manufacturing Technology: Potential Implications for U.S. Manufacturing Competitiveness, J. Int. Commer. Econ. (2014) 1–35.

[4] I. Gibson, D.W. Rosen, B. Stucker, Additive Manufacturing Technologies 3D Printing, Rapid Prototyping, and Direct Digital Manufacturing, Second, Springer Science + Business Media, New York, 2010. doi:10.1007/9781493921133.

[5] S.-H. Ahn, M. Montero, D. Odell, S. Roundy, P.K. Wright, Anisotropic material properties of fused deposition modeling ABS, Rapid Prototyp. J. 8 (2002) 248–257. doi:10.1108/13552540210441166.

[6] S.H. Ko, H. Pan, D. Lee, All-inkjet-printed flexible electronics fabrication on a polymer substrate by low-temperature high-resolution selective laser sintering of metal nanoparticles., Nanotechnology. 18 (2007). http://iopscience.iop.org/article/10.1088/0957-4484/18/34/345202/pdf (accessed September 14, 2017).

[7] E. Sachs, M. Cima, J. Cornie, D. Brancazio, J. Bredt, A. Curodeau, T. Fan, S. Khanuja, A. Lauder, J. Lee, S. Michaels, Three-dimensional printing: the physics and implications of additive manufacturing, in: Ann. CIRP, 1993: pp. 257–260. http://ac.els-cdn.com/S000785060762438X/1-s2.0-S000785060762438X-main.pdf?_tid=3bcff0bc-9983-11e7-8171-00000aacb360&acdnat=1505417638_d44f2398fb9a8245fa00ad4d0119dcf4 (accessed September 14, 2017).

[8] B.N. Turner, R. Strong, S.A. Gold, A review of melt extrusion additive manufacturing processes: I. Process design and modeling, Rapid Prototyp. J. 20 (2014) 192–204. doi:10.1108/RPJ-01-2013-0012.

[9] Y. Huang, M.C. Leu, J. Mazumder, A. Donmez, Additive Manufacturing: Current State, Future Potential, Gaps and Needs, and Recommendations, (n.d.). doi:10.1115/1.4028725.

[10] E. Atzeni, L. Iuliano, P. Minetola, A. Salmi, Redesign and cost estimation of rapid manufactured plastic parts, Rapid Prototyp. J. 16 (2010) 308–317. doi:10.1108/13552541011065704.

[11] V. Kishore, C. Ajinjeru, A. Nycz, B. Post, J. Lindahl, V. Kunc, C. Duty, Infrared preheating to improve interlayer strength of big area additive manufacturing (BAAM) components, Addit. Manuf. 14 (2017) 7–12. doi:10.1016/j.addma.2016.11.008.

[12] J.F. Rodríguez, J.P. Thomas, J.E. Renaud, Mechanical behavior of acrylonitrile butadiene styrene fused deposition materials modeling, Rapid Prototyp. J. 9 (2003) 219–230. doi:10.1108/13552540310489604.
[13] Q. Sun, G.M. Rizvi, C.T. Bellehumeur, P. Gu, Effect of processing conditions on the bonding quality of FDM polymer filaments, Rapid Prototyp. J. 14 (2008) 72–80. doi:10.1108/13552540810862028.
[14] C. Holshouser, C. Newell, S. Palas, L. Martin, C. Duty, L. Love, V. Kunc, R. Lind, P. Lloyd, J. Rowe, R. Dehoff, W. Peter, C. Blue, Out of bounds additive manufacturing, Adv. Mater. Process. 171 (2013) 15–17.
[15] X. Liu, B. Chi, Z. Jiao, J. Tan, F. Liu, W. Yang, A large-scale double-stage-screw 3D printer for fused deposition of plastic pellets, J. Appl. Polym. Sci. 134 (2017) 45147. doi:10.1002/app.45147.
[16] N. Volpato, D. Kretschek, J.A. Foggiatto, C.M. Gomez da Silva Cruz, Experimental analysis of an extrusion system for additive manufacturing based on polymer pellets, Int. J. Adv. Manuf. Technol. 81 (2015) 1519–1531. doi:10.1007/s00170-015-7300-2.
[17] N.S. Hmeidat, J.W. Kemp, B.G. Compton, High-strength epoxy nanocomposites for 3D printing, Compos. Sci. Technol. 160 (2018) 9–20. doi:10.1016/j.compscitech.2018.03.008.
[18] L.J. Love, Utility of Big Area Additive Manufacturing (BAAM) for the Rapid Manufacture of Customized Electric Vehicles, 2014.
[19] B.G. Compton, J.W. Kemp, T. V. Novikov, R.C. Pack, C.I. Nlebedim, C.E. Duty, O. Rios, M.P. Paranthaman, Direct-write 3D printing of NdFeB bonded magnets, Mater. Manuf. Process. 33 (2018) 109–113. doi:10.1080/10426914.2016.1221097.
[20] D. Therriault, S.R. White, J.A. Lewis, Rheological behavior of fugitive organic inks for direct-write assembly, Appl. Rheol. 17 (2007) 1–8.
[21] J.A. Lewis, Direct Ink Writing of 3D Functional Materials**, Adv. Funct. Mater. 16 (2006) 2193–2204. doi:10.1002/adfm.200600434.
[22] J.W. Kemp, N.S. Hmeidat, B.G. Compton, Boron nitride-reinforced polysilazane-derived ceramic composites via direct-ink writing, J. Am. Ceram. Soc. (2020) 1–8. doi:10.1111/jace.17084.
[23] V. Kunc, J. Lindahl, R. Dinwiddie, B. Post, L. Love, M. Matlack, R.L.F. Jr, A.A. Hassen, Investigation of in-autoclave additive manufacturing composite tooling, in: Compos. Adv. Mater. Expo Conf., 2016: pp. 1–9.
[24] L.J. Love, V. Kunc, O. Rios, C.E. Duty, A.M. Elliott, B.K. Post, R.J. Smith, C. a. Blue, The importance of carbon fiber to polymer additive manufacturing, J. Mater. Res. 29 (2014) 1893–1898. doi:10.1557/jmr.2014.212.
[25] M.L. Shofner, K. Lozano, F.J. Rodríguez-Macías, E. V. Barrera, Nanofiber-reinforced polymers prepared by fused deposition modeling, J. Appl. Polym. Sci. 89 (2003) 3081–3090. doi:10.1002/app.12496.

[26] H.L. Tekinalp, V. Kunc, G.M. Velez-garcia, C.E. Duty, L.J. Love, A.K. Naskar, C.A. Blue, S. Ozcan, Highly oriented carbon fiber – polymer composites via additive manufacturing, Compos. Sci. Technol. 105 (2014) 144–150.
[27] C. Duty, V. Kunc, B. Compton, B. Post, D. Erdman, R. Smith, R. Lind, P. Lloyd, L. Love, M.D. Facility, O. Ridge, O. Ridge, Structure and Mechanical Behavior of Big Area Additive Manufacturing (BAAM) Materials, Rapid Prototyp. J. (2016).
[28] V. Kishore, Melt Processability and Post-Processing Treatment of High Temperature Semi-Crystalline Thermoplastics for Extrusion Deposition Additive Manufacturing, University of Tenneessee, 2018. https://trace.tennessee.edu/utk_graddiss/5231.
[29] C. Ajinjeru, V. Kishore, X. Chen, C. Hershey, J. Lindahl, V. Kunc, A.A. Hassen, C. Duty, Rheological survey of carbon fiber-reinforced high-temperature thermoplastics for big area additive manufacturing tooling applications, J. Thermoplast. Compos. Mater. (2019). doi:10.1177/0892705719873941.
[30] V. Kishore, C. Ajinjeru, C. Duty, A. Hassen, J. Lindahl, P. Liu, V. Kunc, Rheological Characteristics of Fiber Reinforced Poly (ether ketone ketone) (PEKK) for Melt Extrusion Additive Manufacturing, in: Int. SAMPE Tech. Conf., Seattle, 2017.
[31] V. Kishore, C. Ajinjeru, A.A. Hassen, J. Lindahl, V. Kunc, C. Duty, Rheological behavior of neat and carbon fiber-reinforced poly(ether ketone ketone) for extrusion deposition additive manufacturing, Polym. Eng. Sci. (2020) 1–10. doi:10.1002/pen.25362.
[32] D.K. Platt, Engineering and High Performance Plastics Market Report, 2003.
[33] A.R.T. Perez, D.A. Roberson, R.B. Wicker, Fracture surface analysis of 3D-printed tensile specimens of novel ABS-based materials, J. Fail. Anal. Prev. 14 (2014) 343–353. doi:10.1007/s11668-014-9803-9.
[34] L.W. McKeen, High-Temperature / High-Performance Polymers, in: Eff. Steriliz. Methods Plast. Elastomers, 2018: pp. 381–415.
[35] B. Macy, Rapid - Affordable Composite Tooling Strategies Utilizing Fused Deposition Modeling.Pdf, in: Int. SAMPE Tech. Conf., Long Beach, CA, 2011: pp. 1–14.
[36] D.R.R. Saini, A. V. Shenoy, Melt Rheology of Some Specialty Polymers, J. Elastomers Plast. 17 (1985) 189–217.
[37] L. Sorrentino, M. Aurilia, S. Iannace, Polymeric Foams from Thermoplastics, Adv. Polym. Technol. 30 (2011) 234–243. doi:10.1002/adv.
[38] R. Johnson, E. Teutsch, Thermoplastic Aromatic Polyimide Composites, Polym. Compos. 4 (1983) 162–166.

[39] J. Vlachopoulos, D. Strutt, Basic Concepts in Polymer Melt Rheology and Their Importance in Processing, in: Appl. Polym. Rheol. Polym. Fluids with Ind. Appl., Wiley, New Jersey, 2011.
[40] A. V. Shenoy, S. Chattopadhyay, V.M. Nadkarni, From melt flow index to rheogram, Rheol. Acta. 22 (1983) 90–101. doi:10.1007/BF01679833.
[41] C. Duty, C. Ajinjeru, V. Kishore, B. Compton, N. Hmeidat, X. Chen, P. Liu, A.A.A.A. Hassen, J. Lindahl, V. Kunc, What makes a material printable? A viscoelastic model for extrusion-based 3D printing of polymers, J. Manuf. Process. 35 (2018) 526–537. doi:10.1016/j.jmapro.2018.08.008.
[42] V. Kishore, X. Chen, C. Ajinjeru, A.A. Hassen, J. Lindahl, J. Failla, V. Kunc, C. Duty, Additive Manufacturing of High Performance Semicrystalline Thermoplastics and their Composites, in: Solid Free. Fabr. 2016, 2016: pp. 906–915.
[43] C. Ajinjeru, V. Kishore, P. Liu, J. Lindahl, A.A. Hassen, V. Kunc, B. Post, L. Love, C. Duty, Determination of melt processing conditions for high performance amorphous thermoplastics for large format additive manufacturing, Addit. Manuf. 21 (2018) 125–132. doi:10.1016/j.addma.2018.03.004.
[44] W.W. Graessley, Polymeric liquids and networks: dynamics and rheology, 1st ed., Garland Science, New York; London, 2008.
[45] L.J. Fetters, D.J. Lohse, D. Richter, T.A. Witten, A. Zirkel, Connection between Polymer Molecular Weight, Density, Chain Dimensions, and Melt Viscoelastic Properties, Macromolecules. 27 (1994) 4639–4647. doi:10.1021/ma00095a001.
[46] J.M. Dealy, R.G. Larson, Structure and Rheology of Molten Polymers, Hanser Publishers, Cincinnati, 2006.
[47] T.A. Vilgis, G. Heinrich, Reinforcement of polymer nano-composites: theory, experiments and applications, Cambridge University Press, Cambridge, UK; New York, 2009.
[48] E.L. Gilmer, D. Miller, C.A. Chatham, C. Zawaski, J.J. Fallon, A. Pekkanen, T.E. Long, C.B. Williams, M.J. Bortner, Model analysis of feedstock behavior in fused filament fabrication: Enabling rapid materials screening, Polymer (Guildf). (2017) 1–11. doi:10.1016/j.polymer.2017.11.068.
[49] A. Bellini, S. Güçeri, M. Bertoldi, Liquefier Dynamics in Fused Deposition, J. Manuf. Sci. Eng. 126 (2004) 237. doi:10.1115/1.1688377.
[50] N. Venkataraman, S. Rangarajan, M.J. Matthewson, B. Harper, A. Safari, S.C. Danforth, G. Wu, N. Langrana, S. Guceri, A. Yardimci, Feedstock material property – process relationships in fused deposition of ceramics (FDC), Rapid Prototyp. J. 6 (2000) 244–253. doi:10.1108/13552540010373344.
[51] D. Roberson, C.M. Shemelya, E. MacDonald, R. Wicker, Expanding the applicability of FDM-type technologies through materials development, Rapid Prototyp. J. 21 (2015) 137–143. doi:10.1108/RPJ-12-2014-0165.

[52] M. Nikzad, S.H. Masood, I. Sbarski, Thermo-mechanical properties of a highly filled polymeric composites for Fused Deposition Modeling, Mater. Des. 32 (2011) 3448–3456. doi:10.1016/j.matdes.2011.01.056.
[53] M. Nikzad, S.H. Masood, I. Sbarski, A. Groth, A Study of Melt Flow Analysis of an ABS-Iron Composite in Fused Deposition Modelling Process, 14 (2009) 29–37.
[54] S. Hwang, E.I. Reyes, K.-S. Moon, R.C. Rumpf, N. Soo Kim, Thermo-mechanical Characterization of Metal/Polymer Composite Filaments and Printing Parameter Study for Fused Deposition Modeling in the 3D Printing Process, J. Electron. Mater. 44 (2015) 771–777. doi:10.1007/s11664-014-3425-6.
[55] H.S. Ramanath, A.C.K. Chua, A.K.F. Leong, A.K.D. Shah, Melt flow behaviour of poly-e-caprolactone in fused deposition modelling, J Mater Sci Mater. Med. 19 (2008) 2541–2550. doi:10.1007/s10856-007-3203-6.
[56] C. Mcilroy, P.D. Olmsted, Deformation of an Amorphous Polymer during the Fused-Filament-Fabrication Method for Additive Manufacturing, n.d. https://arxiv.org/pdf/1611.01522.pdf (accessed October 16, 2018).
[57] T.A. Osswald, J. Puentes, J. Kattinger, Fused filament fabrication melting model, Addit. Manuf. 22 (2018) 51–59. doi:10.1016/j.addma.2018.04.030.
[58] M.E.A. Papon, A. Haque, M.A.R. Sharif, Effect of nozzle geometry on Melt flow simulation and structural property of thermoplastic nanocomposites in Fused deposition modeling, in: 32nd Tech. Conf. Am. Soc. Compos. 2017, 2017: pp. 2167–2182. doi:10.12783/asc2017/15339.
[59] T.J. Coogan, D.O. Kazmer, In-line rheological monitoring of fused deposition modeling, J. Rheol. (N. Y. N. Y). 63 (2019) 141–155. doi:10.1122/1.5054648.
[60] D.D. Phan, Z.R. Swain, M.E. Mackay, Rheological and heat transfer effects in fused filament fabrication, J. Rheol. (N. Y. N. Y). 62 (2018) 1097–1107. doi:10.1122/1.5022982.
[61] V. Nienhaus, K. Smith, D. Spiehl, E. Dörsam, Investigations on nozzle geometry in fused filament fabrication, Addit. Manuf. 28 (2019) 711–718. doi:10.1016/j.addma.2019.06.019.
[62] D.A. Anderegg, H.A. Bryant, D.C. Ruffin, S.M. Skrip, J.J. Fallon, E.L. Gilmer, M.J. Bortner, In-situ monitoring of polymer flow temperature and pressure in extrusion based additive manufacturing, Addit. Manuf. 26 (2019) 76–83. doi:10.1016/j.addma.2019.01.002.
[63] B.G. Compton, J.A. Lewis, 3D-Printing of Lightweight Cellular Composites, Adv. Mater. 26 (2014) 5930–5935. doi:10.1002/adma.201401804.
[64] C. Duty, C. Ajinjeru, V. Kishore, B. Compton, N. Hmeidat, X. Chen, P. Liu, A.A. Hassen, J. Lindahl, V. Kunc, A Viscoelastic Model for Evaluating Extrusion-Based Print Conditions, in: Solid Free. Fabr. 2017, 2017.
[65] M. Dinkgreve, J. Paredes, M.M. Denn, D. Bonn, On different ways of measuring “the” yield stress, J. Nonnewton. Fluid Mech. 238 (2016) 233–241. doi:10.1016/j.jnnfm.2016.11.001.

[66] T.C. Papanastasiou, Flows of Materials with Yield, J. Rheol. . 31 (1987) 385–404. doi:10.1122/1.549709.
[67] D.J. Horrobin, R.M. Nedderman, Die entry pressure drops in paste extrusion, Chem. Eng. Sci. 53 (1998) 3215–3225.
[68] I. Narisawa, Mechanical properties of polymers, Reports Prog. Polym. Phys. Japan. 43 (2000) 347–368. doi:10.1201/9781420057805-14.
[69] S.P. Products, Density Values - Selected Resins, Ansonia, 2016. https://cdn2.hubspot.net/hubfs/2835922/Reference Tables- Density of plastic.pdf?t=1535586246905%0Ahttp://www.stelray.com/reference-tables.html.
[70] Plastemart, Processing of PLA (biopolymer), (2020). http://atozplastics.com/PrintFile.asp?REF=/webtech/upload/literature/processingofpla(biopolymer).asp&.
[71] A.R. Payne, The dynamic properties of carbon black loaded natural rubber vulcanizates. Part I, J. Appl. Polym. Sci. 6 (1962) 368–372. doi:10.1002/app.1962.070062115.
[72] A.A. Hassen, J. Lindahl, X. Chen, B. Post, L. Love, V. Kunc, Additive Manufacturing of composite tooling using high temperature thermoplastic materials, in: Int. SAMPE Tech. Conf., Long Beach, CA, 2016.
[73] F. Stan, N.V. Stanciu, C. Fetecau, Melt rheological properties of ethylene-vinyl acetate/multi-walled carbon nanotube composites, Compos. Part B Eng. 110 (2017) 20–31. doi:10.1016/j.compositesb.2016.10.071.
[74] R.R. Collino, T.R. Ray, R.C. Fleming, J.D. Cornell, B.G. Compton, M.R. Begley, Deposition of ordered two-phase materials using microfluidic print nozzles with acoustic focusing, Extrem. Mech. Lett. 8 (2016) 96–106. doi:10.1016/j.eml.2016.04.003.
[75] J.R. Sangoro, R.C. Pack, N.S. Hmeidat, M.F. Heres, B.G. Compton, Electrical and Mechanical Properties of 3D-Printed Graphene-Reinforced Epoxy, Jom. 70 (2017) 292–297. doi:10.1007/s11837-017-2707-x.
[76] C.S. Davis, K.E. Hillgartner, S.H. Han, J.E. Seppala, Mechanical strength of welding zones produced by polymer extrusion additive manufacturing, Addit. Manuf. 16 (2017) 162–166. doi:10.1016/j.addma.2017.06.006.
[77] C. Ajinjeru, V. Kishore, P. Liu, A.A. Hassen, J. Lindahl, Rheological evaluation of high temperature polymers to identify successful extrusion parameters, in: 28th Annu. Int. Solid Free. Fabr. Symp., 2017: pp. 485–494.
[78] P. Chesser, B. Post, A. Roschli, C. Carnal, R. Lind, M. Borish, L. Love, Extrusion Control for High Quality Printing on Big Area Additive Manufacturing (BAAM) Systems, Addit. Manuf. 28 (2019) 445–455. doi:10.1016/j.addma.2019.05.020.
[79] S.G. Hatzikiriakos, J.M. Dealy, Start-up pressure transients in a capillary rheometer, Polym. Eng. Sci. 34 (1994) 493–499. doi:10.1002/pen.760340606.

[80] E. Mitsoulis, O. Delgadillo-Velazquez, S.G. Hatzikiriakos, Transient capillary rheometry: Compressibility effects, J. Non-Newtonian Fluid Mech. 145 (2007) 102–108. https://ac-els-cdn-com.proxy.lib.utk.edu/S0377025707001231/1-s2.0-S0377025707001231-main.pdf?_tid=1bda35ec-b18e-46aa-b589-a1f4e8291fa4&acdnat=1537470244_4834060a14845fdcb26178fc04293f3d (accessed September 20, 2018).
[81] S.G. Hatzikiriakos, E. Mitsoulis, Excess pressure losses in the capillary flow of molten polymers, Rheol Acta. 35 (1996) 545–555. https://link-springer-com.proxy.lib.utk.edu/content/pdf/10.1007%2FBF00396506.pdf (accessed August 8, 2018).
[82] A. Roschli, B. Post, P. Chesser, M. Borish, L. Love, S. Kim, Creating Toolpaths Without Starts and Stops for Extrusion-Based Systems, in: 30th Annu. Int. Solid Free. Fabr. Symp., Austin TX, 2019: pp. 1113–1125.
[83] M.E. Mackay, Z.R. Swain, C.R. Banbury, D.D. Phan, D.A. Edwards, The performance of the hot end in a plasticating 3D printer; The performance of the hot end in a plasticating 3D printer, (2017). doi:10.1122/1.4973852.
[84] T. Hofstaetter, R. Pimentel, D.B. Pedersen, M. Mischkot, H.N. Hansen, Simulation of a Downsized FDM Nozzle, COMSOL Conf. Grenoble. (2015).
[85] E. Mitsoulis, S.G. Hatzikiriakos, K. Christodoulou, D. Vlassopoulos, E. Mitsoulis, S.G. Hatzikiriakos, K. Christodoulou, D. Vlassopoulos, Sensitivity analysis of the Bagley correction to shear and extensional rheology, 1998. https://link-springer-com.proxy.lib.utk.edu/content/pdf/10.1007%2Fs003970050131.pdf (accessed August 8, 2018).
[86] J. Dvorak, C. Ajinjeru, T. Smith, S. Kim, C. Hershey, J. Lindahl, V. Kunc, C. Duty, Measurement and Analysis of Pressure Profile Within Big Area Additive Manufacturing Single Screw Extruder, in: 30th Annu. Int. Solid Free. Fabr. Symp., Austin TX, 2019: pp. 1242–1250.
[87] A.. Mamalis, K.. Spentzas, G. Kouzilos, I. Theodorakopoulos, N.. Pantelelis, On the High-Density Polyethylene Extrusion: Numerical, Analytical and Experimental Modeling, Adv. Polym. Technol. 29 (2010) 173–184. doi:10.1002/adv.
[88] M. Rahman, N.R. Schott, L.K. Sadhu, Glass Transition of ABS in 3D Printing, Comsol Bost. 2016. (2016) 3.
[89] B.B. Shahriar, C. Arthur, C. France, N. Valérie, Influence of parameters controlling the extrusion step in fused filament fabrication (FFF) process applied to polymers using numerical simulation, AIP Conf. Proc. 1960 (2018). doi:10.1063/1.5034995.
[90] R. Jerez-Mesa, J.A. Travieso-Rodriguez, X. Corbella, R. Busqué, G. Gomez-Gras, Finite element analysis of the thermal behavior of a RepRap 3D printer liquefier, Mechatronics. 36 (2016) 119–126. doi:10.1016/j.mechatronics.2016.04.007.

[91] ASTM D1238-13, Standard test method for melt flow rates of thermoplastics by extrusion plastometer., 2004. doi:10.1520/D1238-10.Procedures.
[92] Q. Zhang, L.A. Archer, Poly(ethylene oxide)/Silica Nanocomposites: Structure and Rheology, (n.d.). doi:10.1021/la026338j.
[93] T.A. Osswald, G. Menges, Material Science of Polymers for Engineers, Hanser Publishers, 2012.
[94] J.X. Hou, C. Svaneborg, R. Everaers, G.S. Grest, Stress relaxation in entangled polymer melts, Phys. Rev. Lett. 105 (2010) 1–4. doi:10.1103/PhysRevLett.105.068301.
[95] D.A. Siginer, S.I. Bakhtiyarov, Flow of drilling fluids in eccentric annuli, J. Nonnewton. Fluid Mech. 78 (1998) 119–132. doi:10.1016/S0377-0257(97)00101-8.
[96] C. Reynolds, R. Thompson, T. McLeish, Pressure and shear rate dependence of the viscosity and stress relaxation of polymer melts, J. Rheol. (N. Y. N. Y). 62 (2018) 631–642. doi:10.1122/1.5012969.
[97] H. Li, G. Taylor, V. Bheemreddy, O. Iyibilgin, M. Leu, K. Chandrashekhara, Modeling and characterization of fused deposition modeling tooling for vacuum assisted resin transfer molding process, Addit. Manuf. 7 (2015) 64–72. doi:10.1016/j.addma.2015.02.003.
[98] H.M. Laun, Orientation effects and rheology of short glass fiber-reinforced thermoplastics, Colloid Polym. Sci. 262 (1984) 257–269. doi:10.1007/BF01410464.
[99] W. Lee, H.H. George, Flow Visualization of Fiber Suspensions *, Polym. Eng. Sci. 18 (1978) 146–156.
[100] R.J. Crowson, M.J. Folkes, Rheology of Short Glass Fiber-Reinforced Thermoplastics and Its Application To Injection Molding - 2. the Effect of Material Parameters, Polym. Eng. Sci. 20 (1980) 934–940. http://www.scopus.com/scopus/inward/record.url?eid=2-s2.0-0019055123&partnerID=40&rel=R8.2.0.
[101] J.P. Greene, J.O. Wilkes, Steady-State and dynamic properties of concentrated fiber-filled thermoplastics, Polym. Eng. Sci. 35 (1995) 1670–1681. doi:10.1002/pen.760352103.
[102] D. Hoskins, C. Ajinjeru, V. Kunc, J. Lindahl, D.M. Nieto, C. Duty, The Effect of Shear-Induced Fiber Alignment on Viscosity for 3D Printing of Reinforced Polymers, Solid Free. Fabr. Symp. (2018) 1102–1111. http://sffsymposium.engr.utexas.edu/sites/default/files/2018/089 TheEffectofShearInducedFiberAlignmentonVis.pdf.
[103] J.K. Kim, J.H. Song, Rheological properties and fiber orientation of short fiber reinforce dplastics, J. Rheol. 41 (1997) 1061–1085.
[104] T. Araki, J.L. White, Shear Viscosity of Rubber Modified Thermoplastics: Dynamically Vulcanized Thermoplastic Elastomers and ABS Resins at Very Low Stress, Polym. Eng. Sci. 38 (1998) 590–595.

[105] M. Bertin, G. Marin, J. Montfort, Viscoelatic Properties of Acrylonitrile-Butadiene-Styrene (ABS) Polymers in the Molten State, Polym. Eng. Sci. 35 (1995) 1394–1406.
[106] M. Nikzad, S.H. Masood, I. Sbarski, A.M. Groth, Rheological Properties of a Particulate-Filled Polymeric Composite through Fused Deposition Process, Mater. Sci. Forum. 654–656 (2010) 2471–2474. doi:10.4028/www.scientific.net/MSF.654-656.2471.
[107] J.Z. Liang, J.N. Ness, Effect of die angle on flow behaviour for high impact polystyrene melt, Polym. Test. 16 (1997) 403–412. doi:10.1016/S0142-9418(97)00001-9.
[108] N. Li, Y. Li, S. Liu, Rapid prototyping of continuous carbon fiber reinforced polylactic acid composites by 3D printing, J. Mater. Process. Technol. 238 (2016) 218–225. doi:10.1016/j.jmatprotec.2016.07.025.
[109] D. Galvan, F. Carneiro, M. Mazzucco, J.R. Bartoli, M.A. D'Ávila, A.R. Morales, E.G. Fernandes, Effect of organoclay mixture on the rheological properties of ABS-clay nanocomposites, Macromol. Symp. 319 (2012) 167–172. doi:10.1002/masy.201100165.
[110] P. Singh, A.K. Ghosh, Torsional, tensile and structural properties of acrylonitrile-butadiene-styrene clay nanocomposites, Mater. Des. 55 (2014) 137–145. doi:10.1016/j.matdes.2013.09.036.
[111] C. Ajinjeru, V. Kishore, Z. Sudbury, C. Duty, J. Lindahl, A. Hassen, B. Post, L. Love, V. Kunc, The influence of rheology on melt processing conditions of fiber reinforced polyetherimide for Big Area Additive Manufacturing, in: Int. SAMPE Tech. Conf., Seattle, 2017.
[112] B.N. Turner, S.A. Gold, A review of melt extrusion additive manufacturing processes: II. Materials, dimensional accuracy, and surface roughness, Rapid Prototyp. J. 21 (2015) 250–261. doi:10.1108/RPJ-01-2013-0012.
[113] R.L. Powell, Rheology of suspensions of rodlike particles, J. Stat. Phys. 62 (1991) 1073–1094. doi:10.1007/BF01128178.
[114] J.K. Kim, J.H. Song, Rheological properties and fiber orientations of short fiber-reinforced plastics, J. Rheol. (N. Y. N. Y). 41 (1997) 1061–1085. doi:10.1122/1.550825.
[115] A. V Shenoy, Unsteady shear viscoelastic properties, in: Rheol. Fill. Polym. Syst., Springer Science + Business Media Dordrecht, 1999: pp. 338–394.
[116] D.M. Bigg, Rheological behavior of highly filled polymer melts, Polym. Eng. Sci. 23 (1983) 206–210. doi:10.1002/pen.760230408.
[117] M.M.M. Khan, R.F. Liang, R.K. Gupta, S. Agarwal, Rheological and mechanical properties of ABS / PC blends, Korea-Australia Rheol. J. 17 (2005) 1–7.
[118] L. Czarnecki, J.L. White, Shear flow rheological properties, fiber damage, and mastication characteristics of aramid-, glass-, and cellulose-fiber-reinforced polystyrene melts, J. Appl. Polym. Sci. 25 (1980) 1217–1244. doi:10.1002/app.1980.070250623.

[119] R.T. Young, D.G. Baird, Processing and properties of injection molded thermoplastic composites reinforced with melt processable glasses, Polym. Compos. 21 (2000) 645–659. http://www.scopus.com/inward/record.url?eid=2-s2.0-0034296094&partnerID=40&md5=1350bef67be4cabfd334a6e7d62c0e9d.
[120] T.W. Hughes, R. Avakian, L. Hu, K.C. Chuang, Reactive extrusion of high temperature resins for additive manufacturing, in: Int. SAMPE Tech. Conf., 2014: pp. 1–17. http://www.scopus.com/inward/record.url?eid=2-s2.0-84907803194&partnerID=40&md5=3f705a519c75557800e266a33042846c.
[121] M.R. Nobile, D. Acierno, L. Incarnato, E. Amendola, L. Nicolais, C. Carfagna, Improvement of the processability of advanced polymers, J. Appl. Polym. Sci. 41 (1990) 2723–2737. doi:10.1002/app.1990.070411119.
[122] S. Lee, S.M. Hong, Y. Seo, T.S. Park, S.S. Hwang, K.U. Kim, J.W. Lee, Characterization and processing of blends of poly(ether imide) with thermotropic liquid crystalline polymer, Polymer (Guildf). 35 (1994) 519–531. doi:10.1016/0032-3861(94)90506-1.
[123] W.P. Cox, E.H. Merz, Correlation of Dynamic and Steady Flow Viscosities, J. Polym. Sci. 28 (1958) 619–622.
[124] R. Guo, J. Azaiez, C. Bellehumeur, Rheology of fiber filled polymer melts: Role of fiber-fiber interactions and polymer-fiber coupling, Polym. Eng. Sci. 45 (2005) 385–399. doi:10.1002/pen.20285.
[125] J.R. Raney, B.G. Compton, J. Mueller, T.J. Ober, K. Shea, J.A. Lewis, Rotational 3D printing of damage-tolerant composites with programmable mechanics, Proc. Natl. Acad. Sci. 115 (2018) 1198–1203. doi:10.1073/pnas.1715157115.

APPENDIX

BAAM as a Rheometer

Determining Power Law Variables from BAAM Data

Coogan and Kazmer were the first to demonstrate the use of an AM system as a rheometer [59]. Their FFF rheometer results showed excellent agreement with capillary and parallel-plate rheometry offline measurements. Given the high accuracy of their findings, they recommended that pressure measurements and predictions in AM can be improved using AM systems as in-line rheometers.

To convert BAAM steady-state pressures to viscosity and shear rate values, the following approach was used.

Given:

$$P_L Q_L \ \& \ P_H Q_H \tag{1}$$

where P_L is the BAAM steady-state pressure at the low screw speed, Q_L is the volume flow rate at the low screw speed, P_H is the BAAM steady-state pressure at the high screw speed, and Q_H is the volume flow rate at the high screw speed.

Governing Equations:

$$P_{TOT} = \Delta P_E + \Delta P_N \tag{2}$$

where P_{TOT} is total pressure drop in the nozzle, ΔP_E is the pressure drop in the exit region of the nozzle, and ΔP_N is the pressure drop in the nozzle region of the die.

Hagen-Poiseuille Equation:

$$\Delta P = \frac{8\,\eta\,Q\,L}{\pi R^4} \tag{3}$$

where Q is the volume flow rate, η is the material viscosity, L is the length of the nozzle and R is the radius of the nozzle.

The power-law is used to model the non-Newtonian behavior of polymer melts:

$$\eta = C\dot{\gamma}^{n-1} \tag{4}$$

where n is the power-law index, C is the consistency index, η is the viscosity and $\dot{\gamma}$ is the shear rate. During extrusion, the apparent shear rate $(\dot{\gamma}_a)$ at the wall (assuming no slip) can be determined from the flow rate by:

$$\dot{\gamma}_a = \frac{4\,Q}{\pi R^3} \tag{5}$$

Therefore, to calculate the P_{TOT}:

$$P_{TOT} = \frac{8}{\pi}\eta_E \frac{L_E}{R_E^4} + \frac{8}{\pi}\eta_N \frac{L_N}{R_N^4} \tag{6}$$

$$P_{TOT} = \frac{8Q}{\pi}\left(C\,\dot{\gamma}_E^{n-1}\frac{L_E}{R_E^4} + C\,\dot{\gamma}_N^{n-1}\frac{L_N}{R_N^4}\right) \tag{7}$$

$$P_{TOT} = \frac{8Q}{\pi}\left[\left(\frac{4Q}{\pi R_E^3}\right)^{n-1}\frac{L_E}{R_E^4} + \left(\frac{4Q}{\pi R_N^3}\right)^{n-1}\frac{L_N}{R_N^4}\right] \tag{8}$$

Equation 1: (P_L @ Q_L)

$$P_L = \frac{8Q_L C}{\pi}\left[\left(\frac{4Q_L}{\pi R_E^3}\right)^{n-1}\frac{L_E}{R_E^4} + \left(\frac{4Q_L}{\pi R_N^3}\right)^{n-1}\frac{L_N}{R_N^4}\right] \tag{9}$$

Solve C

$$C = \frac{\pi P_L}{8Q_L}\left[\left(\frac{4Q_L}{\pi R_E^3}\right)^{n-1}\frac{L_E}{R_E^4} + \left(\frac{4Q_L}{\pi R_N^3}\right)^{n-1}\frac{L_N}{R_N^4}\right]^{-1} \tag{10}$$

Equation 2: (P_H @ Q_H)

$$P_H = \frac{8Q_H C}{\pi}\left[\left(\frac{4Q_H}{\pi R_E^3}\right)^{n-1}\frac{L_E}{R_E^4} + \left(\frac{4Q_H}{\pi R_N^3}\right)^{n-1}\frac{L_N}{R_N^4}\right] \tag{11}$$

Plug in C

$$P_H = P_L\frac{Q_H}{Q_L}\frac{\left[\left(\frac{4Q_H}{\pi R_E^3}\right)^{n-1}\frac{L_E}{R_E^4} + \left(\frac{4Q_H}{\pi R_N^3}\right)^{n-1}\frac{L_N}{R_N^4}\right]}{\left(\frac{4Q_L}{\pi R_E^3}\right)^{n-1}\frac{L_E}{R_E^4} + \left(\frac{4Q_L}{\pi R_N^3}\right)^{n-1}\frac{L_N}{R_N^4}} \tag{12}$$

Equation 12 is used to solve for n and then C. The results are tabulated below along with the viscosity and shear rate graphs.

Power Law Variables from BAAM Data for ABS 20 wt.% CF

Table A.1. BAAM process parameters for ABS 20 wt.% CF

Nozzle diameter (cm)	0.508		0.762		1.016	
Screw speed (RPM)	50	100	50	350	50	350
Q (cc/s)	1.61	3.94	1.76	8.78	1.80	13.02
BAAM P (MPa)	4.07	5.08	2.03	3.19	0.76	1.59

Table A.2. BAAM nozzle dimensions for ABS 20 wt.% CF

Nozzle diameter (cm)	0.508	0.762	1.016
L_E (cm)	1.14	1.14	1.14
D_N (cm)	1.02	1.02	1.02
L_N (cm)	2.42	2.42	1.02
L_E / R_E^4 (cm)	274	55	17
L_N / R_N^4 (cm)	36	36	36

Table A.3. BAAM shear rates for ABS 20 wt.% CF

Nozzle diameter (cm)	0.508		0.762		1.016	
Screw speed (RPM)	50	100	50	350	50	350
Exit shear rate (1/s)	125	306	41	204	17	126
Nozzle shear rate (1/s)	15	38	17	84	17	126

Table A.4. Numerically solved Power-Law exponent, n for ABS 20 wt.% CF

Nozzle diameter (cm)	0.508	0.762	1.016
P_L (BAAM)	4.07	2.03	0.76
Q_L (BAAM)	1.61	1.76	1.80
P_H (BAAM)	5.08	3.19	1.59
Q_H (BAAM)	3.94	8.78	13.02

Table A.5 Guess n values for ABS 20 wt.% CF

Guess (n)	n = 0.248		n = 0.279		n = 0.375	
To make	P_H (Eqn)	5.083	P_H (Eqn)	3.183	P_H (Eqn)	1.593
Equal this	P_H (BAAM)	5.085	P_H (BAAM)	3.189	P_H (BAAM)	1.594
Calculate	C (Pa)	84019	C (Pa)	53880	C (Pa)	18506
& Verify	P_L (BAAM)	4.07	P_L (BAAM)	2.03	P_L (BAAM)	0.76

Power Law Variables from BAAM Data for PPSU 25 wt.% CF

Table A.6. BAAM process parameters for PPSU 25 wt.% CF

Nozzle diameter (cm)	0.508		0.762		1.016	
Screw speed (RPM)	50	100	100	350	50	350
Q (cc/s)	0.83	2.34	1.84	5.89	0.96	4.53
BAAM P (MPa)	3.38	5.52	2.34	3.79	0.71	1.93

Table A.7. BAAM nozzle dimensions for PPSU 25 wt.% CF

Nozzle diameter (cm)	0.508	0.762	1.016
L_E (cm)	1.14	1.14	1.14
D_N (cm)	1.02	1.02	1.02
L_N (cm)	2.42	2.42	1.02
L_E / R_E^4 (cm)	274	55	17
L_N / R_N^4 (cm)	36	36	36

Table A.8. BAAM shear rates for PPSU 25 wt.% CF

Nozzle diameter (cm)	0.508		0.762		1.016	
Screw speed (RPM)	50	100	100	350	50	350
Exit shear rate (1/s)	64	182	43	137	9	44
Nozzle shear rate (1/s)	8	22	18	57	9	44

Table A.9. Numerically solved Power-Law exponent, n for PPSU 25 wt.% CF

Nozzle diameter (cm)	0.508	0.762	1.016
P_L (BAAM)	3.38	2.34	0.71
Q_L (BAAM)	0.83	1.84	0.96
P_H (BAAM)	5.52	3.79	1.93
Q_H (BAAM)	2.34	5.89	4.53

Table A.10 Guess n values for PPSU 25 wt.% CF

Guess (n)	n = 0.471		n = 0.413		n = 0.644	
To make	P_H (Eqn)	5.514	P_H (Eqn)	3.790	P_H (Eqn)	1.931
Equal this	P_H (BAAM)	5.516	P_H (BAAM)	3.792	P_H (BAAM)	1.931
Calculate	C (Pa)	37979	C (Pa)	39488	C (Pa)	12050
& Verify	P_L (BAAM)	3.38	P_L (BAAM)	2.34	P_L (BAAM)	0.71

Calculated Viscosities as a Function of Shear Rate for ABS 20 wt.% CF and PPSU 25 wt.% CF

Melt flow curves showing the calculated viscosities as a function of shear rate for the three nozzle diameters are shown in Figure A.1 along with the parallel-plate measurements for the respective materials. It is observed that the melt viscosity increases with increase in nozzle size in both material resulting in nozzle size dependent n and C values. However, these results are not in agreement with what Coogan and Kazmer observed when they used the FFF printer as a rheometer and therefore warrant further investigation. High viscosity values are observed in instances where the temperature is low but in this work, nothing definitive can be said about the impact of temperature in the nozzle on the viscosity since this was not captured in the tests. The variation in viscosity as a function of nozzle diameter does not seem to be a function of high shear memory in the extruder or material relaxation time either. Although it is evident that different n and C values should be used as inputs for the Hagen-Poiseuille and COMSOL simulations in order to better extrusion pressures, studies involving the incorporation of a thermocouple to the BAAM nozzle need to be done to quantify the impact of temperature on the melt during deposition.

Mesh Sensitivity Study

Systemic mesh independence studies were conducted by refining the mesh successfully for the BAAM nozzle using COMSOL Multiphysics software to determine the optimum mesh resolution. Pressure drops across the axial asymmetric nozzle were observed for different mesh resolutions and are plotted in Figure A.1 for the 0.508 cm and 1.016 cm nozzles using ABS 20 wt.% CF as the material. With increase in the number of mesh elements, there was not a significant difference found. The model appears to be optimized at 54214 elements beyond which no significant changes are noticed. For the simulations in this dissertation, the normal mesh corresponding to element size used was 54214. Figure A.3 shows the mesh distribution for the 1.016 cm nozzle.

Influence of Exit Geometry and Entry Angle on Simulated Pressure Predictions

The exit length and entry angles of the BAAM nozzle were varied for the COMSOL simulated ΔP predictions. The n and C values for ABS 20 wt.% CF (n = 0.369, C = 20499 $Pa.s^n$) and PPSU 25 wt.% CF (n = 0.77, C = 6031 $Pa.s^n$) used were experimentally determined using a parallel plate rheometer. Figures A.4 and A.5 show the different nozzle geometries simulated for the 0.508 cm and

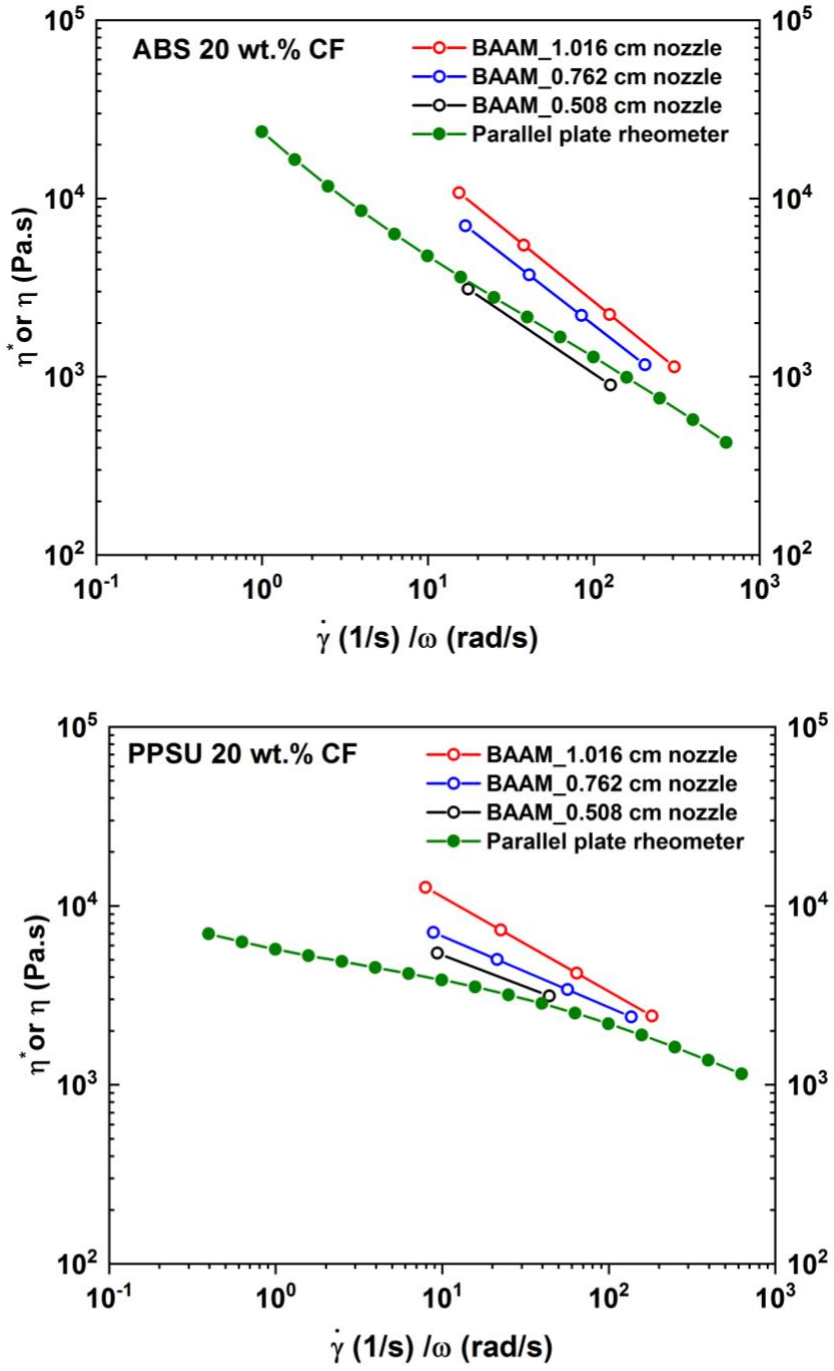
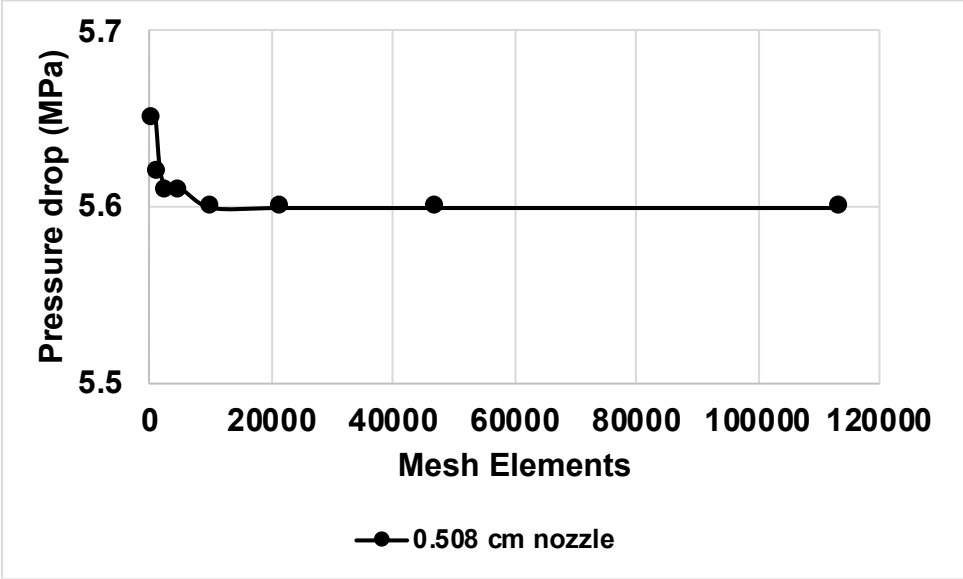


Figure A.1. Viscosity vs shear rate calculated from BAAM steady-state pressure values for ABS 20 wt.% CF and PPSU 25 wt.% CF



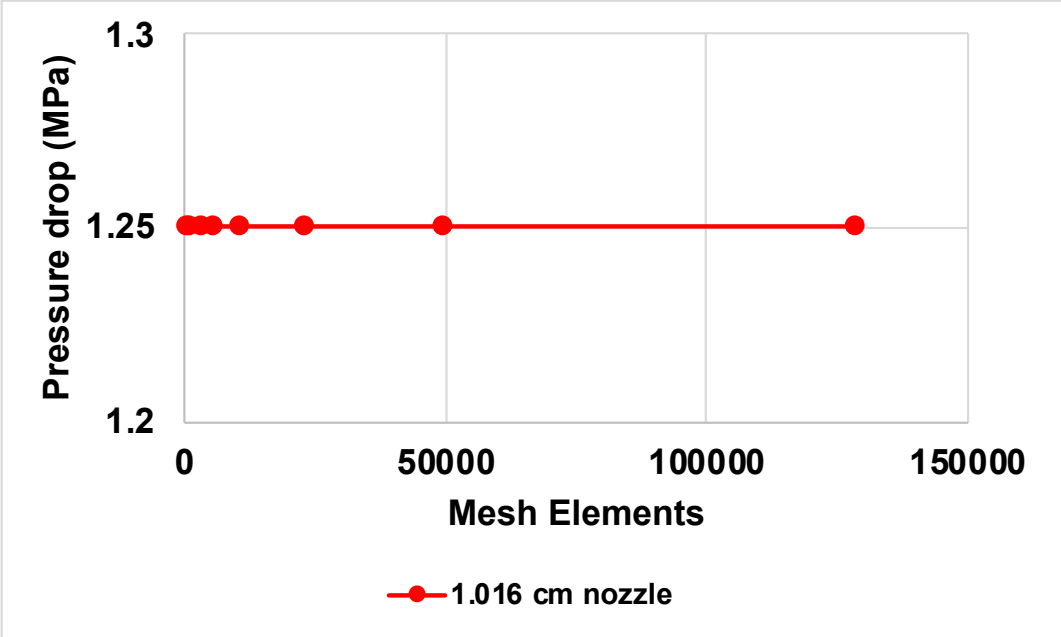


Figure A.2. Mesh independence study for the 0.508 cm and 1.016 cm nozzle

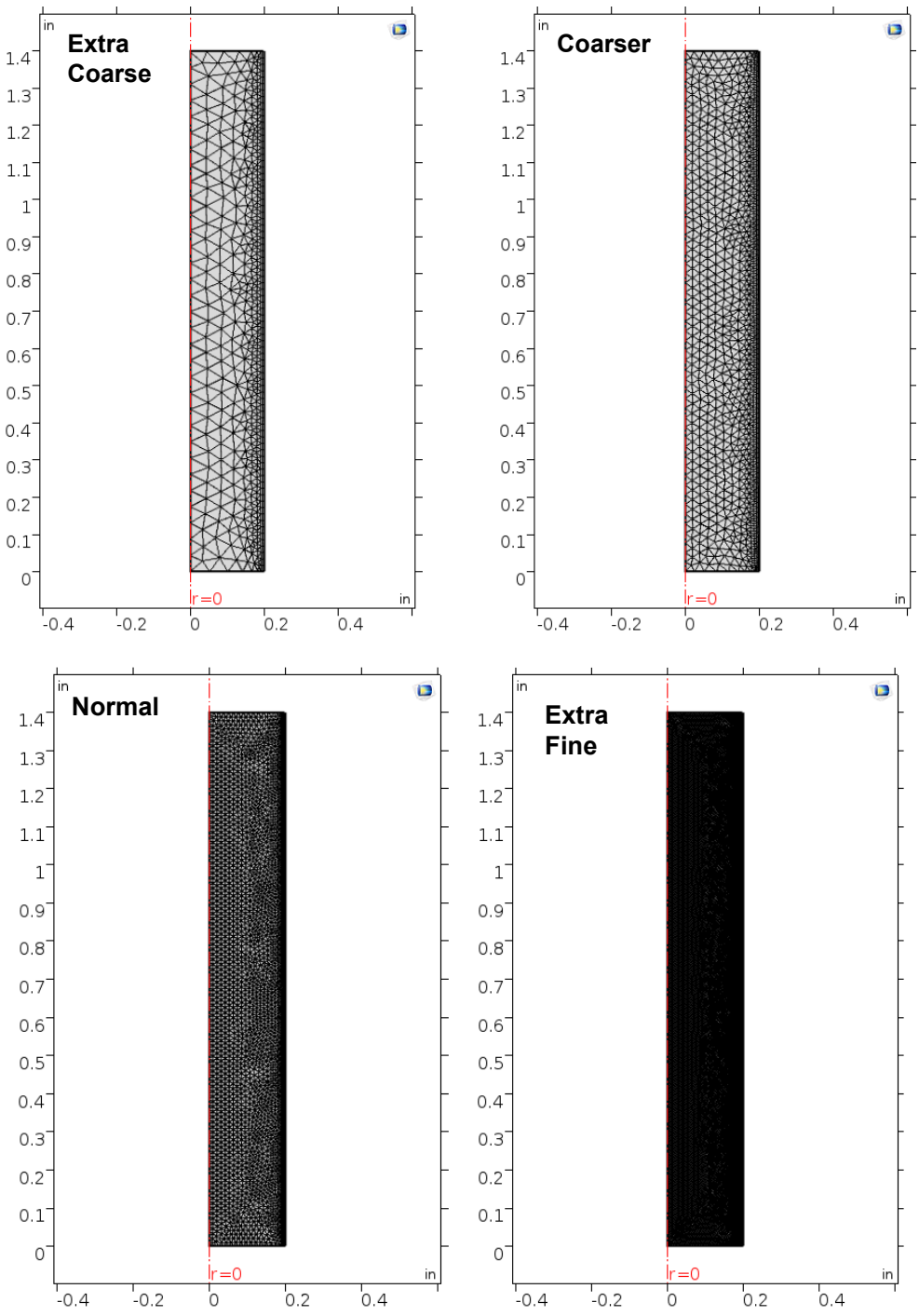


Figure A.3. Exterior image of mesh on the 1.016 cm nozzle

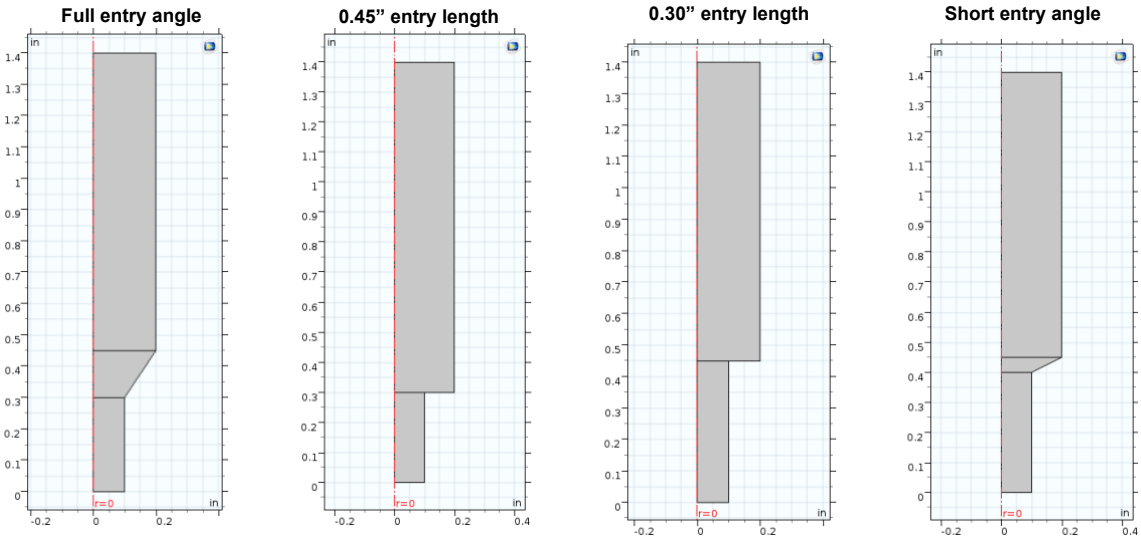


Figure A.4. COMSOL nozzle geometries: 0.508 cm nozzle diameter

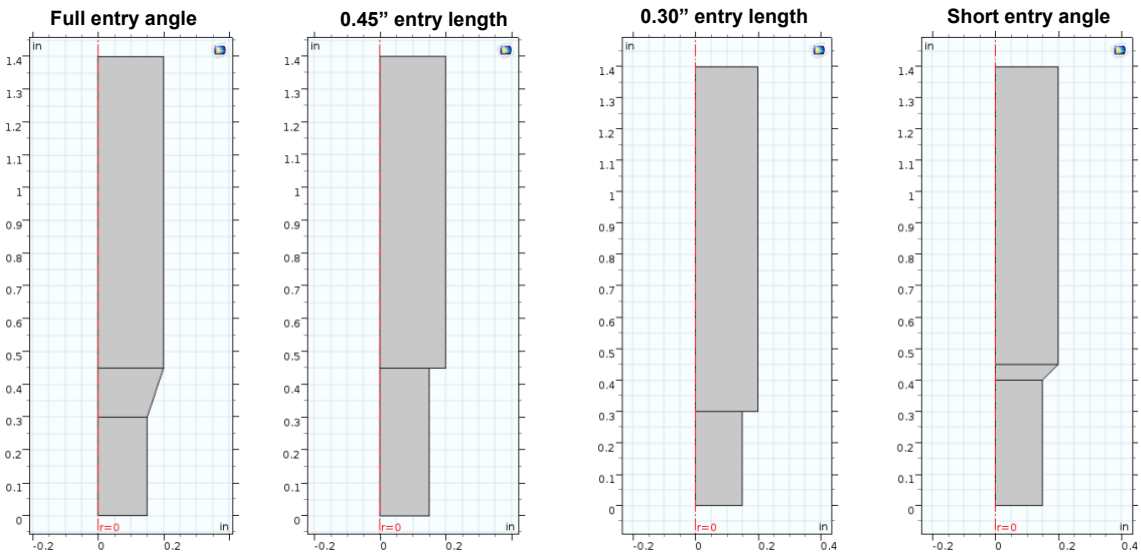


Figure A.5. COMSOL nozzle geometries: 0.762 cm nozzle diameter

0.762 cm nozzles, respectively. It was found that varying nozzle exit length and angle had minimal effect on the COMSOL ΔP predictions for the 0.762 cm nozzle for ABS 20 wt.% CF (Figure A.6). However, for the 0.508 cm nozzle, having a longer exit length region and shorter contraction angle had significant effects on the COMSOL predictions. Since these simulations utilized the parallel-plate rheometer n and C values, HP and COMSOL predictions greatly underpredicted BAAM steady-state pressures.

PPSU 25 wt.% CF COMSOL simulated ΔP predictions are very similar to those of ABS 20 wt.% CF (Figure A.7). Varying the nozzle exit length and entry angle was found to have no impact on the COMSOL ΔP predictions for the 0.762 cm nozzle well as in the 0.508 cm nozzle, a longer exit length region and shorter contraction angle significantly impact the predictions.

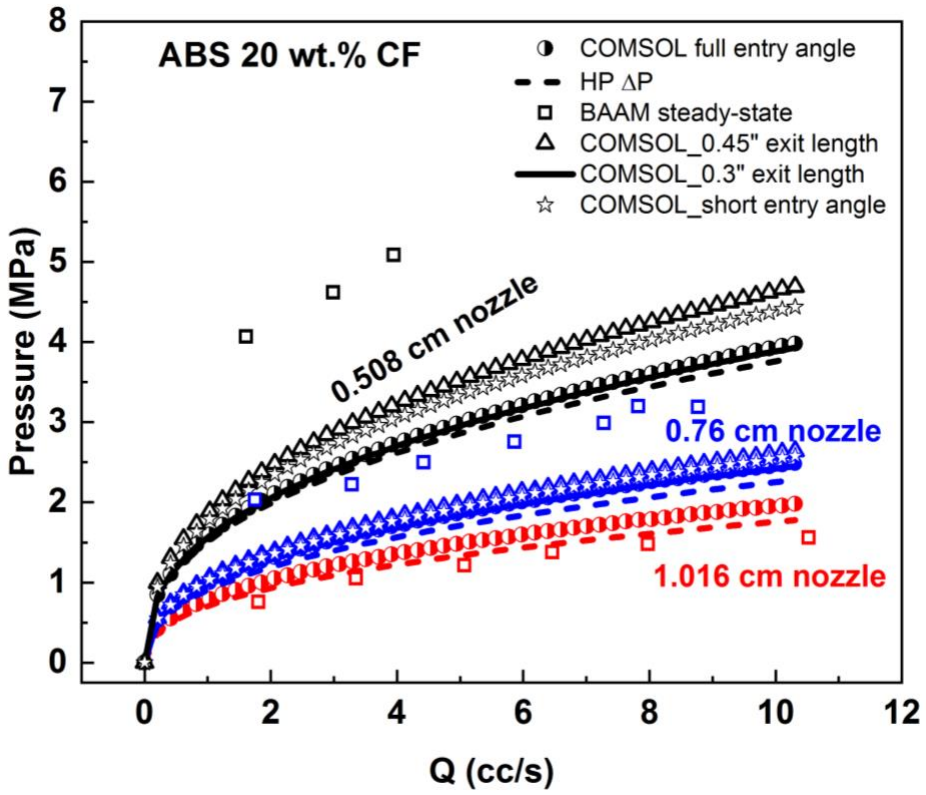


Figure A.6. COMSOL pressure drop predictions for ABS 20 wt.% CF using BAAM nozzles with varying exit lengths and entry angles

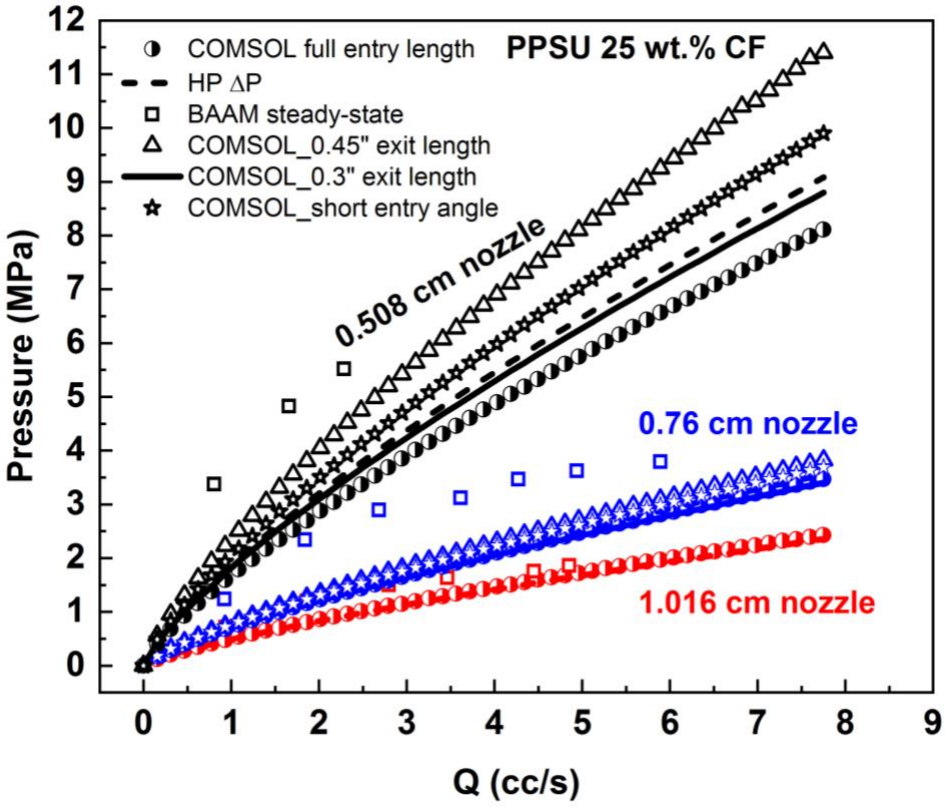


Figure A.7. COMSOL pressure drop predictions for PPSU 25 wt.% CF using BAAM nozzles with varying exit lengths and entry angles

VITA

Christine Ajinjeru was born in Uganda. Growing up, she had a knack for science and a passion for international development. This motivated her to leave Uganda and pursue educational opportunities abroad. She completed her high school at the United World College of the Atlantic in Wales, UK. The long and gloomy winter days played a major part in her decision to leave the UK. She attended Grinnell College in Iowa where she studied Chemistry. Little did she know that Iowa winters were a whole other ordeal. At Grinnell, she was introduced to research and spent her summers conducting Physical Chemistry research. She also spent a semester at Oak Ridge National Laboratory as an intern, where she was exposed to world class research and the plethora of research opportunities. Wanting to nurture her scientific curiosity, she applied to the Energy Science and Engineering PhD program at the University of Tennessee. This program presented an opportunity for her to combine her abilities to use her scientific training to dive deep in a technical area while also using the knowledge gained from the engineering toolkit to solve developmental challenges.